# PROBING THE DETERMINANTS OF THE MOLECULAR RECOGNITION IN METAL-DEPENDENT DEACETYLASE

by

Byung Chul Kim

A dissertation submitted in partial fulfillment
of the requirements for the degree of
Doctor of Philosophy
(Chemical Biology)
in the University of Michigan
2014

Doctoral Committee:
Professor Carol A. Fierke, Chair
Professor Anna K. Mapp
Associate Professor Bruce A. Palfey
Associate Professor Patrick J. O'Brien

# ACKNOWLEDGEMENTS

I would like to take this opportunity to thank all those who supported and helped me during the past 5 years. First of all, I would like to thank my advisor Prof. Carol A. Fierke for being a spectacular advisor and it was a great pleasure to work with you! This work could not become even close to the way it is now without her encouragement and enormous suggestions. Over the past 5 years, her patience and guidance have helped me to become a more independent student, furthermore true scientist. She has also been very supportive and helpful in any idea that I brought to her. I feel so fortunate to join her lab at my second year and graduate from her lab. I would also like to give great thanks to my dissertation committee members, Prof. Anna K. Mapp, Prof. Bruce A. Palfey, and Prof. Patrick J. O'Brien, for their valuable advices during my candidacy, data meeting and dissertation.

I have always enjoyed working with all past / current lab members in the Fierke Lab. I am very grateful for mentoring from Dr. Samuel G. Gattis when I was a rotation student. Dr. Caleb G. Joseph, Dr. Noah Wolfson, and Dr. Ningkun Wang gave numerous discussions with me on how to develop and solve experimental problem. I would like to thank HDAC8 group (Carol Ann Pitcairn, Eric Sullivan, Jeff Lopez, and Katherine Leng) for sharing their idea and help. I also enjoyed working with the labmates, Mike Howard, Elia Wright, Nancy Wu, Amit Pithadia, Dr. Lubomir Dostal, Dr. Benjamin Jennings, Dr. Xin Liu, Chen Yu, Bradley Klemm, lastly, Andrea Stoddard. Also Yaru Zhang for helping me through 5 years. Thanks so much!

I would also like to mention my collaborators who allow me to expand my knowledge to

various field. I'd like to thank Prof Brandon T. Ruotolo and Shuai Niu who helped me to measure protein binding affinity by developing cool mass-spectrometry methodology. I would also like to thank Prof. Seth M. Cohen and Dr. David Puerta for providing quality of compound libraries. In addition to that, I would like to thank Prof. Caroline C. Philpott and Dr. Moon-Suhn Ryu for sharing Co-IP data in chapter 4.

Special thanks to Dr. Hyung Ki Yoon, Dr. Jang Hyun Lee and other Korean friends. I truly enjoyed every moment we spent together in and out of Chemistry building after Fall 2009.

This dissertation could not be accomplished without the endless encouragement and support from my beloved family. I want deliver my sincere appreciation to my parents for their unconditional love. Last but not least I would like to thank my wife, Sujeong and my baby daughter. I couldn't have done this without your support. Thank you.

## TABLE OF CONTENTS

## LIST OF FIGURES

## LIST OF TABLES

## ABSTRACT

## PROBING THE DETERMINANTS OF THE MOLECULAR RECOGNITION IN METAL-DEPENDENT DEACETYLASE

**by**

**Byung Chul Kim**

**Chair: Carol A. Fierke**

Metal-dependent deacetylases catalyze a variety of essential reactions in nature. However, most metallohydrolases can be activated by a number of divalent metal ions, such as Zn(II) or Fe(II). Human metal-dependent metalloenzyme, histone deacetylases 8 (HDAC 8), catalyze the deacetylation of acetylated lysine residues on histones and other protein substrates. Although it was known as a Zn(II)-metalloenzyme, there is growing evidence which indicates it is also activated by Fe(II). HDAC8 was more active with Fe(II) than Zn(II) *in vitro*, and exhibits Fe(II)-like activity *in vivo*, suggesting that many "Zn"-enzymes may utilize either Fe or Zn cofactors *in vivo* depending on cellular conditions. Here I measured the metal (Zn(II) / Fe(II)) binding kinetics and thermodynamics for HDAC8 using newly developed fluorescence polarization assay. Next, the determinants governing the metal specificity of HDAC8 was explored. Alterations in second shell ligand environment significantly affect the reactivity ($k_{cat}/K_M$), binding affinity ($k_{off}$ and $K_D$) for Zn/Fe-bound HDAC8 when compared to the wild-type. Monovalent binding to other metal binding sites in HDAC8 also had an effect on divalent metal binding by decreasing dissociation rate constant. Additionally, the putative binding partner

to HDAC8, poly (rC) binding protein, was investigated to determine the interaction between the two proteins *in vitro* and *in vivo*. This finding revealed that the two proteins bind to each other in a specific manner with μM affinity when apo-apo proteins interact. All these data suggest that HDAC8 is activated by either Zn or Fe based on various factors as a means of metal homeostasis.

Finally, another deacetylase, UDP-3-*O*-(*R*-3-hydroxymyristoyl)-*N*-acetylglucosamine deacetylase (LpxC), was studied to generate a novel potent inhibitor. LpxC catalyzes the committed step in Lipid A biosynthesis. Inhibitors of LpxC affecting lipid A biosynthesis are targets for the development of antibacterials, since lipid A is essential for bacterial cell viability. For the development of more potent non-hydroxamate inhibitors, libraries of metal-binding fragments were screened against *Escherichia coli* LpxC using a high-throughput mass spectrometry assay. A few potent hits ($IC_{50}$ in the nM range) were identified.

These results are important for understanding how best to inhibit the many clinically useful metalloprotein drug targets, as well as for understanding a potentially important new aspect of metal ion homeostasis and metalloprotein regulation.

# CHAPTER 1

# INTRODUCTION

## 1. *Metal homeostasis*

Zinc and iron are essential metal cofactors. However, both metals can be toxic if their homeostasis (such as levels and distribution) is unregulated.[1] The impact of incorrect control of metal homeostasis on human health has generated considerable interest in understanding the principles involved in metal homeostasis. Cells use metal-binding proteins to maintain low cytosolic metal ion concentrations and as protection against cytotoxic increases in intracellular metal ions.

### 1.1 *Zinc homeostasis*

Zinc is an essential element in the cell, playing important structural, and regulatory roles.[2] It forms the catalytic center in numerous metalloenzymes and stabilizes the structure of many other proteins. It is the second most abundant transition metal in the cell, next to iron.[3] Bioinformatic studies revealed that 10% of all proteins in the human genome contain potential binding sites for zinc.[4]

Zinc has several characteristics that enhance its use as a metal cofactor. First, unlike other essential transition metals in the cells such as iron and copper, zinc is redox insensitive and can form stable complexes with macromolecules. Second, as a $d^{10}$ metal, zinc is not susceptible to

ligand field stabilization effects; therefore, zinc can adopt various coordination numbers ranging from 4 to 8, with 4 – 6 commonly observed in protein binding sites[5], although the most typical geometry is tetrahedral or distorted tetrahedral. Third, the specific recognition of a transition metal by a protein-binding site requires discrimination based on ionic size, charge, and chemical nature (i.e., "hardness" or "softness"). Zinc has borderline hardness and easily accommodates nitrogen, oxygen, and sulfur atoms in its biological coordination polyhedral (Table 1). Lastly, in addition to chemical hardness/softness, simple electrostatic effects are also important for protein-metal ion recognition. In metalloproteins, zinc binds to negatively charged residues (e.g., carboxylates and thiolates) and/or neutral dipolar residues (e.g., carbonyls and imidazoles).

Given its importance, zinc homeostasis is regulated through an extensive network of transporters, ligands and transcription factors in the cell (Figure 1).[6,7] The dysregulation of zinc homeostasis is associated with various human health problems.[8,9] For instance, displacement of zinc from zinc-binding structures, e.g., zinc finger structures in DNA repair enzymes, is proposed as a major cause for carcinogenicity of other metals such as cadmium, cobalt, nickel, and arsenic.[10] Furthermore, zinc is suggested to play a role in the development of prostate cancer. Zinc levels in prostate adenocarcinoma are significantly lower than in the surrounding normal prostate tissues, implying a role for zinc in the pathogenesis and progression of prostate malignancy.[11] The proposed mechanism is down-regulation of the zinc transporter Zip1, which is responsible for zinc uptake and accumulation in prostate cells.[12,13] Elevated zinc levels have also been implicated in the development of neurodegenerative diseases, e.g., deregulated zinc homeostasis could be important to onset and progression of Alzheimer's disease.[14]

**Table 1.1** Properties of certain biological metal ions

| Metal ion | Radius (Å )[a] | Hard-soft[b] |
|---|---|---|
| Mg(II) | 0.65 | Hard |
| Ca(II) | 0.99 | Hard |
| Mn(II) | 0.80 | Hard |
| Fe(II) | 0.76 | Borderline |
| Fe(III) | 0.53 | Hard |
| Co(II) | 0.74 | Borderline |
| Ni(II) | 0.69 | Borderline |
| Cu(I) | 0.96 | Soft |
| Cu(II) | 0.72 | Borderline |
| Zn(II) | 0.74 | Borderline |
| Cd(II) | 0.97 | Soft |

a. Radii were calculated by the method of Pauling, abstracted from Cotton and Wilkinson[5]

b. From Pearson (1963)[15]

**Figure 1.1** Zinc homeostasis in mammalian cells reprinted from Da Wang's thesis with permission. MTF-1 is the zinc-dependent transcription factor that is the major regulator of zinc homeostasis in mammalian cells. MTF-1 up-regulates the expression of the membrane zinc exporter ZnT1 and metallothionein to enhance zinc efflux and sequestration by intracellular ligands under high zinc stress. ZIP transporters increase the cytosolic zinc concentration by importing zinc from the outside or releasing zinc from the organelles into the cytosol. ZnT transporters decrease the cytosolic zinc concentration by zinc efflux to the outside or sequestration into organelles. ZIP (blue) and ZnT (green) transporters carry various tissue-specific functions. Some ZnT type transporters shuttle zinc into specialized secretory vesicles, including insulin granules and synaptic vesicles.

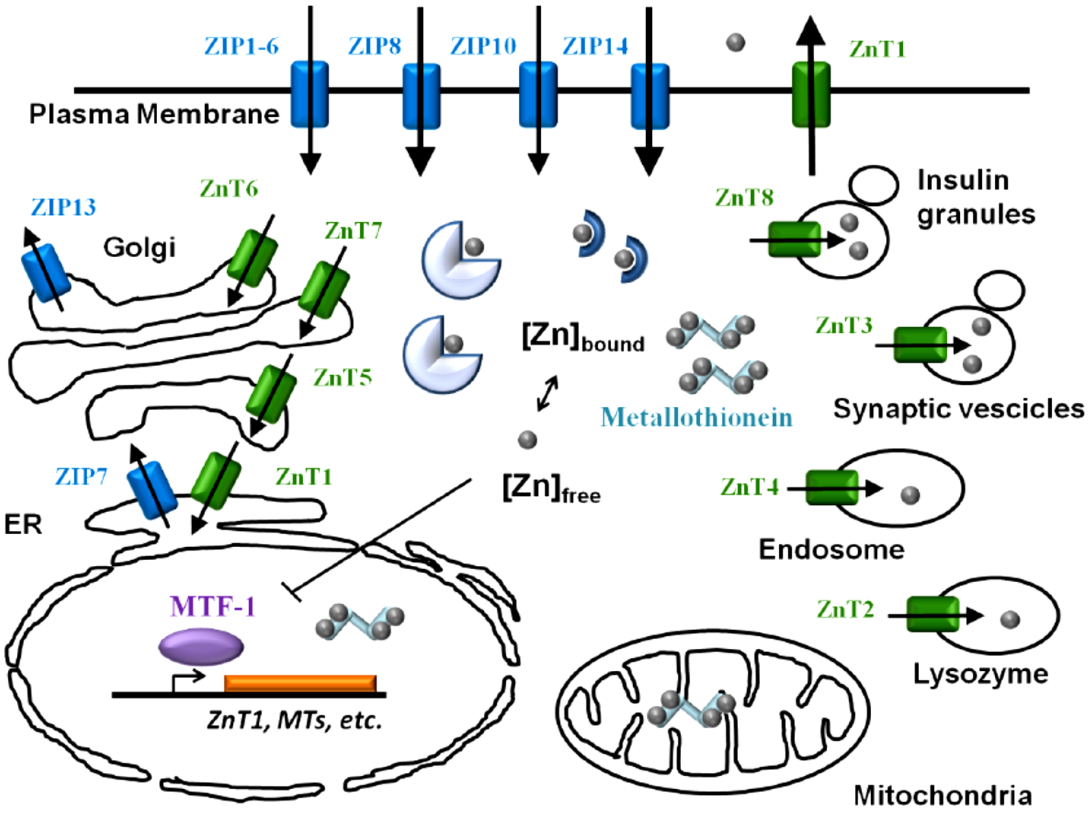


## 1.2 *Iron homeostasis*

Iron is also essential for the function of many metalloenzymes, including heme, iron-sulfur clusters, and non-heme metalloproteins, where it is a cofactor in many major biological processes, including photosynthesis, $N_2$ fixation, methanogenesis, $H_2$ production and consumption, respiration, the trichloroacetic acid (TCA) cycle, oxygen transport, gene regulation

and DNA biosynthesis.[16] Under physiological conditions, cellular iron mainly exists in one of two interconvertible redox states: the reduced Fe(II) ferrous form and the nearly insoluble, oxidized Fe(III) ferric form. Its biological functionality is most frequently dependent upon the formation of a metalloprotein, either as a metal cofactor or as part of iron-sulfur clusters or heme groups. Therefore, sophisticated regulatory mechanisms have evolved to acquire and transport iron across biological membranes to provide adequate amounts for critical biological processes.

Cells must maintain sufficient iron to ensure proper cellular functions but not excess iron that could generate toxic effects, such as promoting the formation of reactive oxygen species (Figure 2). Cells maintain iron homeostasis by a number of mechanisms. First, all mammalian cells produce ferritin, an iron(III) storage protein. Each ferritin can accommodate up to 4500 iron atoms. Ferritin acts as a depot, keeping excess iron and allowing for the mobilization of iron when needed.[17] A second mechanism is a set of iron regulatory proteins (IRPs). When iron is limiting, IRPs bind to RNA stem-loop iron regulatory elements (IREs) found in the untranslated regions of mRNAs involved in iron transport and storage.[18] The IRP-IRE regulatory system enables cells to adjust proteins involved in iron homeostasis to regulate the concentration of available cytosolic iron and optimize the function of numerous iron-dependent cellular components. Therefore, the uptake and export of cellular iron is tightly regulated, as low concentrations of irons impair the function of numerous iron proteins, whereas excess iron can oxidize and damage cellular macromolecules. In addition, several iron-specific metallochaperones are being investigated for roles in iron homeostasis.[19,20] These chaperone candidates include the IscA family of proteins and frataxin for delivery of iron for iron-sulfur

**Figure 1.2** Iron homeostasis in *Saccharomyces cerevisiae,* reprinted from ref. 21 with permission. Yeast cells contain multiple dependent transcription factors, Aft1, Mac1, Zap1 (Zn) and Ace1. Products of genes that are activated under low iron-homeostasis conditions by Aft1 (green), Mac1 (blue), Zap1 (red), and Ace1 (purple) are shown. Extracellular iron that is bound to siderophores has been circled, and stars indicate proteins (Arn1-4 and Aft1) that undergo iron-dependent cellular trafficking. The metal ion specificities of transporters involved in metal ion uptake are indicated; the major iron transporters are Ftr1/Fet3, Fre1/2, Fit1-3 and Fet4. Additionally, free iron is taken into the cell by both high and low-affinity transport systems (Fet3, Ftr1, and Fet4).

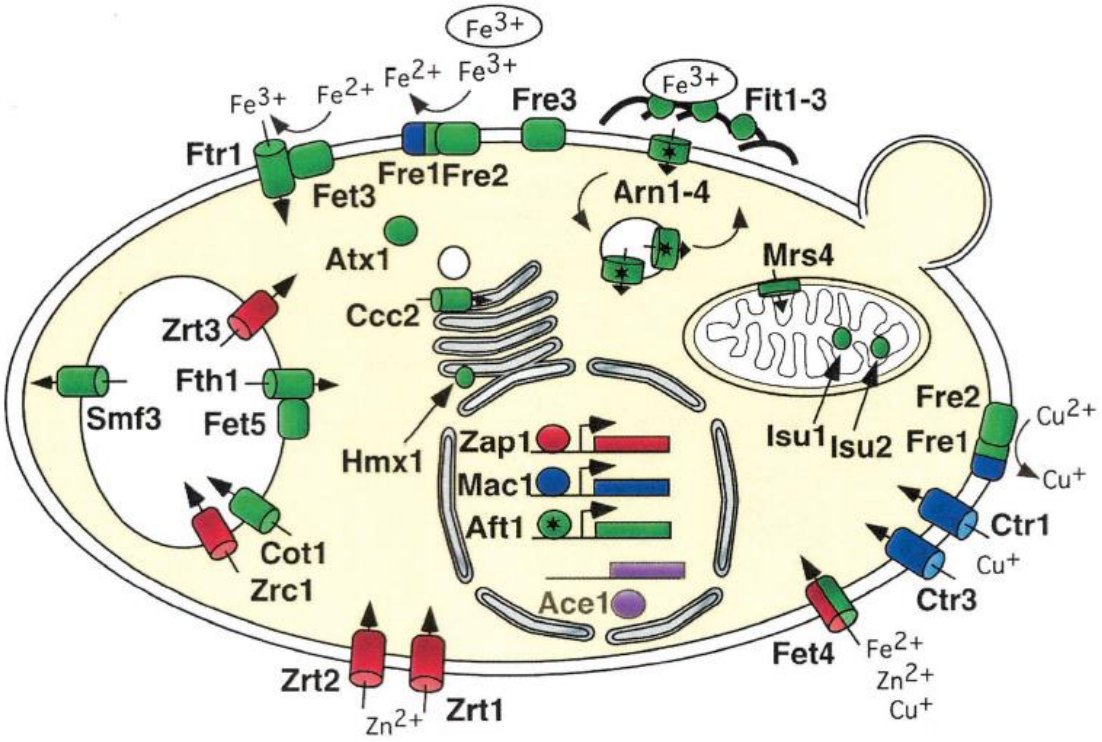


cluster assembly and poly r(C)-binding protein 1 (PCBP1for delivery of iron to ferritin.[22,20,19] Iron deficiency is the most common cause of anemia, which interferes with normal cognitive development in human.[23] Conversely, iron overload, observed in hemochromatosis and thalassemia, causes liver and heart failure.[24,25]

To better understand how cells control metal homeostasis to allow incorporation of the correct metal into metalloproteins, there is a need for more widespread and precise enumeration

of protein metal affinities and selectivities both *in vivo* and *in vitro*.

## 2. Metal selectivity

Metal cations perform a plethora of essential tasks ranging from protein structure stabilization to enzyme catalysis to signal transduction. Currently, about 40% of known proteins contain bound metal cations; Na(I), K(I), Mg(II), Ca(II), Zn(II), Mn(II), Ni(II), Cu(I)/(II), Fe(II)/(III), and Co(II)/(III) are most frequently found to bind to proteins under physiological conditions (Figure 3).[26,27] Understanding the molecular basis of metal binding affinity and selectivity in metalloproteins is of fundamental importance. The exact mechanism and physicochemical principles governing protein-metal recognition remain elusive.

**Figure 1.3** Metals used in metalloproteins for enhancing catalysis reprinted from ref. 28 with permission. The elements used as catalytic cofactors in enzymes are shown in blue. The height of each column represents the proportion of all enzymes with known structures using the respective metal. A systematic bioinformatics survey of 1,371 different enzymes for which three-dimensional structures are known estimated that 47% required metals, with 41% containing metals at their catalytic centers.[28] Magnesium is the most prevalent metal in metalloenzymes, followed by zinc and iron.

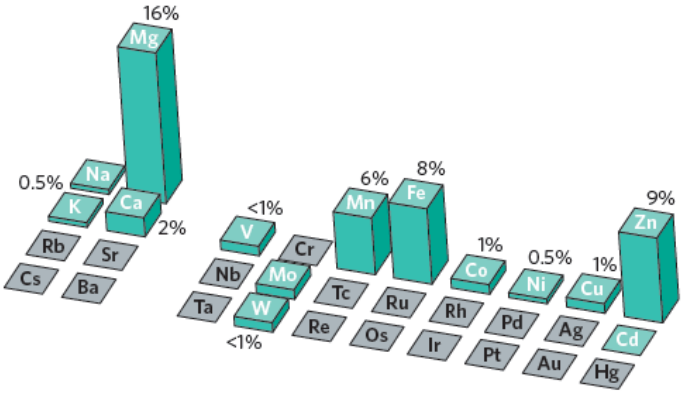


Several questions need further investigatation, including: What is the optimum structure and composition of a protein binding site to provide the best metal affinity and/or selectivity? How does a metal bound to a binuclear site affect the properties of the other metal-binding site? How

and to what extent does the structure of the amino acids in the first and second coordination shell modulate the metal-binding site affinity and selectivity? These questions can be addressed by assessing the role of various factors in metal-protein recognition such as (a) the identity of the metal ion, (b) the structure and composition of the first and second ligation spheres, (c) the structure and properties of the protein matrix, and (d) the cellular environment, such as metallochaperone.

The metal ion selectivity of wild-type carbonic anhydrase II (CAII) $His_3$water zinc coordination polyhedron has been investigated in detail (Figure 4). The metal specificity of this site follows the Irving-Williams series (Mn(II) < Fe(II) < Co(II) < Ni(II) < Cu(II) > Zn(II))[30], similar to small molecule chelators, although the affinity of Zn(II) is increased significantly such that it approaches the affinity of Cu(II).

**Figure 1.4** Schematic diagram of the metal binding affinity of mutants in the active site of WT CA(II), adapted from ref. 29.

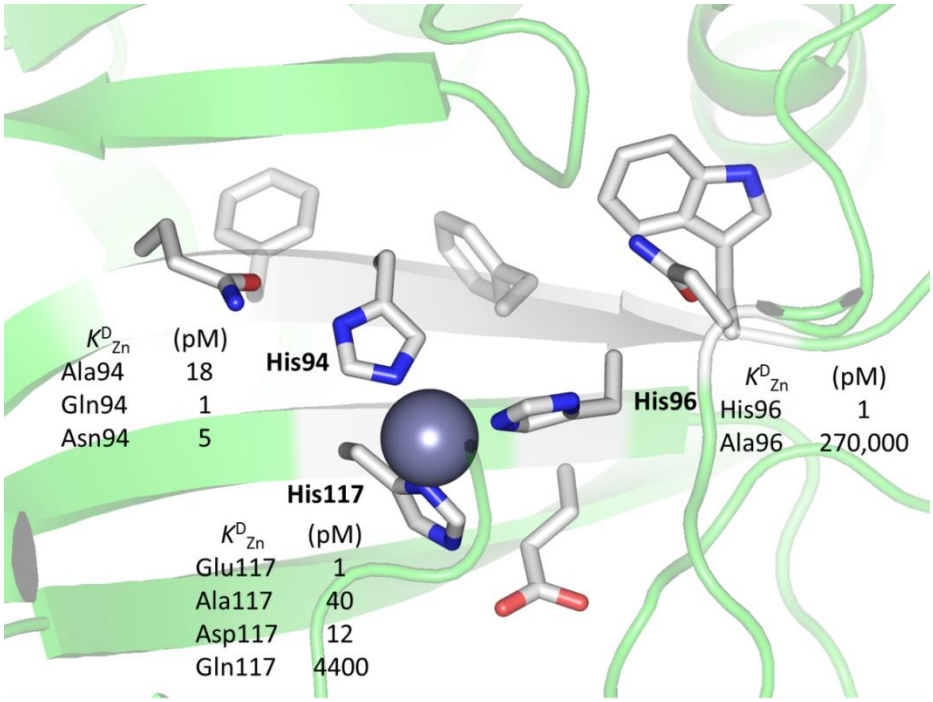

To investigate the determinants of metal ion selectivity, the metal ion affinity and specificity of CAII variants with mutations in the first coordination shell were measured. Substitution of any of the His ligands in the first shell environment with another side chain capable of coordinating the zinc ion, such as Asp, Glu, Gln, Asn decreased zinc affinity by >100 fold.[31–33] Each of the zinc-coordinating His side chains form a hydrogen bond with another protein group. Deletion of any one of the hydrogen bonds with the second shell ligands also reduced zinc affinity by 5~4000-fold.[31,34] Finally, alterations in the hydrophobic residues (Phe93, Phe95 and Trp97) surrounding the zinc binding site also decreased the metal affinity of CA(II) by as much as 100-fold.[35,36] Furthermore, mutations in each of these portions of the metal binding pocket led to alterations in metal selectivity; for example the selectivity of zinc compared to copper ($K_{Zn}/K_{Cu}$) varies from 0.1 for wild-type CAII to $2 \times 10^{-4}$ and 15 for mutations in the His119 ligand (H119N and H119Q, respectively).[33] In summary, these data indicate that the metal ion selectivity of wild-type CAII and the majority of variants follows the Irving-Williams series, demonstrating that the second ionization energy of the metal ion is a dominant factor in thermodynamic metal ion selectivity in proteins, although other influences can alter this trend. These data also demonstrate that changes in metal ion specificity of the variants correlate with the preferred coordination number and geometry of the metal ion. Therefore, we conclude that the primary features driving deviations from the inherent ligand affinity, i.e., the Irving-Williams series, are structural components in the CAII active site that alter the energy required for a bound metal ion to adopt a preferred coordination number and geometry.

## 3. Histone deacetylase (HDAC)

Acetylation / deacetylation, a key posttranslational modification of many proteins, is a dynamic, reversible, and highly regulated chemical modification that is responsible for modulating critical biological pathways. Acetylation is an enzyme-catalyzed reaction involving the transfer of an acetyl group from acetyl-CoA, a metabolic intermediate, to the ε-amino acid of lysine residues in target proteins. Deacetylation is catalyzed by a group of enzymes termed histone deacetylases (HDACs).

There are 18 known HDAC enzymes divided phylogenetically into four classes: class I (HDAC1-3 and HDAC8), class II (HDAC4-7 and HDAC9,10), class III (sirtuins 1-7), and class IV (HDAC11) (Figure 5).[37] Class I, II, and IV HDACs are metalloenzymes that require a divalent metal ion for catalysis. The class III enzymes, termed sirtuins due to their homology with yeast Sir2, have a protein fold and a catalytic mechanism that differs from the metal-dependent enzymes. Although the class I, II, and IV enzymes are referred to as histone deacetylases based on genomic sequence using the first identified enzyme, HDACs catalyze deacetylation of many acetylated protein substrates in addition to histones and in various cellular locations outside of the nucleus.[38] Although histones are the most thoroughly studied of the acetylated protein substrates of HDACs, several recent reports have shown that HDACs are also responsible for deacetylating and thereby modifying the activity of diverse types of non-histone proteins.[39]

These include transcription factors, signal transduction mediators, a microtubule component, and a molecular chaperone.

**Figure 1.5** Classification of classes I, II, and IV HDACs by structure and cellular localization, reprinted from ref. 40 with permission. Eighteen HDACs have been identified in humans, and they are subdivided into four classes based on their homology to yeast HDACs, their subcellular localization and their enzymatic activities. The class I HDACs (1, 2, 3 and 8) are homologous to the yeast RPD3 protein, can generally be detected in the nucleus and show ubiquitous expression in various human cell lines and tissues. Class II HDACs (4, 5, 6, 7, 9 and 10) share homologies with the yeast Hda1 protein and can shuttle between the nucleus and the cytoplasm. HDAC11 is the sole member of the class IV HDACs. It shares sequence similarity with the catalytic core regions of both class I and II enzymes but does not have strong enough identity to be placed in either class.

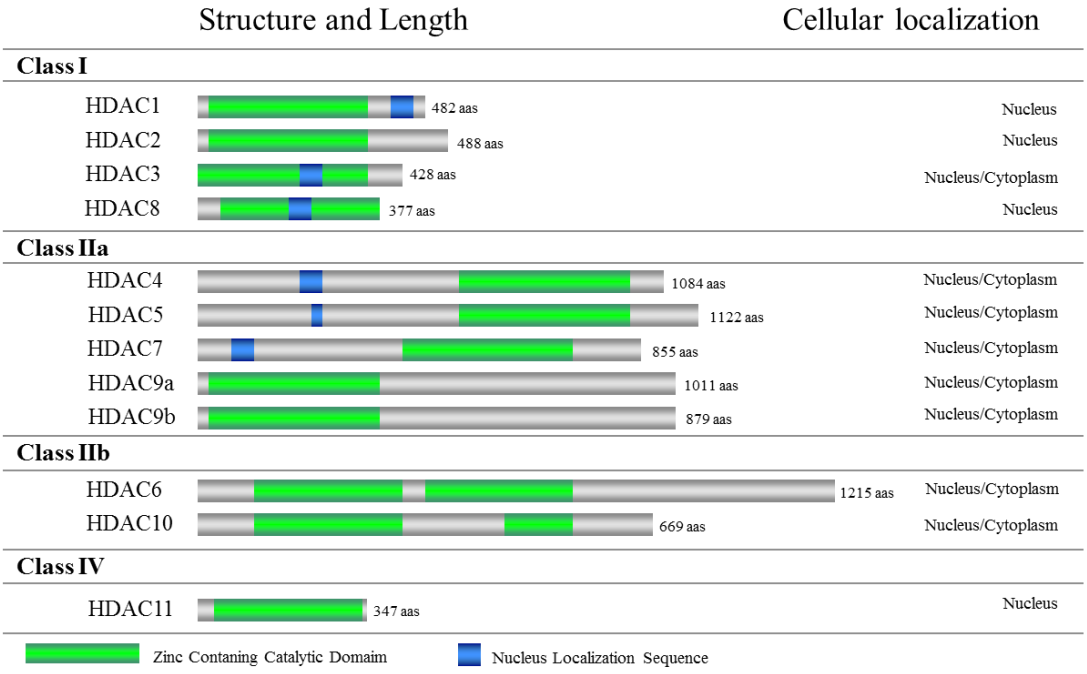


Although histone deacetylases have been shown to be metalloenzymes by crystallography and biochemical analysis, little has been known about the metal ion dependence of HDAC activity.[41,42] Kinetic studies suggest that HDAC8 requires one bound metal ion for maximal activity.[43] The metal-dependent HDACs have been designated as zinc-dependent enzymes because the addition of Zn(II) increases HDAC activity and recombinant HDAC8 isolated aerobically contains bound Zn(II). Furthermore, Zn(II) ion was observed in the active site of the HDAC crystal structure with the bound hydroxamate inhibitor trichostatin A (TSA).[41] However,

HDACs possess an unusual set of metal ligands for a mononuclear Zn(II) enzyme, $Asp_2$-His-water, suggesting that Zn(II) may not be the *in vivo* metal ion.[44] Also, Fe(II)-HDAC8 has a higher value of $k_{cat}/K_M$ than Zn(II)-HDAC8 *in vitro*.[43] Additionally, iron is the most abundant metal in HDAC8-His, immediately following the metal affinity column purification step.[43] For cells grown with iron supplementation, the HDAC8 activity is ~ 4-fold larger when the cells are lysed under anaerobic conditions compared to that under aerobic conditions. All the data above strongly suggest that HDAC8 could function as an Fe(II)-protein in cells.

## 4. Fe(II)-dependent hydrolases

There have been several examples of Zn(II)-dependent hydrolases that have been reclassified as "Fe(II)-dependent" enzymes, including peptide deformylase (PDF), LuxS, γ-class carbonic anhydrase, and UDP-3-*O*-(*R*-3-hydroxymyristoyl)-*N*-acetylglucosamine deacetylase (LpxC) (figure 6). The misidentification of the native metal cofactor as Zn(II) is attributed to the aerobic purification of these enzymes, with the oxidation of Fe(II) to Fe(III) and substitution of Zn(II) at the active site due to higher binding affinity. Identification of these proteins as containing native Fe(II) cofactors comes from a variety of methods, including rapid pull-downs form cells under anaerobic conditions (LpxC)[45] and inhibition of cellular growth using Fe(II)-specific inhibitors (PDF).[46]

The identification of the native metal ion bound to a protein is important because it affects the catalytic activity, substrate selectivity, inhibitor affinities, protein stability and/or regulation. For example, it is proposed that some metalloenzymes are regulated by changes in the oxidation

**Figure 1.6** Reactions catalyzed by Fe(II)-dependent hydrolases. The reactions catalyzed by CA (carbonic anhydrase), LpxC (UDP-3-*O*-(*R*-3-hydroxymyristoyl)-*N*-acetylglucosamine deacetylase), LuxS (S-ribosylhomocysteinase), and PDF (peptide deformylase) are shown.

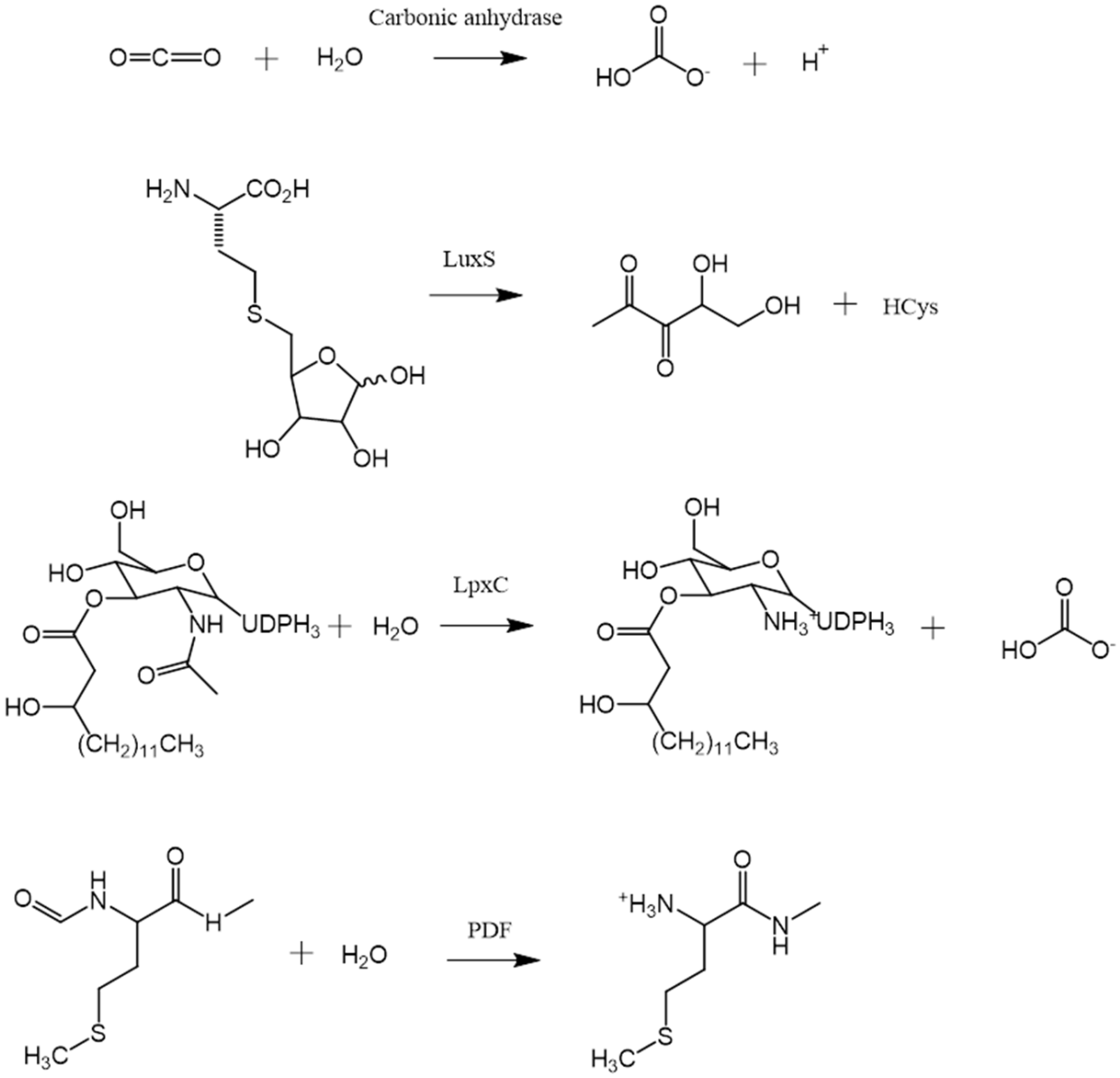

state or the identity of the catalytic metal ion. Furthermore, the unique structural features of the Fe(II)-metalloenzyme active site will facilitate the design of selective inhibitors.

### 4.1. Peptide Deformylase (PDF)

Peptide deformylase is an essential metalloenzyme required for the removal of the formyl group at the N terminus of nascent polypeptide chains in eubacteria. PDF was previously reported to be a zinc metalloenzyme with a $His_2CysWater$ coordination sphere; the Zn(II)-bound protein is very stable but has low catalytic activity ($k_{cat}/K_M \approx 80\ M^{-1}s^{-1}$ with formyl-Met-Ala-Ser as substrate).[47] Later it was found that the *Escherichia coli* enzyme is activated by Fe(II) *in vitro* and retains activity with substitution of Ni(II)[48] for the metal cofactor instead of Zn(II) as previously suggested.[49] The Fe(II)- and Ni(II)-PDF are 1200-fold and 900-fold more active that the Zn(II)-bound form.[50] However, Fe(II)-PDF rapidly loses activity under anaerobic conditions.[50] The dramatically enhanced catalytic activities of PDF with the Fe(II) cofactor compared to Zn(II) despite similar tertiary structures[48,51,52], provided support that the native metal ions are directly involved in the catalytic mechanism.

### 4.2. LuxS

Previous studies have shown that S-ribosylhomocysteinase is encoded by the luxS gene in *Escherichia coli*, which catalyzes the synthesis of the type-2 quorum sensing molecule.[53] LuxS is a small metalloenzyme (157 amino acids for the *Bacillus subtilis* enzyme). Sequence

alignment of this enzyme reveals an invariant HXXEH motif, which is often found in Zn(II)-containing proteins. High resolution structures demonstrated a divalent metal ion bound to the active site via a $His_2Cys$ coordination sphere, which was initially reported to be Zn(II), based on inductively coupled plasma (ICP) metal analysis.[54,55] However, rapid, aerobic purification of overexpressed C-terminally histidine-tagged LuxS using metal affinity chromatography demonstrated that the metal cofactor bound to LuxS was Fe(II).[56] Like the deformylase, native LuxS [Fe(II) bound] rapidly loses activity under aerobic conditions, whereas the activity of the Zn(II)- or Co(II)-substituted LuxS form is stable under these conditions.[56]

### 4.3. γ-Class Carbonic Anhydrase (Cam)

γ-class carbonic anhydrase (Cam) contains a $His_3Water$ metal coordination sphere rather than the $His_3Water$ site in CAII, an α-class enzyme. The initial biochemical, kinetic, and structural characterizations of Cam concluded that the active-site metal ion was Zn(II), which was consistent with zinc reported for all CA's characterized from the extensive α- and β-classes.[57,58] However, the methanoarchaea such as *Methanosarcina thermophile* are strict anaerobes that live in ferrous rich, oxygen-free environments and synthesize an abundance of oxygen-sensitive enzymes. Indeed, it was shown that Cam reconstituted with Fe(II) *in vitro* is exquisitely sensitive to oxygen with rapid loss of activity on exposure to air, leading to the suggestion that aerobic purification of Cam could lead to loss of Fe(II) and incorporation of Zn(II).[59] Overproduction of the archetype γ-class CA in preparative yields provided sufficient material to establish iron as the physiological metal in the active site of this metalloenzyme, establishing a novel catalytic role for iron.[60]

### 4.4. LpxC

UDP-3-*O*-((*R*)-3-hydroxymyristoyl)-*N*-acetylglucosamine deacetylase (LpxC) catalyzes the committed and second overall step in lipid A biosynthesis, the hydrolysis of UDP-3-*O*-myristoyl-*N*-acetylglucosamine to UDP-3-*O*-myristoyl-glucosamine and acetate.[61–63] Lipid A forms the core structure of the lipopolysaccharide cell wall of gram negative bacteria essential for cell growth.[64] Consequently, inhibitors targeting LpxC in the lipid A biosynthetic pathway are an active area of drug development.[65] LpxC was previously identified as a mononuclear Zn(II) metalloenzyme that also contains a weaker, inhibitory metal ion-binding site.[66] However, later studies demonstrated that LpxC is ~6-fold more active with Fe(II) as its metal ion cofactor compared with Zn(II) *in vitro*.[67] Furthermore, rapid anaerobic purifications of tagged LpxC from *E. coli* followed by ICP-MS metal analysis demonstrated that under most growth conditions LpxC is activated by Fe(II) *in vivo*.[45] This identification was also confirmed by the oxygen sensitivity of LpxC activity in crude lysates, indicative of the Fe(II)-bound enzyme. However, the pulldown experiments also demonstrated that in the presence of low Fe(II) and high Zn(II) in the medium, LpxC binds and is activated by Zn(II). These data indicate that LpxC should not be considered an Fe(II)-specific metalloenzyme but rather a Me(II)-dependent enzyme that is generally activated by Fe(II). *In vivo* LpxC can bind either Fe(II) or Zn(II) based on altered cellular conditions, such as variations in metal availability in the medium.[45]

### 4.5. HDAC8

The metal-dependent HDAC8 has been typically described as a Zn(II)-enzyme. However, several lines of evidence suggest a more careful analysis of the metal dependence is warranted,

including the unusual $HisAsp_2$ metal coordination sphere, the higher catalytic activity of Fe(II)-HDAC8 compared to Zn(II)-HDAC8 *in vitro*,[43] and the sensitivity of HDAC activity to oxygen from both *E. coli* lysates containing recombinant HDAC8 and HeLa cell extract.[43]

## 5. Metallochaperones

Access to metals in enzymes can be mediated by specific interactions with metal-delivery proteins, such as metallochaperones. Cells are required to overcome several obstacles in ensuring that apo-proteins receive the correct, cognate metal ion. First, although the first and the second spheres of metal-binding sites can distinguish between ions based on charge, coordination geometry, and polarity, the large differences in intrinsic metal affinity (described by the Irving-Williams series) may overwhelm the capacity of a protein binding site to identify the correct metal ions. In fact, proteins may even bind a non-cognate metal more tightly than the correct one, such as Zn(II)-bound LpxC and Cu(II)-bound CAII.[66,68] Second, some metal ions, such as iron and copper, are redox-active, therefore in the presence of oxygen, can both oxidize to the incorrect metal species (i.e Fe(II) to Fe(III)) and catalyze the formation of reactive oxygen species. Thus, cells must tightly modulate the distribution of transition metals to incorporate them correctly while avoiding the toxicities of mismetallation and oxidative damage. One cellular strategy is to use the metallochaperones that recognize and help deliver a cognate metal ion to a metalloprotein. This strategy has been shown to operate for several copper binding proteins, such as superoxide dismutase[69]; however, no metallochaperones have yet been identified for Zn(II). Therefore, the data suggest that zinc metalloproteins are metallated by equilibration with the cellular exchangeable zinc pools.[6] Eukaryotic metallochaperones for other

metals have not yet been clearly established; however, candidates for the delivery of iron to the sites of iron-sulfur cluster assembly and to ferritin have been identified. Candidates for iron chaperones include frataxin, and poly(rC)-binding proteins (PCBPs).

### 5.1. Frataxin

Frataxin is an essential, highly conserved mitochondrial protein. Frataxin-defective organisms, from unicellular yeast to human beings, exhibit various metabolic disturbances, including the accumulation of iron in the mitochondria of yeast with the deleted frataxin homologue gene (Yfh1).[70] Furthermore, involvement of frataxin in Fe-S formation was suggested by studies showing that patients with Friedreich ataxia (FRDA), and conditional knockout mice have deficiencies in Fe-S cluster proteins.[71]

### 5.2. Poly(rC)-binding proteins (PCBPs)

PCBP1 (also called a-CP1 or hnRNP E1) has previously been shown to function as an RNA- and DNA-binding protein.[72] PCBP1 is one member of a family of four homologous proteins containing three heterogeneous nuclear ribonucleoprotein K-homology (KH) domains. PCBPs have a role in transcriptional regulation and participate in several protein-protein interactions.[73,74] The Philpott laboratory recently identified PCBP1 as a cytosolic iron chaperone that delivers iron for incorporation into ferritin.[75] PCBP1 binds ferrous iron with micromolar affinity in a 3:1 Fe:PCBP1 molar ratio (Figure 7).[19] PCBP1 binds to ferritin and can enhance iron

**Figure 1.7** Simplified model of iron delivery in mammalian cells, adapted from ref. 76. PCBP1 and PCBP2 bind cytosolic Fe(II) and directly deliver it to ferritin, 2-oxoglutarate dioxygenases (such as PHDs and FIH1), and possibly other non-heme iron enzymes such as HDAC8.

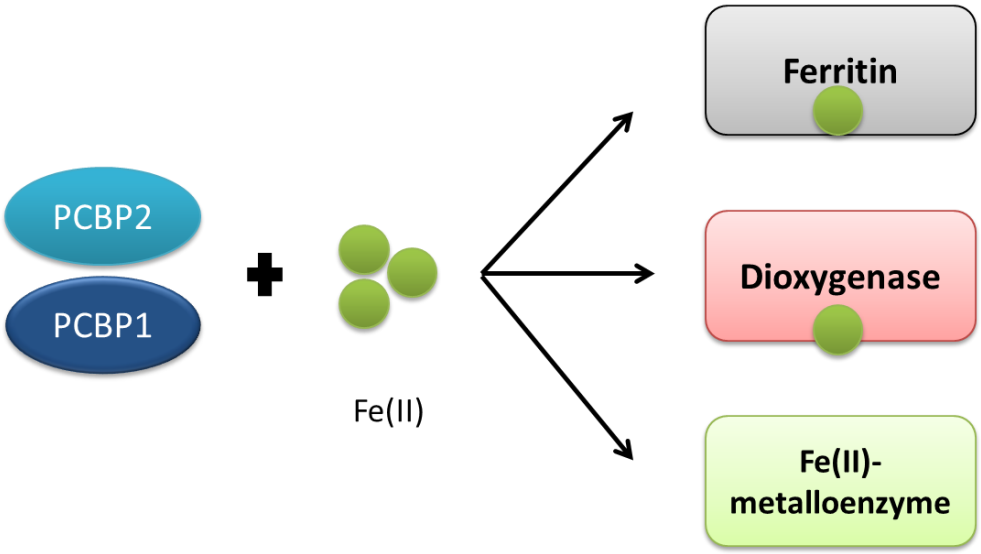


incorporation into ferritin *in vitro* and *in vivo*. Mammalian cells lacking PCBP1 exhibit defective incorporation of iron into ferritin. A previous report indicated that mammalian genomes encode four PCBPs, and suggested that all of the PCBPs may share iron chaperone activity.[77] Subsequently, PCBP1 and 2 have been implicated as metallochaperones for the iron-dependent prolyl hydroxylases (PHDs) and asparaginyl hydroxylase (FIH1) that modifies hypoxia-inducible factor a (HIFa).[78] The activities of the HIF hydroxylases may be regulated by the availability of iron since HIF hydroxylase activity is stimulated by the addition of Fe(II) *in vitro*, and, in cultured cells, activity is inhibited by the addition of iron chelators. Iron-deprived cells lacking PCBP1 or PCBP2 exhibit increased levels of HIF1a due to a decrease in prolyl hydroxylation and Von Hippel–Lindau (VHL)-mediated degradation. The loss of prolyl hydroxylase activity was traced to a decrease in iron loading of the enzyme, which could be restored by addition of

recombinant PCBP1. Furthermore, PCBP1 physically interacts with PHD2 by using pulldown, indicating that PCBP1 likely acts as an iron chaperone for PHD. Similar results suggest a direct role for PCBPs in the activation of asparaginyl hydroxylase.[78] These data indicate PCBP1 facilitates incorporation of iron into ferritin, PHD, and FIH1 and functions as an iron metallochaperone. Since PCBP1 serves as an iron chaperone for these diverse enzymes, it is possible that other enzymes of the Fe(II)-dependent metalloenzyme class will require PCBPs for metallation.

**Objectives of this work**

The overall goal of this thesis is to elucidate the mechanistic features that govern the molecular recognition of metal binding specificity in HDAC8. Growing evidence indicates that HDAC8 could be an Fe(II)-dependent metalloenzyme rather than activated by Zn(II) *in vivo*. Additionally, it is possible that the enzyme is regulated by metal switching depending on cellular conditions, such as concentrations of readily exchangeable metal and/or oxidative stress. However, there is not a clear understanding of how the metal binding of HDAC8 is determined and regulated. In the following chapters, I will develop new assays to measure the binding kinetics and thermodynamics of metal ions bound to HDAC8. This information will aid in identifying the native metal ion. The crystal structure of HDAC8 provides insight into the unique structural features of the metal binding site of HDAC8, such as the lack of hydrogen bonds in the second shell environment and a nearby monovalent cation binding site. These unique structural features may modulate the metal binding of HDAC8. This hypothesis will be analyzed by measuring the metal affinity and selectivity of HDAC8 mutants. These findings shed light on

our understanding of metalloprotein selectivity *in vivo*, and illuminate the potential regulatory mechanism of metal switching which is also suggested by bacterial deacetylase LpxC. Furthermore, the role of the metal identity in determining inhibitor selectivity will be explored for LpxC.

**REFERENCE**

(1) Kozlowski, H., Janicka-Klos, A., Brasun, J., Gaggelli, E., Valensin, D., and Valensin, G. (2009) Copper, iron, and zinc ions homeostasis and their role in neurodegenerative disorders (metal uptake, transport, distribution and regulation). *Coord. Chem. Rev. 253*, 2665–2685.

(2) Vallee, B. L., and Falchuk, K. H. (1993) The biochemical basis of zinc physiology. *Physiol. Rev. 73*, 79–118.

(3) Outten, C. E., and O'Halloran, T. V. (2001) Femtomolar sensitivity of metalloregulatory proteins controlling zinc homeostasis. *Science 292*, 2488–92.

(4) Andreini, C., Banci, L., Bertini, I., and Rosato, A. (2006) Counting the zinc-proteins encoded in the human genome. *J. Proteome Res. 5*, 196–201.

(5) Christianson, D. W. (1991) Structural biology of zinc. *Adv. Protein Chem. 42*, 281–355.

(6) Eide, D. J. (2006) Zinc transporters and the cellular trafficking of zinc. *Biochim. Biophys. Acta 1763*, 711–22.

(7) Colvin, R. a, Holmes, W. R., Fontaine, C. P., and Maret, W. (2010) Cytosolic zinc buffering and muffling: their role in intracellular zinc homeostasis. *Metallomics 2*, 306–17.

(8) Plum, L. M., Rink, L., and Haase, H. (2010) The essential toxin: impact of zinc on human health. *Int. J. Environ. Res. Public Health 7*, 1342–65.

(9) Fukada, T., Yamasaki, S., Nishida, K., Murakami, M., and Hirano, T. (2011) Zinc homeostasis and signaling in health and diseases: Zinc signaling. *J. Biol. Inorg. Chem. 16*, 1123–34.

(10) Beyersmann, D., and Hartwig, A. (2008) Carcinogenic metal compounds: recent insight into molecular and cellular mechanisms. *Arch. Toxicol. 82*, 493–512.

(11) Costello, L. C., and Franklin, R. B. (1998) Novel role of zinc in the regulation of prostate citrate metabolism and its implications in prostate cancer. *Prostate 35*, 285–96.

(12) Costello, L. C., Liu, Y., Zou, J., and Franklin, R. B. (1999) Evidence for a Zinc Uptake Transporter in Human Prostate Cancer Cells Which Is Regulated by Prolactin and Testosterone. *J. Biol. Chem. 274*, 17499–17504.

(13) Franklin, R. B., Feng, P., Milon, B., Desouki, M. M., Singh, K. K., Kajdacsy-Balla, A., Bagasra, O., and Costello, L. C. (2005) hZIP1 zinc uptake transporter down regulation and zinc depletion in prostate cancer. *Mol. Cancer 4*, 32.

(14) Devirgiliis, C., Zalewski, P. D., Perozzi, G., and Murgia, C. (2007) Zinc fluxes and zinc transporter genes in chronic diseases. *Mutat. Res. 622*, 84–93.

(15) Patent, U. S., and Pearson, R. G. (1963) Hard and Soft Acids and Bases. *J. Am. Chem. Soc. 265*, 3533–3539.

(16) Johnson, D. C., Dean, D. R., Smith, A. D., and Johnson, M. K. (2005) Structure, function, and formation of biological iron-sulfur clusters. *Annu. Rev. Biochem. 74*, 247–81.

(17) Theil, E. C. (2003) Metal-Binding Proteins and Trace Element Metabolism Ferritin : At the Crossroads of Iron and Oxygen Metabolism 1 , 2. *J. Nutr. 133*, 1549–1553.

(18) Muckenthaler, M. U., Galy, B., and Hentze, M. W. (2008) Systemic iron homeostasis and the iron-responsive element/iron-regulatory protein (IRE/IRP) regulatory network. *Annu. Rev. Nutr. 28*, 197–213.

(19) Rutherford, J. C., and Bird, A. J. (2004) Metal-Responsive Transcription Factors That Regulate Iron , Zinc , and Copper Homeostasis in Eukaryotic Cells. *Eukaryot. Cell 3*, 1–13.

(20) Shi, H., Bencze, K. Z., Stemmler, T. L., and Philpott, C. C. (2008) A cytosolic iron chaperone that delivers iron to ferritin. *Science (80-. ). 320*, 1207–10.

(21) Bulteau, A.-L., O'Neill, H. a, Kennedy, M. C., Ikeda-Saito, M., Isaya, G., and Szweda, L. I. (2004) Frataxin acts as an iron chaperone protein to modulate mitochondrial aconitase activity. *Science (80-. ). 305*, 242–5.

(22) Jensen, L. T., and Culotta, V. C. (2000) Role of Saccharomyces cerevisiae ISA1 and ISA2 in Iron Homeostasis Role of Saccharomyces cerevisiae ISA1 and ISA2 in Iron Homeostasis. *Mol. Cell. Biol. 20*, 3918–3927.

(23) Clark, S. F. (2008) Iron deficiency anemia. *Nutr. Clin. Pract. 23*, 128–41.

(24) Kowdley, K. V. (2004) Iron, hemochromatosis, and hepatocellular carcinoma. *Gastroenterology 127*, S79–S86.

(25) Olivieri, N. F., and Brittenham, G. M. (1997) Iron-chelating therapy and the treatment of thalassemia. *Blood 89*, 739–61.

(26) Christianson, D. W., and Cox, J. D. (1999) Catalysis by metal-activated hydroxide in zinc and manganese metalloenzymes. *Annu. Rev. Biochem. 68*, 33–57.

(27) Dudev, T., and Lim, C. (2008) Metal binding affinity and selectivity in metalloproteins: insights from computational studies. *Annu. Rev. Biophys. 37*, 97–116.

(28) Waldron, K. J., Rutherford, J. C., Ford, D., and Robinson, N. J. (2009) Metalloproteins and metal sensing. *Nature 460*, 823–30.

(29) Irving, H. Williams, R. J. P. (1948) Order of stability of metal complexes. *Nature 162*, 746–747.

(30) Huang, C. C., Lesburg, C. a, Kiefer, L. L., Fierke, C. a, and Christianson, D. W. (1996) Reversal of the hydrogen bond to zinc ligand histidine-119 dramatically diminishes catalysis and enhances metal equilibration kinetics in carbonic anhydrase II. *Biochemistry 35*, 3439–3446.

(31) Jackman, J. E., Merz, K. M., and Fierke, C. a. (1996) Disruption of the active site solvent network in carbonic anhydrase II decreases the efficiency of proton transfer. *Biochemistry 35*, 16421–8.

(32) McCall, K. a, and Fierke, C. a. (2004) Probing determinants of the metal ion selectivity in carbonic anhydrase using mutagenesis. *Biochemistry 43*, 3979–3986.

(33) Kiefer, L. L., Paterno, S. A., Fierke, C. A., and Carolina, N. (1995) Hydrogen Bond Network in the Metal Binding Site of Carbonic Anhydrase Enhances Zinc Affinity and Catalytic Efficiency ? *J. Am. Chem. Soc. 117*, 6831–6837.

(34) Residues, H. C., Hunt, J. A., Ahmed, M., and Fierke, C. A. (1999) Metal Binding Specificity in Carbonic Anhydrase Is Influenced by Conserved. *Biochemistry 38*, 9054–9062.

(35) Hunt, J. A., and Fierke, C. A. (1997) Selection of Carbonic Anhydrase Variants Displayed on Phage : Aromatic residues in zinc binding site enhance metal affinity and equilibration kinetics selection of carbonic anhydrase variants displayed on phage. *J Biol Chem 272*, 20364–20372.

(36) Hurst, T. K., Wang, D., Thompson, R. B., and Fierke, C. a. (2010) Carbonic anhydrase II-based metal ion sensing: Advances and new perspectives. *Biochim. Biophys. Acta 1804*, 393–403.

(37) Gregoretti, I. V, Lee, Y.-M., and Goodson, H. V. (2004) Molecular evolution of the histone deacetylase family: functional implications of phylogenetic analysis. *J. Mol. Biol. 338*, 17–31.

(38) Lucio-Eterovic, A. K. B., Cortez, M. a a, Valera, E. T., Motta, F. J. N., Queiroz, R. G. P., Machado, H. R., Carlotti, C. G., Neder, L., Scrideli, C. a, and Tone, L. G. (2008) Differential expression of 12 histone deacetylase (HDAC) genes in astrocytomas and normal brain tissue: class II and IV are hypoexpressed in glioblastomas. *BMC Cancer 8*, 243.

(39) Lin, H.-Y., Chen, C.-S., Lin, S.-P., Weng, J.-R., and Chen, C.-S. (2006) Targeting histone deacetylase in cancer therapy. *Med. Res. Rev. 26*, 397–413.

(40) Wolfson, N. a, Ann Pitcairn, C., and Fierke, C. a. (2013) HDAC8 substrates: Histones and beyond. *Biopolymers 99*, 112–26.

(41) Finnin, M. S., Donigian, J. R., Cohen, A., Richon, V. M., Rifkind, R. A., Marks, P. A., Breslow, R., and Pavletich, N. P. (1999) Structures of a histone deacetylase homologue bound to the TSA and SAHA inhibitors. *Nature 401*, 188–193.

(42) Hassig, C. a, Tong, J. K., Fleischer, T. C., Owa, T., Grable, P. G., Ayer, D. E., and Schreiber, S. L. (1998) A role for histone deacetylase activity in HDAC1-mediated transcriptional repression. *Proc. Natl. Acad. Sci. U. S. A. 95*, 3519–24.

(43) Gantt, S. L., Gattis, S. G., and Fierke, C. A. (2006) Catalytic activity and inhibition of human histone deacetylase 8 is dependent on the identity of the active site metal ion. *Biochemistry 45*, 6170–8.

(44) Vallee, B. L., and Auld, D. S. (1990) Zinc coordination, function, and structures of zinc enzymes and other proteins. *Biochemistry 29*, 5647–5659.

(45) Gattis, S. G., Hernick, M., and Fierke, C. a. (2010) Active site metal ion in UDP-3-O-((R)-3-hydroxymyristoyl)-N-acetylglucosamine deacetylase (LpxC) switches between Fe(II) and Zn(II) depending on cellular conditions. *J. Biol. Chem. 285*, 33788–33796.

(46) Apfel, C., Banner, D. W., Bur, D., Dietz, M., Hirata, T., Hubschwerlen, C., Locher, H., Page, M. G., Pirson, W., Rossé, G., and Specklin, J. L. (2000) Hydroxamic acid derivatives as potent peptide deformylase inhibitors and antibacterial agents. *J. Med. Chem. 43*, 2324–31.

(47) Meinnel, T., and Blanquet, S. (1993) Evidence that peptide deformylase and methionyl-tRNA(fMet) formyltransferase are encoded within the same operon in Escherichia coli. *J. Bacteriol. 175*, 7737–40.

(48) Becker, A., Schlichting, I., Kabsch, W., Schultz, S., and Wagner, a F. (1998) Structure of peptide deformylase and identification of the substrate binding site. *J. Biol. Chem. 273*, 11413–6.

(49) Meinnel, T., Blanquet, S., and Dardel, F. (1996) A new subclass of the zinc metalloproteases superfamily revealed by the solution structure of peptide deformylase. *J. Mol. Biol. 262*, 375–86.

(50) Rajagopalan, P. T. R., and Yu, X. C. (2008) Peptide Deformylase : A New Type of Mononuclear Iron Protein. *J. Am. Chem. Soc. 7863*, 12418–12419.

(51) Chan, M. K., Gong, W., Rajagopalan, P. T., Hao, B., Tsai, C. M., and Pei, D. (1997) Crystal structure of the Escherichia coli peptide deformylase. *Biochemistry 36*, 13904–9.

(52) Cell, C., and Peg, S. (1998) Iron center, substrate recognition and mechanism of peptide deformylase. *Nat. Struct. Biol. 132*, 1053–1058.

(53) Schauder, S., Shokat, K., Surette, M. G., and Bassler, B. L. (2001) The LuxS family of bacterial autoinducers: biosynthesis of a novel quorum-sensing signal molecule. *Mol. Microbiol. 41*, 463–76.

(54) Hilgers, M. T., and Ludwig, M. L. (2001) Crystal structure of the quorum-sensing protein LuxS reveals a catalytic metal site. *Proc. Natl. Acad. Sci. U. S. A. 98*, 11169–74.

(55) Lewis, H. a, Furlong, E. B., Laubert, B., Eroshkina, G. a, Batiyenko, Y., Adams, J. M., Bergseid, M. G., Marsh, C. D., Peat, T. S., Sanderson, W. E., Sauder, J. M., and Buchanan, S. G. (2001) A structural genomics approach to the study of quorum sensing: crystal structures of three LuxS orthologs. *Structure 9*, 527–37.

(56) Zhu, J., Dizin, E., Hu, X., Wavreille, A.-S., Park, J., and Pei, D. (2003) S-Ribosylhomocysteinase (LuxS) Is a Mononuclear Iron Protein. *Biochemistry 42*, 4717–26.

(57) Alber, B. E., Colangelo, C. M., Dong, J., Stålhandske, C. M., Baird, T. T., Tu, C., Fierke, C. a, Silverman, D. N., Scott, R. a, and Ferry, J. G. (1999) Kinetic and spectroscopic characterization of the gamma-carbonic anhydrase from the methanoarchaeon Methanosarcina thermophila. *Biochemistry 38*, 13119–28.

(58) Iverson, T. M., Alber, B. E., Kisker, C., Ferry, J. G., and Rees, D. C. (2000) A Closer Look at the Active Site of γ -Class Carbonic Anhydrases : High-Resolution Crystallographic Studies of the Carbonic Anhydrase from. *Biochemistry 39*, 9222–9231.

(59) Tripp, B. C., Bell, C. B., Cruz, F., Krebs, C., and Ferry, J. G. (2004) A role for iron in an ancient carbonic anhydrase. *J. Biol. Chem. 279*, 6683–7.

(60) Macauley, S. R., Zimmerman, S. a, Apolinario, E. E., Evilia, C., Hou, Y.-M., Ferry, J. G., and Sowers, K. R. (2009) The archetype gamma-class carbonic anhydrase (Cam) contains iron when synthesized in vivo. *Biochemistry 48*, 817–9.

(61) Hernick, M., and Fierke, C. a. (2005) Zinc hydrolases: the mechanisms of zinc-dependent deacetylases. *Arch. Biochem. Biophys. 433*, 71–84.

(62) Young, K., Silver, L. L., Bramhill, D., Cameron, P., Eveland, S. S., Raetz, C. R. H., Hyland, S. a., and Anderson, M. S. (1995) The envA Permeability / Cell Division Gene of Escherichia coli Encodes the Second Enzyme of Lipid A Biosynthesis: UDP-3-O-(R-3- hydroxymyristoyl)-N-acetylglucosamine deacetylase. *J. Biol. Chem. 270*, 30384–30391.

(63) Beall, B., and Lutkenhaus, J. (1987) Sequence analysis, transcriptional organization, and insertional mutagenesis of the envA gene of Escherichia coli. *J. Bacteriol. 169*, 5408–15.

(64) Raetz, C. R. H., and Whitfield, C. (2002) Lipopolysaccharide endotoxins. *Annu. Rev. Biochem. 71*, 635–700.

(65) Barb, A. W., Zhou, P., Hsieh, J., Koutmou, K. S., Rueda, D., Koutmos, M., Walter, N. G., and Fierke, C. A. (2008) Mechanism and inhibition of LpxC: an essential zinc-dependent deacetylase of bacterial lipid A synthesis. *Curr Pharm Biotechnol 9*, 9–15.

(66) Jackman, J. E., Raetz, C. R., and Fierke, C. a. (1999) UDP-3-O-(R-3-hydroxymyristoyl)-N-acetylglucosamine deacetylase of Escherichia coli is a zinc metalloenzyme. *Biochemistry 38*, 1902–11.

(67) Hernick, M., Gattis, S. G., Penner-Hahn, J. E., and Fierke, C. a. (2010) Activation of Escherichia coli UDP-3-O-[(R)-3-hydroxymyristoyl]-N-acetylglucosamine deacetylase by Fe2+ yields a more efficient enzyme with altered ligand affinity. *Biochemistry 49*, 2246–55.

(68) Keilin, D., and Mann, T. (1940) Carbonic anhydrase. Purification and nature of the enzyme. *Biochem. J. 34*, 1163–76.

(69) O'Halloran, T. V, and Culotta, V. C. (2000) Metallochaperones, an intracellular shuttle service for metal ions. *J. Biol. Chem. 275*, 25057–60.

(70) Pufahl, R. A. (1997) Metal Ion Chaperone Function of the Soluble Cu(I) Receptor Atx1. *Science (80-. ). 278*, 853–856.

(71) Mühlenhoff, U., Richhardt, N., Ristow, M., Kispal, G., and Lill, R. (2002) The yeast frataxin homolog Yfh1p plays a specific role in the maturation of cellular Fe/S proteins. *Hum. Mol. Genet. 11*, 2025–36.

(72) Chaudhury, A., Chander, P., and Howe, P. H. (2010) Heterogeneous nuclear ribonucleoproteins (hnRNPs) in cellular processes: Focus on hnRNP E1's multifunctional regulatory roles. *RNA 16*, 1449–62.

(73) Choi, H. S., Hwang, C. K., Song, K. Y., Law, P.-Y., Wei, L.-N., and Loh, H. H. (2009) Poly(C)-binding proteins as transcriptional regulators of gene expression. *Biochem. Biophys. Res. Commun. 380*, 431–6.

(74) Makeyev, A. V, and Liebhaber, S. A. (2002) The poly(C)-binding proteins : a multiplicity of functions and a search for mechanisms. *RNA 8*, 265–278.

(75) Shi, H. (2013) A cytosolic iron chaperone that delivers iron to ferritin. *Science (80-. ). 1207*, 1207–1210.

(76) Leidgens, S., Bullough, K. Z., Shi, H., Li, F., Shakoury-Elizeh, M., Yabe, T., Subramanian, P., Hsu, E., Natarajan, N., Nandal, A., Stemmler, T. L., and Philpott, C. C. (2013) Each member of the poly-r(C)-binding protein 1 (PCBP) family exhibits iron chaperone activity toward ferritin. *J. Biol. Chem. 288*, 17791–802.

(77) Nandal, A., Ruiz, J. C., Subramanian, P., Ghimire-Rijal, S., Sinnamon, R. A., Stemmler, T. L., Bruick, R. K., and Philpott, C. C. (2011) Activation of the HIF prolyl hydroxylase by the iron chaperones PCBP1 and PCBP2. *Cell Metab. 14*, 647–57.

(78) Philpott, C. C. (2012) Coming into view: eukaryotic iron chaperones and intracellular iron delivery. *J. Biol. Chem. 287*, 13518–23.

# CHAPTER 2

# MEASUREMENT OF METAL-BINDING PROPERTIES OF HISTONE DEACETYLASE 8 USING FLUORESCEIN-SUBEROYLANILIDE HYDROXAMIC ACID[1]

## INTRODUCTION

Posttranslational modifications are implicated in many human diseases, including cancer and neurodegenerative diseases.[1] Posttranslational acetylation / deacetylation of lysine side chains has been observed at more than 3500 sites in proteins, including histones,[2] and this modification regulates the biological activity of many these proteins. For example, acetylation and deacetylation correlate with the activation and deactivation, respectively, of transcriptional gene expression.[3] The status of acetylation of lysine residues is reversibly regulated by histone acetyltransferase (HAT) and histone deacetylase (HDAC) activity. HDACs are a family of 18 enzymes grouped into 4 classes. Class I comprises four HDAC family members, HDAC 1, 2, 3, and 8. They are expressed ubiquitously and generally display deacetylase activity toward histone substrates.[4] Class II includes HDAC 4, 7, 9, and 10 which generally have lower catalytic activity. HDAC11, the sole member of Class IV, lies at the boundary between the other two classes. Class I, II and IV are metalloenzymes with a largely conserved catalytic core, consistent with a



[1]This was a collaboration with Amit S. Pithadia and synthesis of flSAHA obtained by him is explicitly labeled within the chapter.

common catalytic mechanism.[5] All three classes are distinct from the sirtuin-family enzymes (class III) in the catalytic domain sequence and three-dimensional structure, and in the catalytic mechanism.[6]

High resolution crystal structures of the histone deacetylase-like protein from *Aquifex aeolicus*, human HDAC8, and *Schistosoma mansoni* HDAC8 have been solved illustrating a single α/β domain with a core eight-stranded β-sheet surrounded by eleven α-helices. The substrate binding surface is composed of nine loops and an 11 Å tunnel leading to the active site with a $HisAsp_2$ divalent metal binding site. These crystal structures were solved with zinc(II) as the active site metal ion, although little change in the structure of HDAC8 was observed with other metals (Co(II), Fe(II) and Mn(II)) bound to the active site.[7] Nonetheless, the enzymatic activity of HDAC8 varies with the active site metal ion: Co(II) > Fe(II) > Zn(II) > Ni(II).[8] This result suggests the possibility that either Fe(II) or Zn(II) could activate the enzyme *in vivo*. Recently several "Zn(II)-dependent" enzymes have been reclassified as "Fe(II)-dependent" enzymes, including peptide deformylase (PDF), LuxS and UDP-3-*O*-[(*R*)-3-hydroxymyristoyl]-N-acetylglucosamine deacetylase (LpxC).[9,10,11]

The affinity of HDAC8 for Zn(II) is much higher (5 pM) than the Fe(II) affinity (0.2 μM), as predicted based on the Lewis acidity of Zn(II) compared to Fe(II) and in accord with the Irving-Williams series of stability constants.[12] Although, the total cellular concentrations of zinc and iron are comparable at 0.1 – 0.2 mM in eukaryotes and Escherichia coli[13,14], the readily exchangeable (RE) metal ions differ significantly: $[Zn(II)]_{RE}$ is picomolar (10-400 pM),[15] and $[Fe(II)]_{RE}$ is micromolar (0.2-6 μM).[16,17] Therefore, based on thermodynamic considerations it is possible that HDACs could be activated by Fe(II) rather than Zn(II) in cells. The choice of iron is

intriguing given the redox reactivity of Fe(II)-bound HDAC8[8], suggesting the possibility of regulation of the activity of this enzyme by redox stress and/or Zn(II)/Fe(II) metal switching in cells. Evaluation of the kinetics of metal equilibration with HDAC8 will provide insight into the feasibility and biological relevance of these proposals.

However, previous research showed that HDAC8 could be bound to Fe(II) *in vivo*. First, the $k_{cat}/K_M$ value of HDAC8, stoichiometrically substituted with both metals, is greater for Fe(II). Next, iron was the most abundant metal in HDAC8-His, immediately following the affinity column purification. Also activity of cell-free lysate grown with iron supplementation is ~4-fold higher under anaerobic conditions compared to that under aerobic conditions.[8] Finally, the active site metal ligands of HDAC8 ($Asp_2His$) are unusual for a zinc-dependent hydrolase based on crystal structure of HDAC8 (Figure 1).[7] These findings suggest that HDACs could potentially be activated by Fe(II) rather than Zn(II). The choice of iron is intriguing given that the inherent instability of Fe(II) and that HDAC8 catalyzes a non-redox reaction.

**Figure 2.1** Promiscuity of metal selectivity in HDAC8

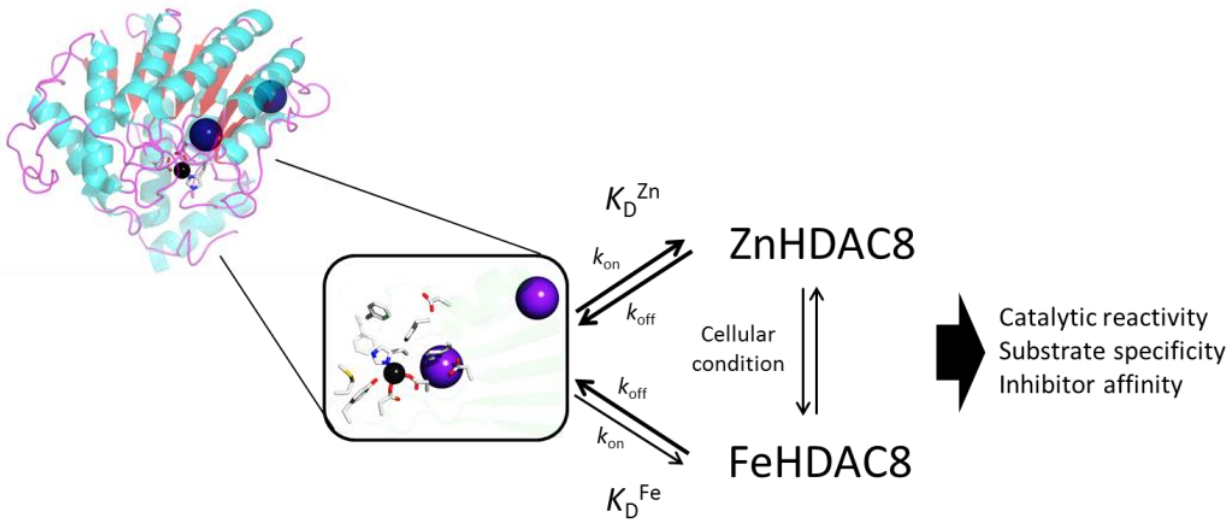

Additionally, there have been several examples of Zn(II)-dependent enzymes that have been reclassified as "Fe(II)- dependent" enzymes including peptide deformylase (PDF), LuxS, and UDP-3-*O*-[(*R*)-3-hydroxymyristoyl]-N-acetylglucosamine deacetylase (LpxC).[9,10,11] These metal constraints limit the utility of HDAC8, thus, a more detailed understanding of binding kinetics is needed to determine the native cofactor.

The crystal structure of HDAC8 also visualized two monovalent binding sites which are conserved in class I and II human HDACs.[18,19] Site 1 and 2 are located 7 Å and 21 Å, respectively, from the divalent metal ion binding site. These monovalent sites could be occupied with either $K^+$ or $Na^+$ depending on the cellular conditions. Previous studies revealed that the monovalent cation (MVC) occupying site 1 inhibits HDAC8 activity, whereas the MVC occupying site 2 increases activity by stabilizing the structure.[20] These monovalent cation binding sites may also play a role in regulating metal selectivity and equilibration kinetics.

To date, a number of assays of HDAC activity have been developed to measure substrate reactivity ($k_{cat}/K_M$), inhibitor potency ($K_i$)[21-22], and enzyme-coupled assay[23]. The most commonly used method is the Fluor de Lys (FdL) assay, which uses the commercially available peptide substrate (R-H-K(Ac)-K(Ac)-coumarin fluorophore) (BIOMOL) derived from the sequence of p53 that is acetylated at Lys381 and Lys382. In this assay, deacetylation is followed by cleavage of the coumarin fluorophore catalyzed trypsin, leading to a measurable change in fluorescence.[8]

However, this assay is not sufficiently rapid to measure the metal-binding kinetics of HDAC8. Recently, a fluorescence-based binding assay has been developed using coumarin-suberoylanilide hydroxamic acid (c-SAHA) as the fluorescent probe; the fluorescence is

quenched 50% upon binding to HDAC8.[24] However, this fluorophore is unsuitable for fluorescence polarization (FP) measurements. Therefore, we developed a FP-based binding assay using fluorescein-labeled SAHA (flSAHA) as a probe. This FP assay measures metal-binding in a simple 96-well format with ease and is ratiometric measurement with great precision. Furthermore, it is also applicable for high-throughput screening of inhibitors against HDAC8.

Here we use the flSAHA assay to demonstrate that despite the differences in the binding affinity of HDAC8 for Zn(II) and Fe(II), the dissociation rate constants are comparable at ~0.001 $s^{-1}$. These data demonstrate that metal binding to HDAC8 occurs in a two-step binding process and that metal selectivity is determined by the apparent slower association rate constant for Fe(II) compared to Zn(II). Furthermore, the metal dissociation kinetics are lowered by the binding of cations to either of the monovalent cation binding sites. These data demonstrate that the metal selectivity (Zn/Fe) occurs in the apparent association step and further implies that association of Fe(II) association is not a diffusion-controlled step. It further implies that Fe(II) binding to HDAC8 could be more than two step mechanism, which is binding followed by a conformational change. These data supports the proposal that HDAC8 could exist as an Fe(II)-dependent metalloenzyme as well as a Zn(II)-dependent enzyme depending on cellular factors.

## MATERIALS AND METHODS

### Materials

Unless specified, chemicals and supplies were purchased from Fisher. All chemicals were of the highest quality available. Ethylenediaminetetraacetic acid (EDTA) and $FeCl_2$ were purchased from Aldrich. Chromatography resins were purchased from GE Healthcare. To prevent

trace metal contamination, all plasticware was presoaked with 1 mM ethylenediaminetetraacetic acid (EDTA) and triple rinsed with Millipure $H_2O$. Plastic disposables, including pipet tips and microcentrifuge tubes, were certified trace metal-free (Corning Incorporated and Costar, respectively). Sodium hydroxide (Sigma, 99.999%) was used to titrate 3-(N-morpholino)propanesulfonic acid (MOPS) buffer (Ambion). Dialysis cassettes (Pierce) and syringes with needles were presoaked with 1 mM EDTA and extensively washed with Millipure $H_2O$.

**Expression and Purification of HDAC8**

Recombinant $His_6$-HDAC8 was expressed in BL21(DE3) *E. coli* transformed with pHD4 and purified as previously described[8] and concentrated to 2-12 mg/mL for metal exchange. Metal-free HDAC8 was generated by dialyzing purified HDAC8 twice into 500 mL of 25 mM MOPS (pH 7.0), 1 mM EDTA for 12-14 hr at 4 ℃, followed by buffer exchange into 25 mM MOPS (pH 7.5), 0.1 mM EDTA and finally 25 mM MOPS (pH 7.5) for 12-14 hr at 4 ℃. When necessary, anaerobic conditions were achieved using either the captair pyramid glove-bag filled with argon or nitrogen or an anaerobic chamber (Coy, Grass Lake, MI)

**Synthesis of flSAHA**

**1)** Synthesis of 2-(3,6-dihydroxy-9H-xanthen-9-yl)-5-(8-methoxy-8-oxooctanamido)benzoic acid: To a flame-dried flask equipped with stir bar and dry DMF (10 mL)

was added 5-fluoresceinamine (100 mg, 0.28 mmol) in one portion. To the stirring solution was added dry NEt3 (43 L, 0.31 mmol). The solution was allowed to stir at room temperature for one hour. Methyl-8-chloro-1-oxooctanate (40 L, 0.28 mmol) was then added to the solution drop wise and the resulting reaction mixture was stirred at 50 ℃ for 24 h. Upon completion the solvent was evaporated in vacuuo and the residue was dissolved in dichloromethane (20 mL). The product was washed with sat. $NaHCO_3$ (3 x 20 mL), brine (2 x 20 mL), dried over anhydrous $MgSO_4$, filtered and dried in vacuuo to yield an deep orange-yellow oil. The product was purified via silica gel chromatography (4% MeOH in $CH_2Cl_2$) and the resulting product was continually washed with hexanes to remove residual impurities. The final product was yielded as an orange oil (yield: 81 mg, 0.16 mmol, 56%). 1H NMR ($CD_3OD$, 400 MHz)/(ppm): 8.23 (d, J = 1.6 Hz, 1H), 7.73 (dd, J = 8.0, 2.0 Hz, 2H), 7.04 (d, J = 8.4 Hz, 2H), 6.56 (d, J = 2.4 Hz, 1H), 6.53 (d, J = 8.8 Hz, 2H), 6.43 (dd, J = 8.4, 2.4 Hz, 2H), 3.54 (s, 3H), 2.34 (t, J = 7.6, 2H), 2.24 (t, J = 7.6, 2H), 1.66-1.52 (m, 4H), 1.32-1.30 (m, 4H). $[M+H]^+$: calcd = 518.13, Found = 518.06

**2)** Synthesis of 2-(3,6-dihydroxy-9H-xanthen-9-yl)-5-(8-(hydroxyamino)-8-oxooctanamido)benzoic acid (flSAHA): Hydroxylamine hydrochloride (104 mg, 1.5 mmol) in methanol (10 mL) was combined with a solution of KOH (1.57 g, 28 mmol) in methanol (16 mL) and cooled to 0 ℃ and then filtered. Product was added to the filtrate from step 1 and slow addition of a solution of KOH (5 mg in 1 mL MeOH). The mixture was stirred at rt for 2 h and then refluxed at 65 ℃ for an additional 34 h. The reaction was quenched by the addition of cold water (15 mL), followed by drop wise addition of glacial acetic acid to until the pH reached approximately 7.0. A solid product precipitated and filtered, washed with water to remove

impurities and dried under vacuum to remove residual water. The resulting product was purified twice by silica gel chromatography (25% MeOH in $CH_2Cl_2$) and the final product was recrystallized in $CH_2Cl_2$ and hexanes to afford an orange solid (yield: 362 mg, 0.70 mmol, 75%). 1H NMR ($CD_3OD$, 400 MHz)/(ppm): 8.24 (d, J = 1.6 Hz, 1H), 7.73 (dd, J = 8.0, 2.0 Hz, 2H), 7.04 (d, J = 8.4 Hz, 2H), 6.56 (d, J = 2.4 Hz, 1H), 6.53 (d, J = 8.8 Hz, 2H), 6.40 (dd, J = 8.4, 2.4 Hz, 2H), 2.32 (t, J = 7.6, 2H), 2.24 (t, J = 7.6, 2H), 1.68-1.51 (m, 4H), 1.37-1.33 (m, 4H). $[M+H]^+$: calcd = 518.14, Found = 518.11

**Affinity of HDAC8 for flSAHA**

FP experiments were performed in a half-area black 96-well microplate (Corning Incorporation, #3686) and FP values were measured with excitation at 485 nm (30 nm bandpass) and emission at 535 nm (40 nm bandpass) using a TECAN Plate Reader. Binding experiments for determining the $K_D$ values of metal-bound HDAC8 for flSAHA included 50 nM flSAHA in assay buffer [20 mM HEPES (pH 8), 137mM NaCl, 3mM KCl] and FP was measured as HDAC8 (≤5 μM) was titrated into the reaction. The fluorescence intensity was corrected for dilution and background fluorescence. The value of $K_D$ for flSAHA was obtained by fitting a binding isotherm to the dependence of the FP signal on the concentration of HDAC8 (equation 1). In the equation, $Pf$ is the polarization of unbound flSAHA and *P*b is signal from fully bound flSAHA·HDAC8 complex.

$$\text{Equation 1 : } Y = Pf + (Pb - Pf) \times \frac{([L]+\{E\}+Kd) - \sqrt{([L]+[E]+Kd)^2 - 4[L][E]}}{2[E]}$$

**Kinetics for Binding flSAHA to HDAC8**

Fluorescence stopped-flow measurements were carried out on a model SF-2001 stopped-flow spectrofluorometer (KinTek Corp., Austin, TX) fitted with a 75W xenon arc lamp in two syringe mode. flSAHA was excited at 495 nm (slit width, 0.1-2 mm). flSAHA fluorescence emission was monitored using a long-pass filter (N500nm; Corion, LL-500-F). All kinetic traces were an average of four to six independent determinations. To measure the dissociation rate constant, flSAHA (0.1 μM) was preincubated with metal-bound HDAC8 (2 μM) for at least 30 min at RT in assay buffer. The reaction was initiated by mixing the HDAC8•flSAHA complex with an equal volume of unlabeled SAHA (final concentration of 20 μM) in assay buffer at 25℃ to trap HDAC8 and an increase in fluorescence intensity was measured. The dissociation rate constant was determined from a fit of a single exponential to the fluorescence signal (equation 2). To determine the association rate constant for HDAC8 binding flSAHA, flSAHA in assay buffer (50 nM final concentration) was mixed with an equal volume of metal-bound HDAC8 (final concentration of 1-6 μM) in assay buffer at 25 °C and a decrease in fluorescence measured. The apparent association rate constants were determined from a fit of a single/double exponential to the time-dependence of the fluorescence signal using KinTek software, and the reported errors are the asymptotic standard errors (equation 3 and 4). The dependence of the observed rate constants on the metal-bound HDAC8 concentration was analyzed using GraphPad Prism 4.0 software.

Equation 2 : $Y = A * \exp(-k_{off} * X) + c$

Equation 3 : $Y = A_1 * \exp(-k_{obs1} * X) + c$

Equation 4 : $Y = A_1 * \exp(-k_{obs1} * X) + A_2 * \exp(-k_{obs2} * X) + c$

**HDAC8 Metal Ion Binding Affinity**

For Zn(II) affinity measurements, apo-HDAC8 (1–200 μM) was incubated in a metal ion and pH buffer containing 1 mM nitrilotriacetic acid (NTA), 10 mM MOPS, pH 7, and 0–0.5 mM $Zn_{tot}$ (0–3.3 nM $Zn_{free}$) at 30 ℃ for 30 min in an anaerobic chamber.[25] Free and bound metal were separated by ultrafiltration, described above and the total metal concentration in each fraction was measured using Inductively coupled plasma mass spectrometry (ICP-MS). The concentration of $Zn_{free}$ in the metal buffers was calculated using the program MINEQL-(Environmental Research software). The value of $K_D$ Zn was obtained by fitting a binding isotherm to the dependence of the bound metal ion on the concentration of $Zn_{free}$ (equation 1). The affinity of HDAC8 for Fe(II) was measured by assaying catalytic activity in the presence of varying $Fe(II)_{free}$ concentrations in an anaerobic glove box in 1 mM NTA, 5 mM MOPS, pH 7, serving as both a pH and metal buffer. The affinity was not dependent on NTA concentration (data not shown). The assays contained 0–950 μM total iron (Sigma, 99.99%, $Fe(II)_{free}$ = 0–2.6 μM, as calculated by MINEQL-(Environmental Research Software)), and 1 μM HDAC8, in the presence of 3 mM KCl and 137 mM NaCl. The assay mixtures were incubated for 2 h on ice to pre-equilibrate in the anaerobic glove box. Assays were initiated by the addition of enzyme (200 nM final), and processed as described above. The affinity is not dependent on the concentration of metal buffer.

**Metal Ion Dissociation Rates Constants**

The first order rate constant for M(II) dissociation from HDAC8•M(II) complex was measured by the time-dependent loss of activity upon incubation with EDTA. HDAC8 reconstituted with stoichiometric Zn(II) or Fe(II) (final concentration = 1 μM) was diluted into assay buffer containing 1 mM EDTA at 30 ℃. At various times (0–60 min) an aliquot was diluted 10-fold into assay buffer containing 50 μM FdL substrate. The reactions were quenched by the addition of TSA followed by trypsin developer as described above. The initial rate for product formation was determined for each time point. The dissociation rate constant was determined from a single exponential fit to the decrease in the initial rates as a function of time (equation 2).

**Dependence of Metal Dissociation Rate constant**

For measurement of the dependence of Zn(II) $k_{off}$ on the concentration of MVC, reconstituted Zn(II)-HDAC8 was incubated with varying concentration of potassium and sodium ([KCl] = 1-100mM, [NaCl] = 100-2000mM) on ice for 1 h in 20mM HEPES, pH 8.0 and then at 25 ℃ for 4 min. The reaction was started by the addition of 1 mM EDTA. The metal dissociation rate constant was measured from the decrease in catalytic activity using the FdL assay and calculated from an equation 5 fit to the data, as described below.

Equation 5 : $k_{obs} = \frac{koff,1+\frac{koff,2*[MVC]}{K1}+\frac{koff,3*[MVC]2}{K1*K2}}{1+\frac{[MVC]}{K1}+\frac{[MVC]2}{K1*K2}}$

## RESULTS

### Design of a fluorescein-SAHA probe for HDAC8

Recently, the pan-HDAC inhibitor, SAHA, was derivatized with a coumarin fluorophore to form coumarin-suberoylanilide hydroxamic acid (c-SAHA)[24]. The fluorescence of this molecule is quenched 50% upon binding to HDAC8 and this property has been used to measure the binding kinetics and dissociation rate constants for HDAC inhibitors. However, the small change in the fluorescence intensity limits the utility of this approach for measuring the affinity of HDAC ligands. Therefore, we developed a similar small molecule probe, flSAHA (Figure 2 and 3), that employs a fluorescein derivative (6-aminofluorescein) to optimize its use as a fluorescence polarization probe and we have used this inhibitor to measure the metal binding affinity of HDAC8 for Zn(II) and Fe(II).

**Figure 2.2** Synthetic scheme of fluorescein-SAHA (flSAHA) and comparison of flSAHA derivatives.

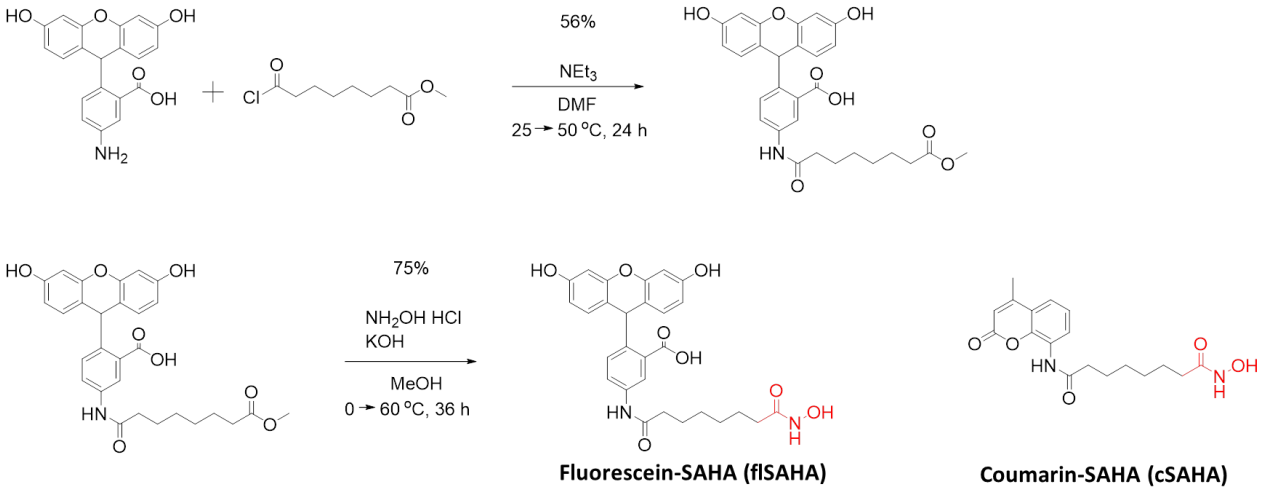

**Figure 2.3** Excitation and emission spectra of flSAHA. The spectra were taken in 10 mM HEPES (pH 8) containing 137 mM NaCl, 3mM KCl and 1 mM TCEP. [flSAHA] = 0.5 μM, (λex = 497 nm, λem = 515 nm). The ultraviolet–visible (UV–vis) spectra of flSAHA showed a prominent absorption band at 497 nm. It shows the fluorescence excitation and emission spectra of flSAHA (0.5 μM) in 10 mM HEPES buffer (pH 8) containing 137 mM NaCl, 3mM KCl and 1 mM TCEP.

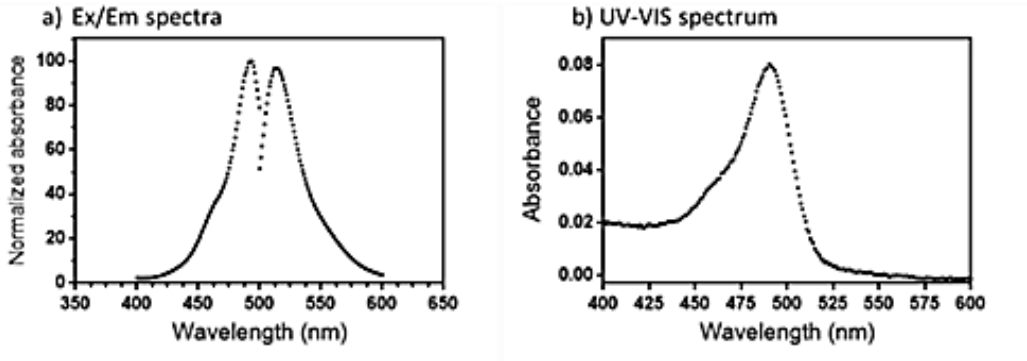


**Binding affinity of apo and metal-bound HDAC8 for fluorescein-SAHA**

To probe the affinity and selectivity of flSAHA for metal-bound HDAC8, we measured the fluorescence anisotropy of flSAHA upon titration with either apo or metal-bound HDAC8 under equilibrium conditions in an assay buffer (137 mM NaCl and 3 mM KCl, Figure 4). Upon addition of metal-bound HDAC8, the fluorescence anisotropy increases with a hyperbolic dependence on the HDAC8 concentration, as predicted for binding of a small molecule to the larger protein (MW = 42.5 kDa).

A single binding isotherm fit to these data allows calculation of an apparent dissociation constant of flSAHA ($K_D$,$^{app}$) for Zn-bound and Fe-bound HDAC8 of 0.3 ± 0.1 μM and 0.2 ± 0.08 μM respectively. The affinity of HDAC8 for flSAHA is enhanced by a bound divalent metal ion as little or no change in fluorescence anisotropy is observed upon titration with BSA or apo-HDAC8 ($K_D$,$^{app}$ > 5 μM assuming that the anisotropy endpoint is the same as flSAHA bound to

Zn-HDAC8). These results demonstrate that flSAHA only binds to metal-bound HDAC8 under the assay conditions. Therefore, flSAHA can be used as a probe to visualize metal-bound HDAC8 and to interrogate metal selectivity and affinity.

**Figure 2.4** Measurement of the binding affinity ($K_D$) of flSAHA with $Zn^{2+}$/$Fe^{2+}$ bound HDAC8 using FP assay. Total florescence change was adjust. Binding of ZnHDAC8 (•) and FeHDAC8 (■) to flSAHA measured by FP in Buffer (20 mM HEPES, pH8, 137 mM NaCl, 3 mM KCl, and 1mM TCEP), at 30˚C with 50 nM flSAHA. $K_D$ of ZnHDAC8 and FeHDAC8 to flSAHA are 0.4 ± 0.1 μM and 0.1 ± 0.1 μM, respectively.

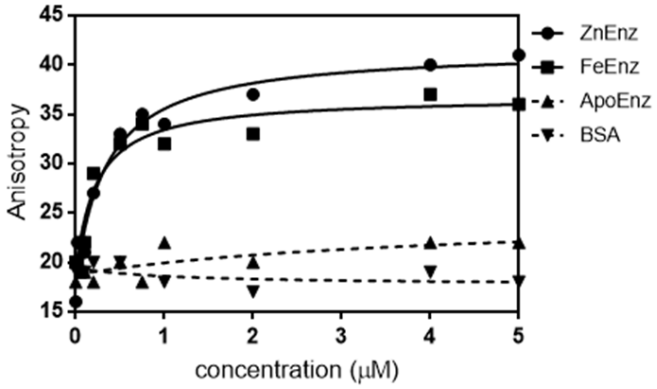


**Binding kinetics of fluorescein-labeled SAHA with metal-bound HDAC8**

The association kinetics for formation of the metal-bound HDAC8-flSAHA complex were assessed by mixing limiting flSAHA with excess metal-bound HDAC8 complex in a stopped-flow fluorescence spectrometer and measuring the time-dependent changes in fluorescence intensity. flSAHA exhibited a decrease in fluorescence over time at each metal-bound HDAC8 concentration tested, producing time courses that are best fit by a single exponential for Zn-HDAC8 and a double exponential for Fe-HDAC8 at 25 ℃ (Figure 5). Biphasic kinetic behavior in ligand binding can be explained by mechanisms that include a

conformational change of the macromolecule either before or after the bimolecular collision event (Scheme 1).[26] The rate constant for both of the phases increases linearly with the concentration of Zn(II)-HDAC8 or Fe(II)-HDAC8, suggesting a bimolecular collision event with an apparent association rate constant for flSAHA ($k_{obs,1}$ in Equation 3 and 4 for Zn and Fe) of 4 x $10^5$ $M^{-1}sec^{-1}$ and 1 x $10^5$ $M^{-1}sec^{-1}$, respectively.

**Figure 2.5** Measurement of the association rate constant ($k_{on}$) of flSAHA with Zn(II)/Fe(II) bound HDAC8 using stopped-flow kinetics. Dependence of $k_{obs}$ on the concentration of Zn-HDAC8 and Fe-HDAC8. The linear least-squares fits to the dependence of $k_{obs}$ on the [$M^{2+}$-HDAC8] yield a slope of (4.1 ± 0.5 ) x $10^5$ $M^{-1}s^{-1}$ for Zn-HDAC8 and (1.0 ± 0.3 ) x $10^5$ $M^{-1}s^{-1}$ for Fe-HDAC8.

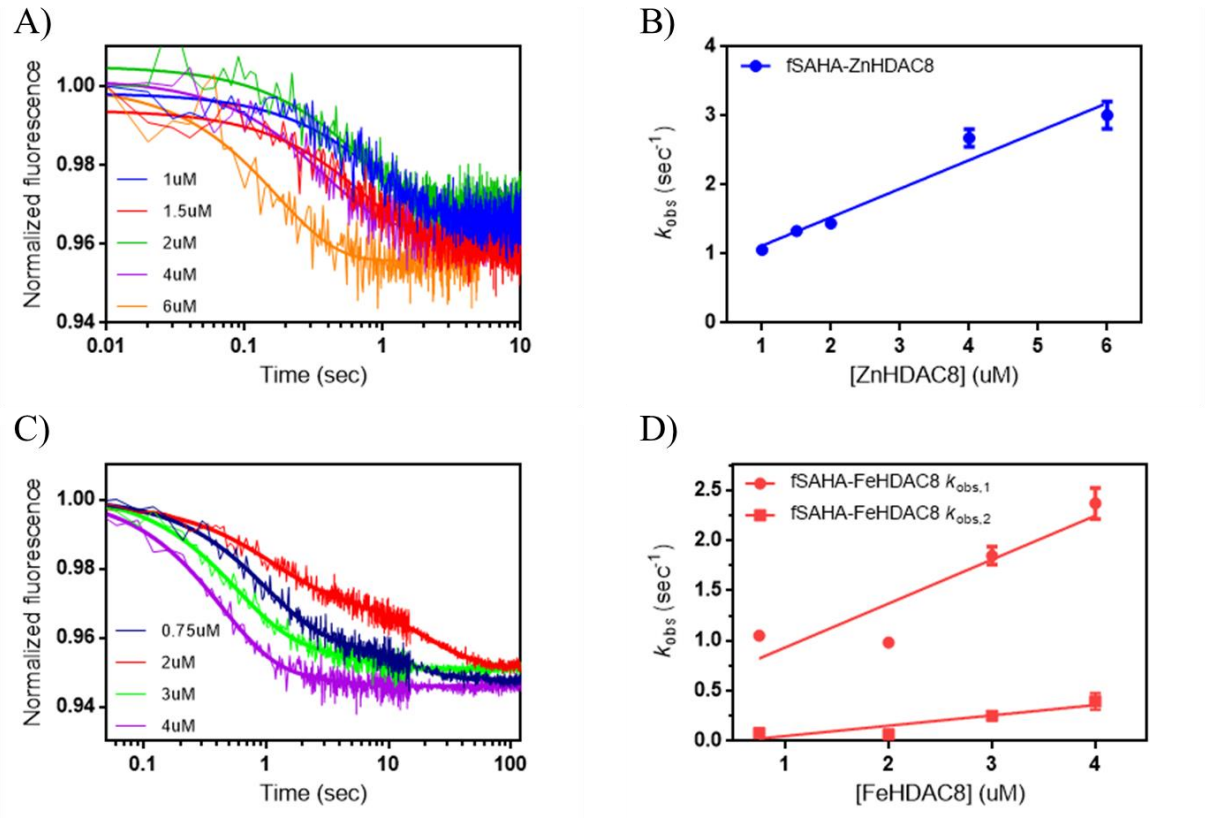

**Scheme 1.** Minimal kinetic mechanism of metal binding to HDAC8

$$E + M^{2+} \underset{k_2}{\overset{k_1}{\rightleftharpoons}} EM^{2+} \underset{k_4}{\overset{k_3}{\rightleftharpoons}} E^{*}M^{2+}$$

The extrapolation of the apparent bimolecular rate constant to the y-axis for flSAHA binding to Zn(II)-HDAC8 is 0.7 $sec^{-1}$, approximating the dissociation rate constant for flSAHA (Equation 3). For Fe(II)-bound HDAC8, the y-intercept is too small to determine (< 0.1 $sec^{-1}$). Assuming a single binding step, a value for the dissociation constant, $K_D$, for flSAHA complexed with Zn-HDAC8 can be estimated from the equilibration rate constants: $K_D = k_{off} / k_{on}$ = 0.6 $s^{-1}$ / 8 x $10^5$ $M^{-1}s^{-1}$ = 0.9 μM. This value is about 2-fold higher than the measured equilibrium value for $K_D$ (Table 1) suggesting that the assumption of a single biomolecular step is reasonable. The biphasic kinetics demonstrate that this assumption cannot be true for Fe-HDAC8.

**Table 2.1** Kinetic parameters of flSAHA for Zn(II) / Fe(II)-HDAC8

| | $K_D^{flSAHA}$ (μM) | $k_{off}$ ($sec^{-1}$) | $k_{on}$ ($M^{-1}s^{-1}$) |
|---|---|---|---|
| Zn(II)-HDAC8 | 0.4 ± 0.01 | 0.6 ± 0.06 | 4 x $10^5$ |
| Fe(II)-HDAC8 | 0.1 ± 0.01 | 0.04 ± 0.0005 | 1 x $10^5$ |

**Determination of rate constant for dissociation of flSAHA complexed with HDAC8**

To measure the dissociation rate constant for flSAHA, the HDAC8•flSAHA was mixed with excess SAHA to bind to HDAC8 to form the HDAC8•SAHA complex rapidly upon dissociation of flSAHA. The replacement of SAHA for flSAHA bound to HDAC8 leads to an

increase in the fluorescent intensity ($\lambda_{ex}$ = 495 nm), allowing measurement of the flSAHA dissociation rate constant.

The time-dependent increase in fluorescence observed after mixing metal-bound HDAC8•flSAHA complex with 20 μM SAHA in the stopped flow fluorometer (Figure 6) is well-described by a single exponential with flSAHA dissociation rate constants of 0.6 ± 0.06 and 0.04 ± 0.0005 $s^{-1}$ for Zn-bound and Fe-bound HDAC8, respectively. These rate constants are unchanged when the concentration of SAHA is increased by two-fold (data not shown), demonstrating that trapping of HDAC8 by SAHA is rapid and therefore the measured rate constants reflect the dissociation rate constant of flSAHA from the HDAC8 complex. These values for $k_{off}$ are consistent with those calculated from the concentration dependence of the association kinetics.

**Figure 2.6** Measurement of the dissociation rate constant ($k_{off}$) of flSAHA with Zn(II)/Fe(II) bound HDAC8 using a stopped-flow assay. The dissociation of flSAHA with the metal-bound HDAC8 was triggered on mixing of the HDAC8–flSAHA complex with an excessive concentration of SAHA. The concentrations of the individual species in the stopped-flow syringes were as follows: [$M^{2+}$-HDAC8] = 2 μM + [flSAHA] = 0.1 μM (syringe 1) versus [SAHA] = 20 μM (syringe 2). The solid lines are the best fit of the experimental data according to the single exponential rate equation for a dissociation off-rate constant. a) $k_{off}$ of flSAHA with Zn-HDAC8. b) $k_{off}$ of flSAHA with Fe-HDAC8

a) ZnHDAC8

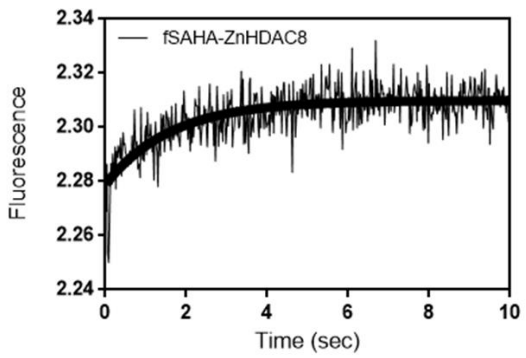


b) FeHDAC8

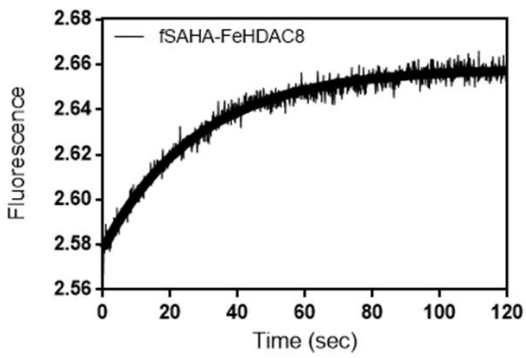

**Metal binding properties of HDAC8**

Zn(II) and Fe(II) are the most likely native cofactors for HDAC8 since they exist in high amounts in the cell. To determine the metal binding affinity of HDAC8, metal binding was coupled to the binding of flSAHA. The fluorescence anisotropy of flSAHA in the presence of HDAC8 was measured as a function of free metal concentration in nitrilotriacetate (NTA)-buffered solutions under equilibrium conditions. The fluorescence anisotropy increased with a hyperbolic dependence on the free metal concentration (Figure 7) while the total fluorescence intensity remained constant (data not shown). Dissociation constants ($K_D$) were obtained from fitting a single binding isotherm to these data ($K_{D,Zn}$ = 6 ± 1 pM and $K_{D,Fe}$ = 0.2 ± 0.1 μM), demonstrating that HDAC8 has a significantly higher affinity for Zn(II) than Fe(II).

**Figure 2.7** Measurement of metal affinity of HDAC8 by the FdL activity assay and the FP assay. The activity and anisotropy of HDAC8 was assayed in the presence of increasing concentrations of free Zn(II) (circles) or Fe(II) (squares) using a 1 mM NTA metal buffer. a) The relative initial velocity ($v_{obs}/v_{max}$) is plotted to simplify the graph. b) Anisotropy is plotted as a function of free metal concentration. The metal dissociation constant was determined from fitting a single binding isotherm (eq 3) to these data.

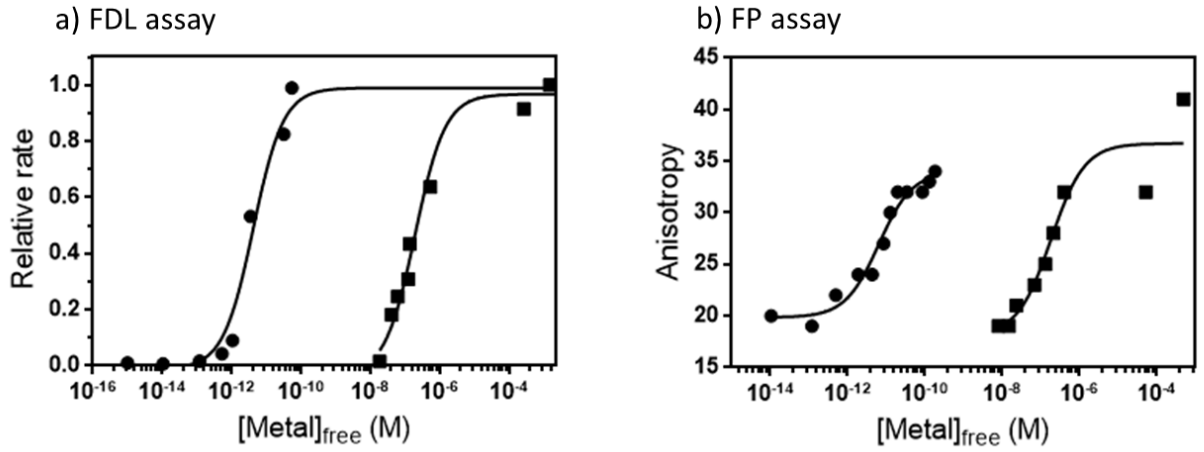

To validate the FP method for measuring metal affinity, the binding affinities of HDAC8 for Zn(II) and Fe(II) were measured from the metal-dependent activation of catalytic activity (Figure 7, $K_D$ = 5 ± 1 pM for Zn(II) and $K_D$ = 0.2 ± 0.03 μM for Fe(II)). These values are also slightly lower than previously measured metal affinities for HDAC8.[7] The higher Zn(II) affinity is consistent with the higher Lewis acidity of Zn(II).[27]

The rate constants for dissociation of HDAC8-bound metal ions were also determined from the time-dependent decrease in activity upon dilution of the enzyme into the high affinity metal chelator, EDTA. The measured rate constants are not dependent on the concentration of EDTA (data not shown), indicating that the metal chelator is trapping the metals after dissociation from the enzyme. These measurements revealed that the rate constants for dissociation ($k_{off}$) of Zn(II) and Fe(II) from HDAC8 are 0.0006 ± 0.0001 and 0.001 ± 0.0002 $s^{-1}$, respectively (Figure 8). The similarity in the dissociation rate constants for Zn(II) and Fe(II) is unexpected given the significantly different affinity of HDAC8 for these metal ions.

**Figure 2.8** Measurement of the metal dissociation rate constant ($k_{off}$) from the HDAC8•Me(II) complex using the FdL assay. The $k_{off}$ values for HDAC8-bound metal ions were determined from the time-dependent decrease in activity measured using the FdL assay after dilution of the enzyme into 1 mM EDTA in 20 mM HEPES, pH8, 3 mM KCl, 137 mM NaCl..

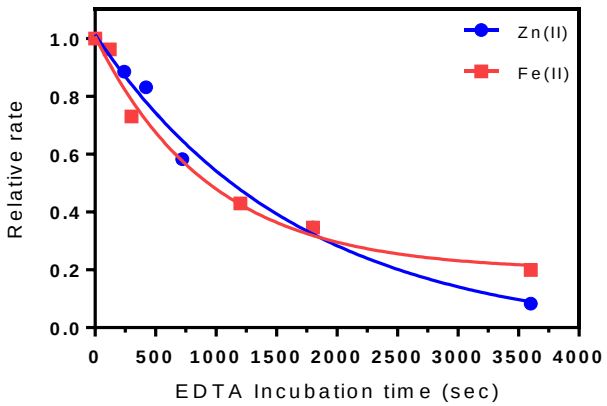

Therefore, the discrimination between the two metal ions originates mainly from the apparent association rate constants that are estimated assuming a one-step binding mechanism from the $K_D$ and $k_{off}$ values ($k_{on} = k_{off} / K_D$) as 1 x $10^8$ $M^{-1}s^{-1}$ (Zn(II)) and 5 x $10^3$ $M^{-1}s^{-1}$ (Fe(II)). The calculated association rate constant for zinc is near the diffusion-controlled limit, consistent with a single-step binding mechanism. However, the association rate constant for Fe(II) is significantly lower than the diffusion-limit suggesting a two-step binding mechanism, perhaps formation of an initial encounter complex followed by a unimolecular conformational rearrangement.

**KCl and NaCl Modulate metal-binding property of HDAC8**

To evaluate whether monovalent cations bound to HDAC8 regulate the metal binding kinetics, the HDAC8 metal affinity and metal dissociation rate constants as a function of the concentration of either $K^+$ or $Na^+$ was measured. As the monovalent cation concentration increases, the observed value of $k_{off}$ for Me(II) decreases significantly until it reaches a plateau near 100 mM KCl or 1500 mM NaCl (Figure 9). Data were fit assuming that two non-cooperative monovalent cations bind to and decrease the metal dissociation rate constant (equation 4). These data indicate that binding potassium or sodium to HDAC8 decreases the Me(II) dissociation rate constant by 30-fold and 15-fold, respectively. Previous research demonstrated that one bound MVC activates catalytic activity ($K_{1/2}$ = 3.4 mM for $K^+$), whereas the second, weaker- binding MVC ($K_{1/2}$ = 26 mM for $K^+$) decreases catalytic activity.[20]

**Figure 2.9** Dependence of metal dissociation rate constant ($k_{off}$) from the HDAC8•Me(II) complex on the concentration of monovalent cations. The rate constants were determined as described in the legend of Figure 8. It show the dependence of $k_{off}$ on the concentration of KCl (circle) and NaCl (triangle), respectively. The solid line is a fit of equation 5 to the data.

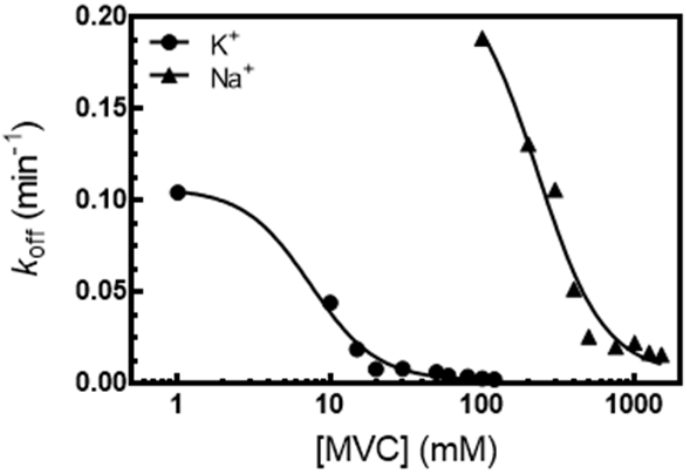


These data also suggest that monovalent cations increase the affinity of HDAC8 for Zn(II) and that the enzyme with two bound potassium ions has the highest affinity for Zn(II). Therefore, Zn(II) had the highest affinity for the MVC-occupied form of HDAC8 ($EK_2$) with the affinity increasing at least up to 15-fold.

## DISCUSSION

Here, we developed a new fluorescent probe that can be utilized in a FP assay to measure the kinetics and thermodynamics of metal binding to HDAC8. With this assay, the metal binding kinetics of HDAC8 have been determined for the first time. Notably, this FP assay can be used to measure the metal binding kinetics of HDAC8 variants and other HDAC isozymes. This assay could also be useful as a high-throughput screen for HDAC inhibitors.

flSAHA binds to metal-bound HDAC8 in the submicromolar range, which is comparable to that of cSAHA. This is reasonable since both SAHA analogs contain the same hydroxamate moiety chelates the metal ion in active site and an aliphatic chain that can be accommodated in the hydrophobic tunnel of HDAC8.[18] Additionally, flSAHA displays similar $K_D$ values for the Zn(II)- and Fe(II)-bound HDAC8 forms, as previously observed for SAHA.[8] Apparent association rate constants of flSAHA to metal-bound HDAC8 were measured as 4 x $10^5$ $M^{-1}s^{-1}$ and 1 x $10^5$ $M^{-1}s^{-1}$ for Zn(II)- and Fe(II)-HDAC8, respectively. These association rate constants are lower than the diffusion-limit and biphasic binding kinetics are observed for Fe(II)-HDAC8 suggesting a two-step binding mechanism. One mechanism consistent with these data is the formation of an encounter complex followed by a slow conformational change. Dissociation rate constants ($k_{off}$) of flSAHA from metal-bound HDAC8 were also determined using stopped-flow spectrometry to be 0.7 $s^{-1}$ and 0.04 $s^{-1}$ for Zn(II)- and Fe(II)-HDAC8, respectively.

By using flSAHA, we have measured the metal binding thermodynamics and kinetics of HDAC8. $K_D$ measurements of dissociation of metal from the HDAC8•Me(II) complex using the flSAHA FP assay were comparable to values determined from metal-dependent activation of catalytic activity.[7] The binding affinity of Zn(II) to HDAC8 is in the picomolar range while the Fe(II) affinity is in the micromolar range, a difference of $10^5$-fold comparable to previous measurements.[7] Unexpectedly, the dissociation rate constants ($k_{off}$) of both metals (0.001 $s^{-1}$) are similar, despite the difference in the binding affinities. This result indicates that metal selectivity primarily occurs in the apparent association rate constant, estimated as $10^8$ and $10^3$ $M^{-1}s^{-1}$ for Zn(II) and Fe(II), respectively (Table 2). Importantly, these data show that apparent association rate constant for Fe(II) is much lower than that of Zn(II). The Zn(II) association rate step is likely diffusion-controlled, while the Fe(II) association is likely a two-step binding mechanism

(Scheme 1).

**Table 2.2** Kinetic parameters of metal for HDAC8

| | $K_D^{metal}$ | $k_{off}$ ($sec^{-1}$) | $k_{on}$ ($M^{-1}s^{-1}$) |
|---|---|---|---|
| Zn(II)-HDAC8 | 5 ± 1 pM | 0.001 ± 0.0001 | 1 x $10^8$ |
| Fe(II)-HDAC8 | 0.2 ± 0.03 μM | 0.001 ± 0.0002 | 5 x $10^3$ |

Previously, metal association kinetics of human carbonic anhydrase II (CAII) were determined with association rate constants for Zn(II) and Cu(II) of $10^4$–$10^5$ and $10^9$ $M^{-1}s^{-1}$, respectively.[28] Analysis of the zinc binding kinetics of CAII mutants suggests a two-step binding mechanism. In the first step zinc binds to CAII at near diffusion-controlled rates to form an initial complex with two protein ligands followed by a second slower step that includes exchange of inner-sphere water molecules with the third protein ligand.[28] This may be a paradigm for two-step metal binding to proteins, including HDAC8. Metal binding kinetics similar to HDAC8 have been measured for another deacetylase, LpxC, where the association rate constants for Zn(II) and Fe(II) are $10^6$ and $10^4$ $M^{-1}s^{-1}$, respectively, also suggesting a two-step binding mechanism for Fe(II) association.[11] In this case, the physiological metal in *E. coli* is Fe(II) under most conditions, although LpxC binds Zn(II) *in vivo* when Fe(II) concentrations are very low. In LpxC and CAII, the physiological metal ion (Fe(II) and Zn(II), respectively) has a low association rate constant, leading to a very low dissociation rate constant. This may be important for metal selectivity *in vivo*, decreasing kinetic traps for the higher affinity, but incorrect metal ion. Furthermore, the similarities between the *in vitro* metal binding kinetics of LpxC and HDAC8 lead to the hypothesis that HDAC8 might behave similarly to LpxC in cells

by being activated by Fe(II) undermost conditions but switches to the Zn(II) bound enzyme at high cellular zinc..[11]

Two bound monovalent cations are observed in the crystal structures of HDAC8.[18,19] Subsequently, it was determined that HDAC8 is activated by low concentrations of KCl and NaCl, and inhibited at higher concentrations of these MVCs. Inhibition is proposed to occur by binding to MVC site1 (nearest the metal site) which depresses the p*Ka* of His-142 near the active site.[20] In this work, we investigated the regulation of the metal binding kinetics by monovalent cations by measuring the metal dissociation rate constant as a function of MVC concentration. This is consistent with previous finding that the occupancy of MVC2 site (distal from the metal site) stabilizes an active HDAC8

HDAC8 is activated by a number of divalent metal ions, including zinc, iron(II), nickel(II), and cobalt(II) *in vitro*[8]. The use of a Fe(II) as the physiological catalytic metal ion has been previously demonstrated for multiple metallohydrolases, such as peptide deformylase, methionyl aminopeptidase, LuxS, γ-carbonic anhydrase, cytosine deaminase, and atrazine chlorohydrolase.[9,10,29,30],[31],[32] These enzymes were originally misidentified as a Zn(II)-metalloenzyme due to oxidation of the Fe(II) to Fe(III), dissociation of this metal and re-binding of Zn(II) upon purification under aerobic conditions. Additionally, measurement of the native activity under anaerobic condition is difficult. Previous data show that the HDAC8 is likely another non-heme Fe(II) hydrolase that was previously identified as a zinc metalloenzyme.[8] HDAC8 may use Fe(II) as a metal cofactor under many physiological conditions, but the Fe(II) metal ion may exchange with zinc as a function of cellular condition, such as oxidative stress, increased cellular zinc concentration, or activity of a metallochaperones..

## REFERENCES


(1) Strahl, B. D., and Allis, C. D. (2000) The language of covalent histone modifications. *Nature 403*, 41–45.

(2) Choudhary, C., Kumar, C., Gnad, F., Nielsen, M. L., Rehman, M., Walther, T. C., Olsen, J. V, and Mann, M. (2009) Lysine acetylation targets protein complexes and co-regulates major cellular functions. *Science (80-. ). 325*, 834–40.

(3) Backs, J., and Olson, E. N. (2006) Control of cardiac growth by histone acetylation/deacetylation. *Circ. Res. 98*, 15–24.

(4) Gregoretti, I. V, Lee, Y.-M., and Goodson, H. V. (2004) Molecular evolution of the histone deacetylase family: functional implications of phylogenetic analysis. *J. Mol. Biol. 338*, 17–31.

(5) Saadi Khochbin , André Verdel, C. L. and. (2001) Functional significance of histone deacetylase diversity 162–166.

(6) Blander, G., and Guarente, L. (2004) The Sir2 family of protein deacetylases. *Annu. Rev. Biochem. 73*, 417–35.

(7) Dowling, D. P., Gattis, S. G., Fierke, C. A., and Christianson, D. W. (2010) Structures of metal-substituted human histone deacetylase 8 provide mechanistic inferences on biological function . *Biochemistry 49*, 5048–56.

(8) Gantt, S. L., Gattis, S. G., and Fierke, C. A. (2006) Catalytic activity and inhibition of human histone deacetylase 8 is dependent on the identity of the active site metal ion. *Biochemistry 45*, 6170–8.

(9) Cell, C., and Peg, S. (1998) Iron center, substrate recognition and mechanism of peptide deformylase. *Nat. Struct. Biol. 132*, 1053–1058.

(10) Zhu, J., Dizin, E., Hu, X., Wavreille, A.-S., Park, J., and Pei, D. (2003) S-Ribosylhomocysteinase (LuxS) Is a Mononuclear Iron Protein. *Biochemistry 42*, 4717–26.

(11) Gattis, S. G., Hernick, M., and Fierke, C. A. (2010) Active site metal ion in UDP-3-O-((R)-3-hydroxymyristoyl)-N-acetylglucosamine deacetylase (LpxC) switches between Fe(II) and Zn(II) depending on cellular conditions. *J. Biol. Chem. 285*, 33788–33796.

(12) Irving, H. Williams, R. J. P. (1948) Order of stability of metal complexes. *Nature 162*, 746–747.

(13) Outten, C. E., and O'Halloran, T. V. (2001) Femtomolar sensitivity of metalloregulatory proteins controlling zinc homeostasis. *Science (80-. ). 292*, 2488–92.

(14) Wang, D., Hosteen, O., and Fierke, C. A. (2012) ZntR-mediated transcription of zntA responds to nanomolar intracellular free zinc. *J. Inorg. Biochem. 111*, 173–81.

(15) Vinkenborg, J. L., Nicolson, T. J., Bellomo, E. a, Koay, M. S., Rutter, G. a, and Merkx, M. (2009) Genetically encoded FRET sensors to monitor intracellular Zn2+ homeostasis. *Nat. Methods 6*, 737–40.

(16) Petrat, F., Groot, H. D. E., and Rauen, U. (2001) Subcellular distribution of chelatable iron: a laser scanning microscopic study in isolated hepatocytes and liver endothelial cells. *Biochem. J 69*, 61–69.

(17) Meguro R, Asano Y, Odagiri S, Li C, Iwatsuki H, S. K. (2007) Nonheme-iron histochemistry for light and electron microscopy - a historical, theoretical and technical review.pdf. *Arch Histol Cytol* 1–19.

(18) Vannini, A., Volpari, C., Filocamo, G., Casavola, E. C., Brunetti, M., Renzoni, D., Chakravarty, P., Paolini, C., De Francesco, R., Gallinari, P., Steinkühler, C., and Di Marco, S. (2004) Crystal structure of a eukaryotic zinc-dependent histone deacetylase, human HDAC8, complexed with a hydroxamic acid inhibitor. *Proc. Natl. Acad. Sci. U. S. A. 101*, 15064–15069.

(19) Somoza, J. R., Skene, R. J., Katz, B. a, Mol, C., Ho, J. D., Jennings, A. J., Luong, C., Arvai, A., Buggy, J. J., Chi, E., Tang, J., Sang, B.-C., Verner, E., Wynands, R., Leahy, E. M., Dougan, D. R., Snell, G., Navre, M., Knuth, M. W., Swanson, R. V, McRee, D. E., and Tari, L. W. (2004) Structural snapshots of human HDAC8 provide insights into the class I histone deacetylases. *Structure 12*, 1325–34.

(20) Gantt, S. L., Joseph, C. G., and Fierke, C. A. (2010) Activation and inhibition of histone deacetylase 8 by monovalent cations. *J. Biol. Chem. 285*, 6036–43.

(21) Mazitschek, R., Patel, V., Wirth, D. F., and Clardy, J. (2008) Development of a fluorescence polarization based assay for histone deacetylase ligand discovery. *Bioorg. Med. Chem. Lett. 18*, 2809–12.

(22) Wegener, D., Wirsching, F., Riester, D., and Schwienhorst, A. (2003) A Fluorogenic Histone Deacetylase Assay Well Suited for High-Throughput Activity Screening. *Chem. Biol. 10*, 61–68.

(23) Wolfson, N. A., Pitcairn, C. A., Sullivan, E. D., Joseph, C. G., and Fierke, C. A. (2014) An enzyme-coupled assay measuring acetate production for profiling histone deacetylase specificity. *Anal. Biochem. 456*, 61–9.

(24) Singh, R. K., Mandal, T., Balasubramanian, N., Cook, G., and Srivastava, D. K. (2011) Coumarin-suberoylanilide hydroxamic acid as a fluorescent probe for determining binding affinities and off-rates of histone deacetylase inhibitors. *Anal. Biochem. 408*, 309–15.

(25) McCall, K. A., and Fierke, C. A. (2004) Probing determinants of the metal ion selectivity in carbonic anhydrase using mutagenesis. *Biochemistry 43*, 3979–3986.

(26) Hsieh, J., and Fierke, C. A. (2009) Conformational change in the Bacillus subtilis RNase P holoenzyme – pre-tRNA complex enhances substrate affinity and limits cleavage rate. *RNA 15*, 1565–1577.

(27) Patent, U. S., and Pearson, R. G. (1963) Hard and Soft Acids and Bases. *J. Am. Chem. Soc. 265*, 3533–3539.

(28) Huang, C. C., Lesburg, C. A., Kiefer, L. L., Fierke, C. A., and Christianson, D. W. (1996) Reversal of the hydrogen bond to zinc ligand histidine-119 dramatically diminishes catalysis and enhances metal equilibration kinetics in carbonic anhydrase II. *Biochemistry 35*, 3439–3446.

(29) Tripp, B. C., Iii, C. B. B., Krebs, C., Ferry, J. G., and Cruz, F. (2004) A role for iron in an ancient carbonic anhydrase. *J. Biol. Chem. 279*, 21677–21679.

(30) D'souza, V. M., and Holz, R. C. (1999) The methionyl aminopeptidase from Escherichia coli can function as an iron(II) enzyme. *Biochemistry 38*, 11079–11085.

(31) Porter, D. J. T., Austiny, E. A., and Carolina, N. (1993) Cytosine deaminase : The roles of divalent metal ions in catalysis. *J. Biol. Chem. 268*, 24005–24011.

(32) Seffernick, J. L., McTavish, H., Osborne, J. P., de Souza, M. L., Sadowsky, M. J., and Wackett, L. P. (2002) Atrazine chlorohydrolase from Pseudomonas sp. strain ADP is a metalloenzyme. *Biochemistry 41*, 14430–14437.

# CHAPTER 3

# SECOND SHELL RESIDUES MODULATE THE METAL SELECTIVITY AND REACTIVITY OF HISTONE DEACETYLASE 8[1]

## INTRODUCTION

Histone deacetylases (HDACs) catalyze the hydrolysis of the ε-*N*-acetyl group from lysine residues that were previously acetylated by histone acetyltransferases. To date, more than 4500 acetylated lysine residues have been identified in human proteins and this posttranslational modification is proposed to regulate multiple cellular processes, including DNA replication, DNA damage and repair, or transcription factors.[1] Among 18 human HDACs, HDAC8 is a member of the class I metal-dependent histone deacetylases and has been shown by immunochemistry to localize mainly with the cytoskeleton in smooth muscle cells.[2] HDAC8 was also found to be located in nucleus of NIH3T327 and HEK293 cells.[3,4] A recent study has also shown that a loss of function mutation in HDAC8 leads to increased SMC3 acetylation which results in Cornelia de Lange syndrome (CdLS), a developmental disorder.[5]

HDAC8 was originally characterized as a $Zn^{2+}$-dependent metalloenzymes.[6] However, subsequent studies have shown that the catalytic efficiency ($k_{cat}/K_M$) of HDAC8 with peptides is enhanced with $Co^{2+}$ or $Fe^{2+}$ as the active site metal ion compared with $Zn^{2+}$. HDAC8 has significantly higher affinity for $Zn^{2+}$ ($K_D$ = 5 ± 1 pM) than $Fe^{2+}$ ($K_D$ = 0.2 ± 0.03 μM) with affinities that are comparable to estimates of the readily exchangeable metal concentrations in cells.[7] Previous measurements in eukaryotic cells indicate that the concentration of readily



[1]The contents of this chapter are adapted and reproduced from a manuscript by Byungchul Kim and Carol A .Fierke.

exchangeable Zn ($[Zn^{2+}]_{free}$ ~10-400 pM)[8] is also orders of magnitude lower than the concentration of readily exchangeable Fe, where $[Fe^{2+}]_{free}$ ~0.2-6 μM.[4,9] These data suggest that either $Zn^{2+}$ or $Fe^{2+}$ could be the native metal cofactor in cells[10] leading to a number of biologically relevant implications. First, the activity and/or substrate selectivity of HDAC8 could be regulated by a metal switching mechanism in response to changes in the readily exchangeable concentrations of $Zn^{2+}$ and $Fe^{2+}$ depending on cellular conditions, such as oxidative stress.[11] Second, the cellular metal cofactor could affect inhibitory affinity, as previously observed for other enzymes, such as methionine aminopeptidase.[12] Therefore, HDAC inhibitors should be screened using the native metal cofactor. Identification of the determinants of metal selectivity in HDAC8 *in vitro* could provide insight into metal specificity *in vivo*.

For cells grown with iron supplementation, the HDAC8 activity is ~4-fold larger when the cells are lysed and assayed under anaerobic conditions compared to that under aerobic conditions.[10] This increase in activity is consistent with the ratio of activities of $Fe^{2+}$- and $Zn^{2+}$-substituted HDAC8s. This evidence suggests that $Fe^{2+}$-HDAC is the major species when recombinantly expressed in *E. coli*.

The metal selectivity of proteins is governed both by direct interactions with side chains that coordinate the metal ion and indirectly by the protein structure surrounding the metal binding site.[13] Carbonic anhydrase II (CAII) is a prototypical Zn(II)-metalloenzyme, where the role of conserved structural features of metal binding sites in determining metal ion affinity and specificity has been probed.[14–21] In CAII three conserved features regulate the properties of the metal ion binding site (Figure 1). First, the first direct ligands (H94, H96, and H119) and a hydroxide ion coordinate to zinc in a tetrahedral array. Second, indirect second ligands (Q92, E117, the backbone carbonyl of N244 and T199) form hydrogen bonds to the zinc-coordinated

histidine and hydroxide moieties. These second-shell interactions enhance the basicity of the direct histidine ligands and allow the positioning of the direct ligands for optimal metal

**Figure 3.1** Comparison of the active site of CAII and HDAC8. **A)** Structure of the active site of wild-type carbonic anhydrase II (CAII) taken from the crystal structure (PDB ID: 3KS3). Zinc coordinated to three imidazole ligands, H94, H96, and H119 in the first shell. H94 and H119 donate a hydrogen bond to the side chains of Q92, E117, respectively. H96 donates a hydrogen bond to the backbone carbonyl oxygen of N244. Direct metal coordination interactions are indicated by black dashed lines. F93, F95, and W97 that form an aromatic cluster underneath the zinc site are also depicted. **B)** Structure of the active site of wild-type HDAC8 taken from the crystal structure (PDB ID: 2V5W). D178, H180, and D267 are coordinating to the metal. Hydrophobic shell residues F207, F208, and M274 are located on the near H180 at the active site. The zinc ion appears as a large sphere.

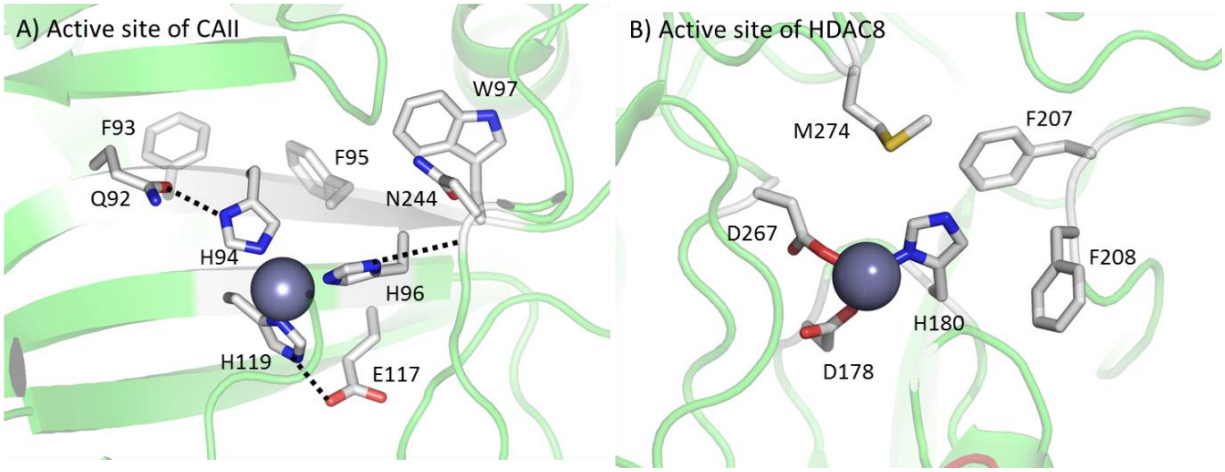


coordination.[14,22,15] Finally, hydrophobic residues (F93, F95, and W97) anchor the β-strand containing H94 and H96 in the hydrophobic core of the enzyme. This hydrophobic shell is proposed to enhance protein-metal affinity by both positioning the ligands and establishing a metal site environment with a lower dielectric constant[23] that increases electrostatic interactions.

X-ray crystal structures of zinc-bound HDAC8 show that the divalent metal ion is pentacoordinated to carboxylate oxygens of D178 and D267, and to the N$\delta$1 atom of H180 as direct ligands in addition to the hydroxamic acid group of the inhibitor.[24,25]

Similar to CAII, the hydrophobic side chains (M274, F207, and F208) are embedded

near the H180 metal ligand. Two of these hydrophobic residues (F207 and F208) are highly conserved across both class I human HDACs and HDAC8 homologues from different organisms (Figure 2). However, M274 is a leucine in other class I HDACs and a histidine in *Schistosoma mansoni* HDAC8 (smHDAC8).[26]

**Figure 3.2** Multiple sequence alignment of HDAC8 from different organisms showing conserved first shell ligands and hydrophobic residues of the second shell. Protein sequences of HDAC8 were identified from PSI-BLAST search and aligned by Clustal Omega. Red color-shading indication of sequence conservation were generated by ESPript 3. Secondary structure is annotated based on human HDAC8 structure using ESPript 3. Sequences in black boxes correspond to the first shell elements. Putative second shell ligands are marked by yellow boxes.

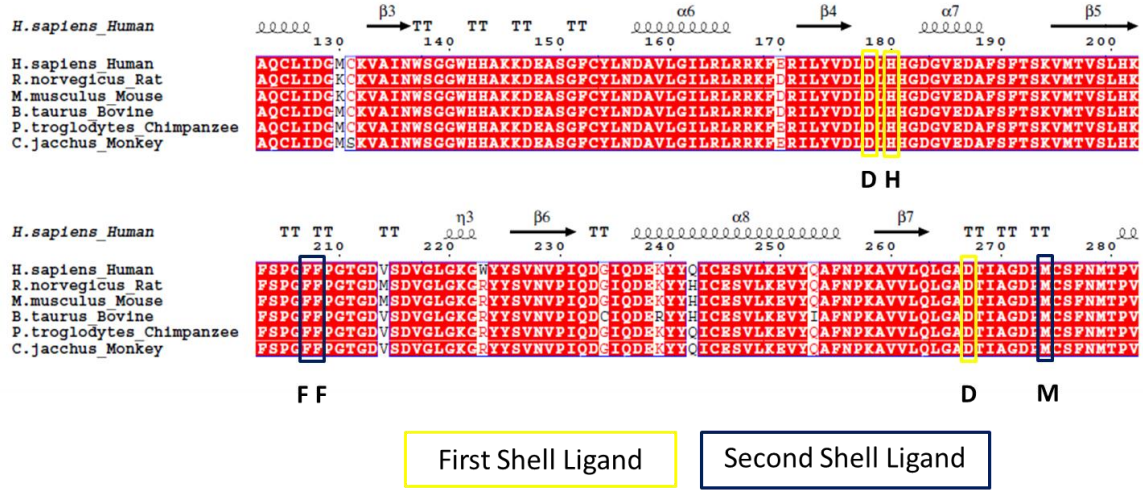


Additionally, the crystal structure visualizes hydrophobic interactions between F207 and F208 and the HDAC inhibitor suberanilohydroxamic acid (SAHA).[27,28] However, in contrast to CAII and other zinc metalloenzymes[29,30] hydrogen bonding interactions with the first shell H180 are absent, replaced by hydrophobic interactions (Figure 3). This structural alteration may be a signature of metalloenzymes that may be activated by multiple metal species *in vivo* (i.e. $Zn^{2+}$ or $Fe^{2+}$), allowing subtle alterations in the active site structure to accommodate different metal ions. The role of the hydrophobic shell in HDAC8 was investigated by measuring the effect of mutants in F207, F208 and M274 on the catalytic activity, metal binding affinity and metal equilibration

kinetics. These data demonstrated that catalytic reactivity ($k_{cat}/K_M$) and metal selectivity, primarily $K_D$, are governed by the second shell environment, which is unique structural feature when compared to CAII. This could be a physiologically relevant way for metalloproteins to recognize and switch Zn/Fe based on cellular conditions.

**Figure 3.3** Crystal structure of Zn(II)-HDAC8 active site with bound acetyl-lysine methyl coumarin. Figures derived from PDB file 2V5W using Pymol. A close-up of $Zn^{2+}$-HDAC8 active site with bound acetyl-lysing methyl coumarin using surface representation of first and second shell ligands. Second shell residues are depicted as follows: F207 as light blue, F208 as purple, M274 as blue. First shell residues are yellow.

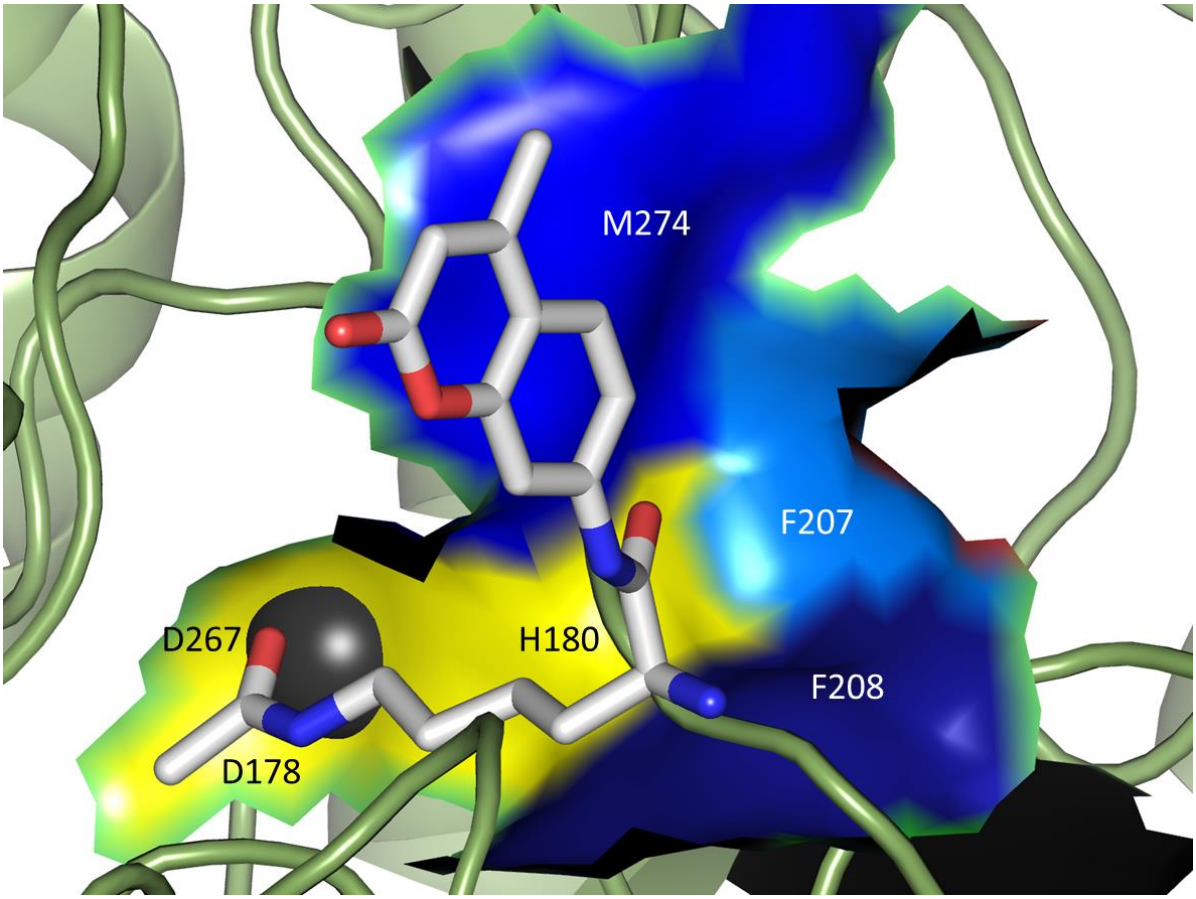

## MATERIALS AND METHODS

*General*

All experiments were performed in metal-free plastic ware using reagents without extraneous metal ions, as verified by Inductively Coupled Plasma Mass Spectrometry (Ted Huston, University of Michigan). Reagents were of the highest quality available from Sigma-Aldrich, unless otherwise noted. For $Fe^{2+}$ experiments, a freshly made 10 mM $FeCl_2$ stock was prepared in 50 mM ascorbic acid and diluted to 100 μM with 1X assay buffer (20mM HEPES, pH8, 3mM KCl, 137mM NaCl) prior to incubation with apo-HDAC8. Similarly, a 10 mM $ZnSO_4$ solution was prepared in 20 mM HEPES pH 8, 1 mM triscarboxyethylphosphine (TCEP) and diluted to 100 μM with 1X assay buffer prior to incubation with apo-HDAC8.

*Preparation of HDAC8 variants using site-directed mutagenesis*

All second shell ligand mutations were introduced into the pHD2 plasmid using QuikChange site-directed mutagenesis methodology (Stratagene). The M274A, M274Q, M274E,F207A, and F208A HDAC8 variant was produced by replacing the wild-type Met-274 codon (ATG) with the codon for Ala (GCG), Gln (CAG), and Glu (GAG) and Phe-207 codon (TTT) with the codon for Ala (GCT) and Phe-208 codon (TTC) with the codon Ala (GCC) using oligonucleotide-directed mutagenesis. The pET-20b-derived HDAC8 *E. coli* expression plasmid, pHD2-His, was modified to add a TEV NIa protease cleavage site with the linker recommended by Invitrogen (ENLYFQG-DYDIPTT) upstream of the C-terminal $His_6$ tag.[10]

Following confirmation of the desired mutation by sequencing, each mutant was expressed in *E.coli* BL21(DE3) and purified similar to WT enzyme.[10] After transforming the

plasmid into the BL21(DE3) strain of *E. coli*, the cells were grown in 2X-YT media supplemented at 37 ℃ until $OD_{600}$ = 0.6, incubated at 25 ℃ for 30 min, and then 0.5 mM isopropyl β-D-1-thiogalactopyranoside was added and the cells were incubated for 12–15 h. The cells were pelleted and resuspended in buffer A (20 mM Hepes, 150 mM NaCl, 0.5 mM imidazole, pH 8.0), lysed using a microfluidizer and the resulting extract was clarified by centrifugation. The cell extract was loaded onto a metal affinity (IMAC) column charged with nickel chloride, washed with buffer A with 25 mM imidazole and then the protein was eluted with buffer A containing 250 mM imidazole. The $His_6$-TEV tag was removed by incubation with recombinant TEV protease and then dialyzed overnight in buffer A containing 1 mM tris(2-carboxyethyl) phosphine (TCEP). The IMAC column was run a second time and HDAC8 was collected in the flow-through. Metal-free HDAC8 was prepared by dialyzing the purified enzyme twice overnight against 20 mM 4-morpholinepropanesulfonic acid (MOPS), 3 mM KCl, 137 mM NaCl, and 1 mM EDTA, pH 8.0, followed by dialysis against 20 mM MOPS, 3 mM KCl, 137 mM NaCl, pH 8.0. The enzyme was then concentrated using an Amicon Ultra Microcon centrifugal filtration device (10,000 MWCO) and the buffer was exchanged using a PD-10 gel filtration column (GE Healthcare) equilibrated with 20 mM MOPS, pH 8.0 (pretreated with metal chelating resin, Chelex 100).

*Measurement of catalytic activity ($k_{cat}$ / $K_M$)*

The catalytic reactivity of wild-type and mutant HDAC8 reconstituted with $Zn^{2+}$ or $Fe^{2+}$ was measured using a commercially-available fluorescent assay (BIOMOL) with the Fluor de Lys (FdL) HDAC8 substrate (RHK(ac)K(ac)-methyl-coumarin). All assay buffers were pre-treated with Chelex resin (Bio-Rad) to remove trace divalent metal ions. Metal-free HDAC8

variants were reconstituted with $Zn^{2+}$ or $Fe^{2+}$ by incubation with a stoichiometric concentration of metal in assay buffer (20mM HEPES pH 8.0, 137 mM NaCl, 3 mM KCl, and 1mM TCEP). The reaction was quenched by the addition of stoichiometric amounts of trichostatin A (TSA), a potent inhibitor of HDAC8. Fluorescence intensity was monitored at $\lambda_{ex}$ = 340 and $\lambda_{em}$ = 450 for the deacetylated and cleaved product, and at $\lambda_{ex}$ = 340 and $\lambda_{em}$ = 380 for the starting acetylated substrate. The ratio of product fluorescence divided by substrate fluorescence was observed and linearly increases with product concentration up to 30% product. The amount of product formed was determined from comparison to the fluorescence rations of a standard curve made up of known concentrations of products and substrates. The linear initial rates catalyzed by 0.5 μM wtHDAC8 or 10 μM HDAC8 mutants with varying concentrations of peptide substrate (50 – 1500 μM) in assay buffer at 25 ℃ were measured. The steady-state parameters $k_{cat}$, $K_M$ and $k_{cat}/K_M$ were obtained by fitting the Michaelis-Menten equation to the dependence of the initial velocities on the substrate concentration using the curve-fitting program Prism.

*Measurement of metal (*$Zn^{2+}$ / $Fe^{2+}$*) dissociation rate constant (*$k_{off}$*)*

The first order rate constant for metal ion dissociation from HDAC8 was measured by the time-dependent loss of activity upon incubation with EDTA. WT and HDAC8 variants (2-10 μM) reconstituted with stoichiometric $Zn^{2+}$ or $Fe^{2+}$ were diluted into assay buffer containing 1 mM EDTA. At various times (0 – 60 min) an aliquot was diluted 10-fold into assay buffer. The reactions were quenched by the addition of TSA and analyzed as described above. The observed rates are not dependent on the concentration of EDTA (0.5-5 mM).

Equation 2 : $Y = A * \exp(-k_{off} * X) + c$

*Measurement of metal ($Zn^{2+}$ / $Fe^{2+}$) dissociation constant ($K_D$)*

The affinity of HDAC8 for $Zn^{2+}$ or $Fe^{2+}$ was measured in an anaerobic glove box ($H_2/N_2$ mix) from an increase in activity measured with the FdL assay in the presence of increasing concentrations of free $Zn^{2+}$ or $Fe^{2+}$ maintained using a metal ion buffer. The standard assay buffer[10] was replaced with 1 mM nitrilotriacetic acid (NTA), 137 mM NaCl, 3 mM KCl, 10 mM MOPS, pH 7 buffer[31] with $[Fe^{2+}]_{total}$ = 0-950 μM ($[Fe^{2+}]_{free}$ 0-2.6 μM) or $[Zn^{2+}]_{total}$ = 0-200 μM ($[Zn^{2+}]_{free}$ 0-532 pM) and 0.5 μM HDAC8. The concentration of bound versus free metal ion was calculated using the program MINEQL+ (Environmental Research Software). The assay mixtures, containing all components except substrate, were incubated for 2 hours on ice in the anaerobic glove box. Assays were incubated at 30℃ for 30 min, initiated by the addition of enzyme and the products analyzed as described above. Activity was dependent on the concentration of $[Me^{2+}]_{free}$ and not the total concentration of the metal ion and buffer as determined by varying the concentration of the buffer. The metal dissociation constant ($K_{Me}$) was determined from fitting a binding isotherm (Equation 1) to the $[Me^{2+}]_{free}$ dependence of activity using the program Prism where A is the activity at saturating metal ion.

Equation 1 : $Y = A^* X / (K_D + X) + c$

**RESULTS**

*Second Shell HDAC8 mutants*

Crystal structures of HDAC8 show three hydrophobic residues, M274, F207, and F208, flanking the zinc ligand H180. In crystal structure, there is no water molecule placed within hydrogen-bonding distance of H180 and the S of M274 is positioned to be within hydrogen

bonding distance to N of H180.[25] The side chains surround the εN of H180 (within 4 Å), replacing the hydrogen bonding interaction observed in a number of other metalloenzymes (Figure 1)[14–16]. We hypothesize that these side chains contribute to the structure and environment important for modulating the properties of the catalytic metal ion site. To delineate the role of these residues in determining catalytic activity and metal selectivity of HDAC8, site-directed mutagenesis was used to prepare mutations where the side chain was truncated to Ala. Additionally, to further explore the role of hydrophobicity and hydrogen bonding in controlling the properties of HDAC8, the M274 side chain was also replaced with Asn and Gln. These hydrophobic residues are highly conserved across HDAC8s from different species.

These residues were mutated by site-directed mutagenesis to determine their role in contributing to metal ion selectivity and affinity within the HDAC8 active site. To delineate the effect of the second shell substitution on the reactivity of zinc/iron-bound mutants, we measured catalytic reactivity of metal-reconstituted HDAC8 WT and second shell ligand mutants using Fluor-de-lys (FdL) acetyl-peptide as a substrate. This assay utilized the commercially available peptide substrates containing a methylcoumarin fluorophore conjugated to the C-terminal side of the p53 transcription factor (RHKacKac-methylcourmarin).

*Steady-State Turnover ($k_{cat}/K_M$) of Mutants*

To define the role of these residues in determining the reactivity of HDAC8, we measured the catalytic activity of HDAC8 WT and mutants, reconstituted with either $Fe^{2+}$ or $Zn^{2+}$, using the Fluor-de-lys (FdL) assay with the commercially available acetyl-peptide substrate containing a methylcoumarin fluorophore conjugated to the C-terminal side of the p53 transcription factor (RHKacKac-methylcoumarin). The steady-state kinetic parameters were

determined from the substrate dependence of the initial rate for product formation from a fit of the Michaelis–Menten equation to the data or, in cases where little or no curvature was observed, the value of $k_{cat}/K_M$ was determined from a linear fit to the data (Figure 4).

Truncating the side chains of each hydrophobic residue by substitution with Ala significantly diminishes the catalytic activity of $Zn^{2+}$-HDAC8; the value of $k_{cat}/K_M$ decreases 25- and 700-fold for M274A and F207A, respectively (Figure 4, Table 1). The F208A mutation has an even larger effect; no detectable catalytic activity was observed for $Zn^{2+}$-F208A even at 1.5 mM substrate concentration, suggesting a decrease in activity of > 130-fold. These data indicate

**Figure 3.4** Deacetylation activity of HDAC8 mutants of second shell residues important for metal ion binding specificity in HDAC8 by measuring the reactivity of variants with $Zn^{2+}$ or $Fe^{2+}$ by using FdL peptide. Apo-HDAC8 mutant (20 μM) was incubated with divalent metal ions ($Fe^{2+}$ and $Zn^{2+}$) at 4 ℃ for 1 h and then assayed at 5 μM HDAC8 mutant with 0 – 1500 μM Fluor de Lys HDAC8 substrate at 25 ℃ in 20 mM HEPES, pH 8.0, 137 mM NaCl and 3 mM KCl. The initial rates for deacetylation were determined from time-dependent changes in fluorescence. The resulting rates fit to the Michaelis-Menten equation to obtain $k_{cat}$ and $K_M$, which are listed in Table 1.

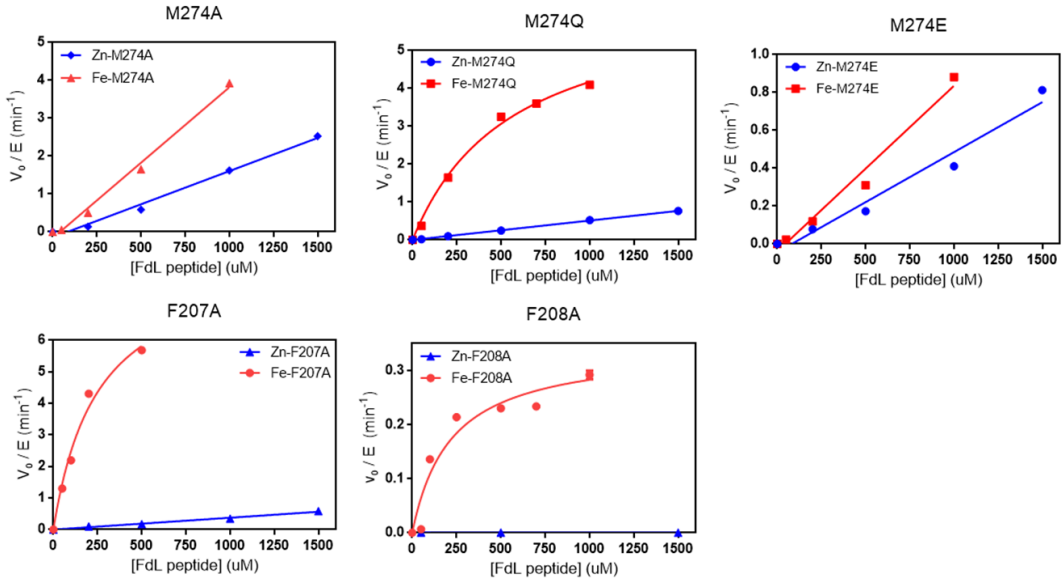


that the hydrophobic shell surrounding H180 is essential for the catalytic efficiency of HDAC8

by enhancing substrate recognition or increasing the reactivity of the catalytic metal site either directly or indirectly through stabilization of the overall protein structure. As previously observed[10], the value of $k_{cat}/K_M$ for deacetylation catalyzed by $Fe^{2+}$-HDAC8 is increased 3-fold compared to $Zn^{2+}$-HDAC8, at least partially due to a decrease in the value of $K_M$, likely reflecting substrate affinity for these weak-binding substrates[10]. Similarly, all of the Ala mutants have higher catalytic activity (2- to 100-fold) using $Fe^{2+}$ as the catalytic metal ion compared to $Zn^{2+}$.

**Table 3.1** Catalytic reactivity of HDAC8 variants with $Zn^{2+}$ / $Fe^{2+}$

| | Zn $k_{cat}/K_M$ ($M^{-1}s^{-1}$) [a] | Fe $k_{cat}/K_M$ ($M^{-1}s^{-1}$) [b] | Fe $k_{cat}/K_M$ / Zn $k_{cat}/KM$ [d] | Fe $K_M$ (uM) | Fe $k_{cat}$ (min-1) |
|---|---|---|---|---|---|
| WT | 800[c] | 2300[c] | 3 | 210 [e] | 30 [e] |
| M274A | 30 | 67 | 2 | n.d.[g] | n.d.[g] |
| M274Q | 9 | 193 | 21 | 560 [e] | 6.5 [e] |
| M274E | 9 | 15 | 2 | n.d.[g] | n.d.[g] |
| F207A | 6 | 580 | 97 | 250 [e] | 8.8 [e] |
| F208A | low [f] | 26 | NA | 220 [e] | 0.3 [e] |

a. Enzyme reconstituted 1:1 with $Zn^{2+}$ was assayed at pH 8 at 30℃
b. Enzyme reconstituted 1:1 with $Fe^{2+}$ was assayed at pH 8 at 30℃
c. Obtained from reference[10]
d. Value of $k_{cat}/K_M$ for $Fe^{2+}$-substituted relative to $Zn^{2+}$-HDAC8
e. Steady-state kinetic parameters calculated from a fit of the Michaelis-Menten equation to the dependence of the initial rate on the substrate concentration
f. Initial velocity was not detectible
g. Value was not determined

The F207A variant is particularly interesting because it retains a high degree of activity (4-fold decrease from WT) for $Fe^{2+}$-bound form despite the 130-fold decrease for the $Zn^{2+}$-bound enzyme. The $K_M$ values of $Fe^{2+}$-bound F207A and F208A are comparable to that of WT HDAC while the $k_{cat}$ values decrease 3- and 100-fold. Assuming that the $K_M$ reflects substrate affinity, these data suggest that alterations at 207 and 208 affect the reactivity of the metal site rather than substrate affinity. In contrast, the M274A mutation increases the $K_M$ value, suggesting that this mutation alters substrate affinity. These data clearly demonstrate that the hydrophobic residues surrounding the metal site modulate the activity of HDAC8. Further, these side chains are generally more important for enhancing the reactivity of the $Zn^{2+}$-bound enzyme than the $Fe^{2+}$-bound enzyme.

To further explore the importance of hydrophobicity on catalytic activity, M274 was substituted with Gln, introducing additional hydrogen-bonding ability, or Glu, introducing a negative charge. For the $Zn^{2+}$-bound enzyme, both the Gln and Glu mutants decrease the activity by 90-fold compared to WT, to a value 3-fold lower than the Ala substitution at this position. However, these isosteric substitutions differentially alter the activity of the $Fe^{2+}$-enzymes; $Fe^{2+}$-M274Q HDAC8 activity decreased 11-fold, a smaller effect than the Ala substitution, while the $Fe^{2+}$-M274E HDAC8 activity lessened by 150-fold. This suggests that the activity of $Fe^{2+}$-HDAC8 is particularly sensitive to the structure or electrostatic environment in the second sphere of the metal site. Furthermore, the M274Q mutation in the $Fe^{2+}$-bound enzyme both increases the value of $K_M$ by ~2-fold and decreases the value of $k_{cat}$ by ~5-fold suggesting effects on both substrate affinity and metal site reactivity. These data pinpoint interactions with M274 as modulating the relative reactivity of the $Zn^{2+}$ and $Fe^{2+}$-substituted enzymes.

*Measurement of dissociation constant ($K_D$)*

Given that mutations in the hydrophobic residues near the metal site differentially alter the activity of $Zn^{2+}$- and $Fe^{2+}$-HDAC8, we tested the importance of these side chains in determining metal selectivity by measured the dissociation constant ($K_D$) for both $Zn^{2+}$ and $Fe^{2+}$ from metal-bound HDAC8. We assayed metal affinity from the metal-dependence of either catalytic activity or binding of fluorescein-labeled SAHA (flSAHA). For these experiments apo-HDAC8 was equilibrated with varying concentrations of total metal ions in nitrilotriacetate (NTA)-buffered solutions to maintain a readily exchangeable zinc/iron pool with a constant free metal ion concentration, calculated using the MINEQL program.[32] The fraction of metal-bound HDAC8 was determined from the catalytic activity measured using the FdL assay or by the binding of flSAHA, which has high affinity only for metal-HDAC8, monitored by fluorescence anisotropy[7]. Both the catalytic activity and fluorescence anisotropy showed a hyperbolic dependence on the free metal concentration (Figure 5) which is well-described by a single binding isotherm (Eq. 1). Both methods yield identical results for the affinity of WT-HDAC8 for metal binding ($K_D^{Zn}$: 5 pM vs. $K_D^{Fe}$: 0.2 μM); this is reasonable since the concentration of flSAHA used is below the $K_D$ for this inhibitor. Consistent with previous results[7], WT HDAC8 binds $Zn^{2+}$ nearly $10^5$-fold more tightly than $Fe^{2+}$.

Mutations in hydrophobic residues near the metal site alter both metal affinity and selectivity. Replacement of the Met ligand at position 274 with Ala, Gln, or Glu significantly decreased the zinc affinity relative to WT (by 10-, 110-, and 12-fold, respectively). However, these Met mutants had smaller and differential effects on the $Fe^{2+}$ binding affinity; M274Q and M274E decreased affinity by 3-, and 8-fold, respectively, while M274A enhanced the affinity by 3-fold. Therefore, alterations in this side chain increased the selectivity for $Fe^{2+}$, alter the metal

selectivity ratio ($K_D^{Fe}/K_D^{Zn}$) from the WT value of 60,000 to 1,300 for M274Q.

**Figure 3.5** Measurement of a $Zn^{2+}$ / $Fe^{2+}$ dissociation constant ($K_D$) for mutants of second shell residues of HDAC8 by activity assay and FdL assay. ApoHDAC8 was equilibrated with NTA-buffered metal solutions. Bound zinc (left) was analyzed by enhancement of HDAC8 activity and FP assay ($K_D^{Zn}$); bound iron (right) was analyzed by HDAC8 activity and FP assay ($K_D^{Fe}$), as described in Materials and Methods. $K_D$ values are listed in Table 2.

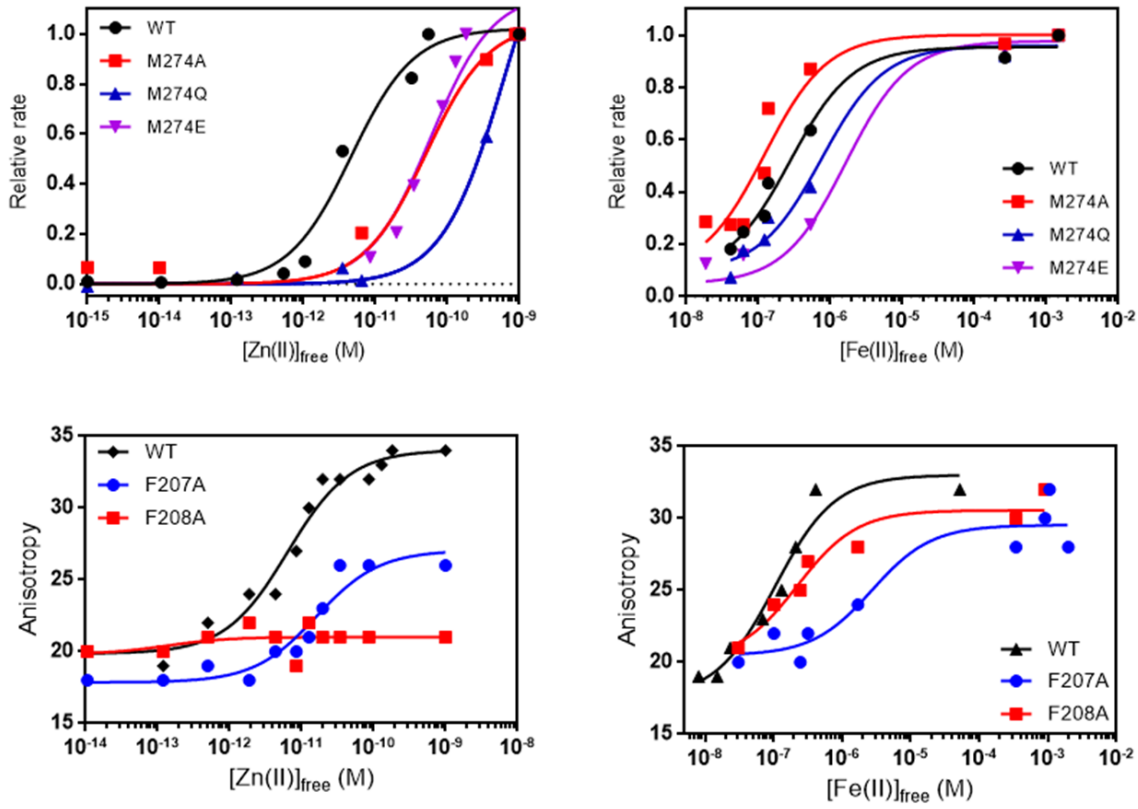


The Gln substitution at M274Q leads to both the highest selectivity for $Fe^{2+}$ affinity and the highest ratio of catalytic activity for the $Fe^{2+}$- and $Zn^{2+}$-substituted enzymes. In contrast, substitution of Ala for Phe at position 207 decreased the affinity of HDAC8 for $Fe^{2+}$ (3-fold) more than for $Zn^{2+}$ (9-fold) compared to that of wild-type HDAC8. This leads to a HDAC8 mutant with higher selectivity for Zn ($K_D^{Fe}/K_D^{Zn}$ =193,000).

**Table 3.2** Metal dissociation constants and dissociation rate constants of HDAC8 WT and second shell ligand variants

| Enzyme[a] | Zn $K_D$ (pM)[b] | Fe $K_D$ (μM)[b] | Zn $K_D$ / Fe $K_D$ (μM)[c] | Zn $k_{off}$ ($min^{-1}$)[d] | Fe $k_{off}$ ($min^{-1}$)[d] |
|---|---|---|---|---|---|
| WT | 5 ± 1 | 0.3 ± 0.08 | 1.7 E-05 | 0.04 ± 0.004 | 0.07 ± 0.01 |
| M274A | 50 ± 30 | 0.1 ± 0.07 | 4.2 E-04 | 0.04 ± 0.02 | 0.03 ± 0.01 |
| M274Q | 620 ± 200 | 0.8 ± 0.3 | 8.2 E-04 | 0.06 ± 0.008 | 0.06 ± 0.01 |
| M274E | 60 ± 30 | 1.6 ± 1.2 | 3.6 E-05 | 0.03 ± 0.02 | 0.02 ± 0.006 |
| F207A | 14 ± 5 | 2.7 ± 2.3 | 5.2 E-06 | 0.26 ± 0.06 | 2.6 ± 0.1 |
| F208A | NA | 0.2 ± 0.1 | - | - | - |

a. Metal substituted HDAC8 WT and variants was reconstituted with stoichiometric metal ion (1:1) as described in the "Materials and Methods for measuring $k_{off}$ values
b. Metal binding affinity to HDAC8 was measured at 30 ℃ (20 mM HEPES, pH 7.5, 3 mM KCl, 137 mM NaCl, 1 mM NTA) using fluorescence anisotropy or FdL activity assay as described in the "Materials and Methods". The $K_D$ values were obtained by fitting Eq.1 to the data.
c. Value of $K_D$ for $Zn^{2+}$ relative to $Fe^{2+}$ in HDAC8
d. Metal-reconstituted HDAC8 variants were incubated 1 mM EDTA for various times and then the activity was determined by dilution into an assay to measure metal dissociation rate constant ($k_{off}$), as described in Materials and Methods.

Unexpectedly, for the F208A mutant, no zinc-dependent binding of flSAHA was observed even at nM zinc concentrations (Figure 5), suggesting that the zinc affinity of this mutant is decreased >1000-fold compared to WT HDAC8. This result is consistent with the absence of detectable catalytic activity even at high substrate concentrations for $Zn^{2+}$-F208A HDAC8. However, the F208A enzyme retains $Fe^{2+}$-dependent flSAHA binding (Figure 5), with a $K_D^{Fe}$ value that is comparable to wild-type. The retention of high $Fe^{2+}$ affinity demonstrates that

the loss of zinc affinity is not caused by global unfolding of this mutant. Surprisingly, truncation of the F208 side chain drastically lowers the binding affinity for $Zn^{2+}$ while having no effect on the $Fe^{2+}$ affinity, leading to a HDAC8 mutant with increased selectivity for Fe ($K_D^{Fe}/K_D^{Zn} > 150$). In summary, the hydrophobic second shell residues play a significant role in modulating the metal affinity and Zn/Fe selectivity of HDAC8.

*Measurement of metal dissociation rate constant ($k_{off}$)*

To further examine the importance of the hydrophobic side chains in the second shell (residue F207, F208, and M274) in determining the properties of the HDAC8 metal site, we measured the rate constant ($k_{off}$) for dissociation of $Zn^{2+}$ or $Fe^{2+}$ bound to the HDAC8 variants. The metal dissociation rate constants ($k_{off}$) were determined from the time-dependent decrease of enzyme activity after dilution into 1 mM EDTA to trap the dissociated free metal. The measured values of $k_{off}$ are not dependent on the EDTA concentration (1 – 5 mM) demonstrating that this chelator does not catalyze metal dissociation but functions by lowering the free metal ion concentration (data not shown).

The rate constants for dissociation ($k_{off}$) of $Zn^{2+}$ or $Fe^{2+}$ from WT HDAC8 at 25℃, pH 8 are 0.04 ± 0.004 $min^{-1}$ and 0.07 ± 0.01 $min^{-1}$, respectively (Figure 6). The comparable dissociation rate constant for $Zn^{2+}$ and $Fe^{2+}$ is unexpected given the large differential in the affinity of HDAC8 for these metals. This result suggests a two-step binding mechanism, which has previously been observed in other metalloenzymes, including carbonic anhydrase II and UDP-3-*O*-(*R*-3-hydroxymyristoyl)-*N*-acetylglucosamine deacetylase (LpxC).[31,33] Consistent with a multi-step metal binding mechanism, the measured dissociation constants for the HDAC8 mutants at M274 do not scale with the measured alterations in the metal affinity.

**Figure 3.6** Measurement of a $Zn^{2+}$ and $Fe^{2+}$ dissociation rate constant ($k_{off}$) for mutants of HDAC8 second shell residues. 5 μM $Zn^{2+}$-bound (left) or $Fe^{2+}$-bound (right) HDAC8 mutants were incubated with 1 mM EDTA at various times and then at those times the activity was determined by dilution (10-fold) into an assay, as described in Materials and Methods. A single exponential equation (Equation 2) was fit to the time-dependence of activity to obtain $k_{off}$ (solid lines). $k_{off}$ values are listed in Table 2.

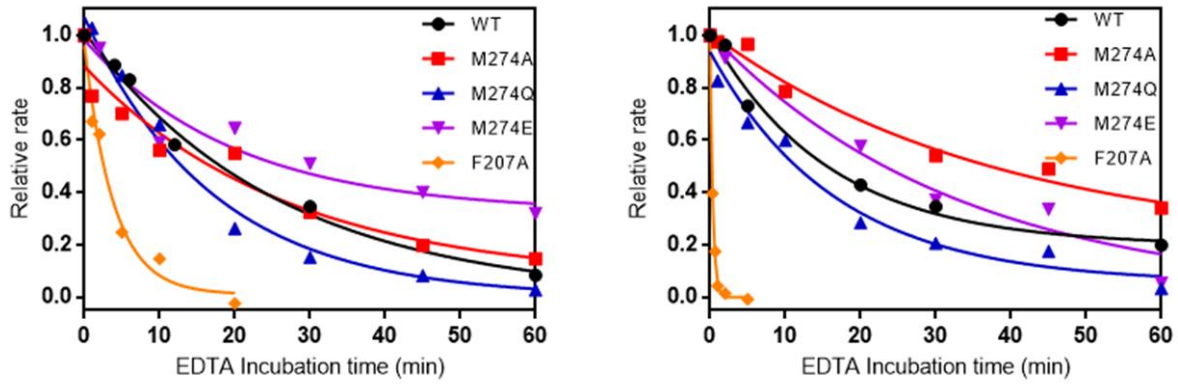


The substitution of M274 with Ala, Gln, and Glu led to minor changes (<3-fold) on the $Zn^{2+}$ and $Fe^{2+}$ dissociation rate constants relative to that of wild-type despite decreases in the zinc affinity of >100-fold (Table 2). In contrast, the F207A mutation results in an increase in $k_{off}$ of 6-fold and 30-fold for $Zn^{2+}$-HDAC8 and $Fe^{2+}$-HDAC8, respectively, consistent with the decreased affinity of this mutant for both $Zn^{2+}$ and $Fe^{2+}$ (3-fold and 9-fold, respectively). Therefore, these hydrophobic shell residues differentially regulate the metal binding kinetics of HDAC8.

## DISCUSSION

In all of the crystal structures of HDAC8•hydroxamate complexes solved to date, the metal geometry is square-pyramidal with the metal ion coordinated by three protein ligands (Asp, Asp, and His side chains) and two oxygens from the hydroxamate inhibitor which are presumably replaced by water molecules in the absence of the inhibitor.[7,25,34] The unusual ligand set ($Asp_2His$) for HDAC8 compared to prototypical zinc-dependent hydrolases (frequently $His_3$

or $His_2Glu$[35]) called into question the identity of the physiological metal cofactor. The refined metal ion coordination geometries and distances in $Fe^{2+}$-substituted HDAC8 are comparable to those observed in $Zn^{2+}$-HDAC8, although some uninterpretable difference density is observed for $Fe^{2+}$-HDAC8 that may reflect incomplete changes in metal coordination.[7] These structural data are consistent with activation of the enzyme by either $Fe^{2+}$ or $Zn^{2+}$. However, the enhanced activity of $Fe^{2+}$-HDAC8 suggested that iron could be the metal cofactor *in vivo*. Although the affinity of HDAC8 for $Fe^{2+}$ is $10^5$-fold weaker than $Zn^{2+}$, the biologically readily exchangeable concentration of $Fe^{2+}$ is estimated to be $10^4$-fold higher than that of $Zn^{2+}$ and both concentrations are on the same order of magnitude as the HDAC8 metal affinity. This correlation suggests that HDAC8 could be activated by either zinc or iron under physiological conditions. However, the factors contributing to the Zn/Fe metal selectivity in HDAC8 have not been delineated.

In this study, we performed site-directed mutagenesis of second shell residues for the following reasons: (i) to understand which residues surrounding the first shell residues play a pivotal role in regulating metal ion selectivity (ii) to explore the possibility of manipulating metal selectivity by varying these residues (iii) to gain insights into a potential mechanism of metal ion switching that regulate HDAC8 activity, and (iv) to investigate if we could develop an iron-specific sensor for measuring free iron concentration *in vivo*. To investigate the essential features that may lead to $Zn^{2+}$ versus $Fe^{2+}$ selectivity in HDAC8, we altered the size and hydrophobicity of the amino acids at positions F207, F208, and M274 that form hydrophobic interactions with the first shell ligand at the active site. We mutated these 3 hydrophobic residues into smaller and hydrophilic ones in HDAC8 to determine the effect on catalytic activity and metal ion binding affinity for $Zn^{2+}$ or $Fe^{2+}$.

*Second Shell Residues affect catalytic activity*

Measurement of HDAC8 activity with the non-physiological Fluor de Lys substrate yields low values of $k_{cat}/K_M$ and high $K_M$ values. Thus, it is reasonable to assume that the kinetic mechanism is rapid, reversible substrate binding followed by rate-limiting cleavage. The enhancement of cleavage for peptide substrates containing trifluoro-acetyl modifications is consistent with the model that $k_{cat}$ reflects the rate constant of the hydrolytic step.[36] For this mechanism, $K_M$ equals $K_D^{Substrate}$, reflecting the affinity of HDAC8 for the peptide substrate.

Mutation of the F207, F208, or M274 side chain to alanine diminished the catalytic activity of zinc-bound HDAC8 significantly (27- to 133-fold) (Table 3). Since wild-type and mutant $Zn^{2+}$-HDAC8s have such a high $K_M$ (> 1 mM), it is not possible to determine whether the decrease in activity is mainly due to changes in substrate affinity or the hydrolytic rate constant.

**Table 3.3** Fold decrease in reactivity of HDAC8 variants [a,b]

| Residue | M274 | | | F207 | F208 |
|---|---|---|---|---|---|
| Enzyme | Ala | Gln | Glu | Ala | Ala |
| $Zn^{2+}$ | x27 | x89 | x89 | x133 | n.d. |
| $Fe^{2+}$ | x34 | x12 | x153 | x4 | x88 |

a. Activity of metal-reconstituted HDAC8 was measured at 25 ℃ (20 mM HEPES, 3 mM KCl, 137 mM NaCl, pH 8) using FdL assay as described in the "Materials and Methods" and as listed in Table 1

b. Fold-decrease observed for mutant relative to wild-type HDAC8

However, the $K_M$ values for hydrolysis catalyzed by $Fe^{2+}$-HDAC8 mutants vary significantly less (<3-fold) than the changes in $k_{cat}/K_M$ suggesting that the mutations mainly alter

the reactivity of the active site metal ion. Similarly, replacement of hydrophobic interactions with hydrogen bonding by incorporating a carbamide or carboxylate side chain (M274Q, M274E) also resulted in a dramatic decrease in the reactivity of $Zn^{2+}$-HDAC8.

Intriguingly, the mutations in the second shell had differential effects on the activity of $Fe^{2+}$- and $Zn^{2+}$-HDAC8 (Table 3). For example, the F207A mutation decreases the activity of the zinc enzyme by 133-fold compared to the modest (4-fold) decrease observed when the mutant is reconstituted with $Fe^{2+}$. Similarly, the M274Q mutation has a significantly smaller deleterious effect on $Fe^{2+}$-HDAC8 compared to the zinc enzyme. In contrast, the M274E and M274A have a comparable or larger effect on the iron enzyme. These differential effects of mutations in the second shell demonstrate that these side chains are important for tuning the reactivity of the metal site and thus differentially altering the hydrolytic rate of the metal-substituted enzymes. This could be mediated by changes in the electrostatic environment of the metal site due to replacement of a hydrophobic side chain with water or a polar group. Alternatively, replacement of a hydrophobic side chain with a group that could hydrogen bond with the His metal ligand, such was a water molecule (Ala mutants) or Gln or Glu side chain could potentially lead to alterations in geometry of the bound metal and the $Fe^{2+}$- and $Zn^{2+}$-HDAC8 sites could respond differently to these new interactions. For example, it is possible that these mutations allow the geometry of the bound zinc ion to become tetrahedral rather than the 5-coordinate square-pyramidal geometry observed in the wild-type crystal structures. This alteration in geometry is predicated to decrease reactivity as it would limit the ability of the metal to coordinate 2 non-protein ligands to both activate a water nucleophile and polarize the carbonyl of the substrate oxygen.

For previously studied $Fe^{2+}$-dependent hydrolases, including γ–carbonic anhydrase and

peptide deformylase, the $k_{cat}/K_M$ value for the $Fe^{2+}$-enzyme is 1.7- to 100-fold higher than the $Zn^{2+}$-bound enzyme form.[37,38] Consistent with the other enzymes, WT-HDAC8 has a 2.8-fold higher $k_{cat}/K_M$ value for activation by $Fe^{2+}$ compared to $Zn^{2+}$. The ratio of $k_{cat}/K_M$ values for the $Fe^{2+}$ and $Zn^{2+}$-substituted HDAC8 mutants in the second shell are also within this range (Table 1).

In summary, these results demonstrate that the conserved hydrophobic residues in the context of the native protein fine-tune the reactivity of the $Zn^{2+}$ and $Fe^{2+}$ enzymes such that they have similar reactivity.

*Mutations Alter Metal Affinity and Specificity*

The affinity of WT-HDAC8 for $Zn^{2+}$ is ~$10^5$-fold tighter than the $Fe^{2+}$ affinity. A preference for $Zn^{2+}$ binding can be expected by the increased Lewis acidity of $Zn^{2+}$ compared to $Fe^{2+}$ and is also in accordance with the Irving-Williams series of stability constants.[39] However, HDAC8 could still bind either $Zn^{2+}$ or $Fe^{2+}$ *in vivo* since the intracellular concentration of readily exchangeable $Zn^{2+}$ in cells is orders of magnitude lower than the concentration of readily exchangeable $Fe^{2+}$ (5-400 pM $Zn^{2+}$ vs. 0.2-6 μM $Fe^{2+}$).[8,40–42] The determinant of metal selectivity of cellular proteins is currently unclear and could be facilitated by the unique second shell ligand environment in the HDAC8 active site. In cells, it is possible that metal selectivity is determined by equilibration with the metal pools and is therefore under thermodynamic control. Since zinc and iron ions are dissimilar (Chapter 1, Table 1) in size and preferred geometry, alterations in the metal binding site are not expected to affect the $Zn^{2+}$ and $Fe^{2+}$ binding affinities to the same extent.[43] Consistent with this, mutations in HDAC8 differentially alter the binding affinities for $Zn^{2+}$ and $Fe^{2+}$ (Table 4).

**Table 3.4** Fold decrease in metal affinity parameters of HDAC8 variants [a,b]

| Residue | M274 | | | F207 | F208 |
|---|---|---|---|---|---|
| Enzyme | Ala | Gln | Glu | Ala | Ala |
| $Zn^{2+}$ | x10 | x124 | x12 | x3 | n.d |
| $Fe^{2+}$ | x0.3 | x2.7 | x5.3 | x9 | x0.7 |

a. Metal binding to HDAC8 was measured at 25 ℃ (20 mM HEPES, 1 mM NTA, 3 mM KCl, 137 mM NaCl, pH 7.5) using FdL or FP assay as described in the "Materials and Methods". The $K_D$ values were obtained by fitting Eq. 1 to the data.
b. Fold-decrease observed for mutant relative to wild-type HDAC8 for binding to metal

Metal binding kinetic from wild-type HDAC8 was similar to that previously measured from UDP-3-*O*-(*R*-3-hydroxymyristoyl)-*N*-acetylglucosamine bacterial deacetylase (LpxC). LpxC was shown to perform metal switching depending on cellular condition as the rate constants for dissociating $Zn^{2+}$ and $Fe^{2+}$ from the LpxC-metal complex were comparable (0.03 and 0.067 $s^{-1}$, respectively) despite the large differential in binding affinity (60 ± 20 pM and 112 ± 43 nM, respectively).[33] HDAC8 also showed similar dissociation rate constants for $Zn^{2+}$ and $Fe^{2+}$ (0.0006 and 0.001 $s^{-1}$, respectively) while it has significantly different binding affinity for $Zn^{2+}$ and $Fe^{2+}$ (5 pM and 0.2 μM, respectively).

Mutation of M274 to a smaller side chain (M274A) or replacement with carboxylate group (M274E) both showed a similar 10-fold decrease in binding affinity for $Zn^{2+}$. Remarkably, substitution of Met with Gln (M274Q) resulted in a 100-fold decrease in binding affinity for $Zn^{2+}$ with only a 3-fold decrease in the $Fe^{2+}$ affinity. Similar behavior was observed with carbonic anhydrase II (CAII) for alteration of E117 that forms a hydrogen bond with the H119 zinc ligand.

In the E117Q CAII variant the amide side chain is a hydrogen bond donor that preferentially stabilizes the H119-histidinate-$Zn^{2+}$ interaction. The alteration of a negatively charged metal ligand in CAII profoundly decreased catalytic activity and increased the protein-zinc equilibration kinetics[21]. A similar hydrogen bond polarity reversal has been proposed in the D102N variant of the catalytic triad of the serine protease trypsin where the activity is reduced 4 orders of magnitude. These alterations have modest effects on the active site structure but large effects on the electrostatic environment.[21,44,45]

Surprisingly no measurable $Zn^{2+}$ binding was observed for the F208A mutant using the flSAHA assay. This could reflect a dramatic decrease in the binding affinity of F208A for $Zn^{2+}$ (>200-fold) or the inability of flSAHA to bind to $Zn^{2+}$-substituted F208A. This latter explanation is less likely since the $Fe^{2+}$ affinity of the F208A mutant, measured using the flSAHA assay, is comparable to the WT $Fe^{2+}$ affinity. Loss of zinc affinity would explain the complete absence of catalytic activity of the $Zn^{2+}$-F208A mutant (Table 3).

Most of the mutations in the second shell have little effect on the dissociation rate constant ($k_{off}$) for $Zn^{2+}$ and $Fe^{2+}$ despite significant decreases the metal dissociation constant ($K_D$). This lack of correlation between $k_{off}$ and $K_D$ provide additional evidence for multiple steps in the metal association mechanism where $k_{off}$ is mainly limited by a conformational change rather than the metal-ligand interaction. In contrast, the F207A mutation has a larger effect on $k_{off}$ (7- and 37-fold for $Zn^{2+}$ and $Fe^{2+}$, respectively) than on $K_D$ (3- and 9-fold for $Zn^{2+}$ and $Fe^{2+}$, respectively). These data indicate that the M274 and F207A mutations alter different steps in the metal binding pathway. These data also suggest that exchange of the protein metal ligands is at least partially rate-limiting in $Zn^{2+}$/$Fe^{2+}$ dissociation for F207A variant, indicating that the conformational rearrangement that limits zinc dissociation for WT HDAC8 is accelerated by the F207A mutation.

This suggests that rearrangement of F207 occurs during dissociation of metal from wild-type HDAC8 or that the enhanced solvent access in this mutant facilitates exchange of the protein metal ligands with solvent water, resulting in an increased rate constant for $Zn^{2+}/Fe^{2+}$ dissociation.

Overall, mutations in second shell residues decreased the affinity for zinc more than iron. Interestingly, the ratio of Fe/Zn specificity ($K_D^{Fe}/K_D^{Zn}$) varied by 50-fold, from 1.7 x $10^{-5}$ for wild-type to 8.2 x $10^{-4}$ for the M274Q variant. (Figure 7) When Fe/Zn specificity ($K_D^{Fe}/K_D^{Zn}$) for WT was normalized to 1, metal selectivity for M274Q was calculated as ~50. Notably, F208A was estimated to be more than 150. This could be due to the total loss of binding affinity for $Zn^{2+}$-bound HDAC8 structural conformation or the decreased affinity for flSAHA which leads to significantly weak $K_D$ for $Zn^{2+}$.

**Figure 3.7** $Fe^{2+}$ / $Zn^{2+}$ selectivity profiles of HDAC8 second shell mutants. The $K_D$ for metal in HDAC8 was measured at 30 °C as described in "Materials and Methods" and ratio of $K_D^{Zn}$ to $K_D^{Fe}$ was calculated. Those are normalized to the ratio of $K_D$ values for WT enzyme.

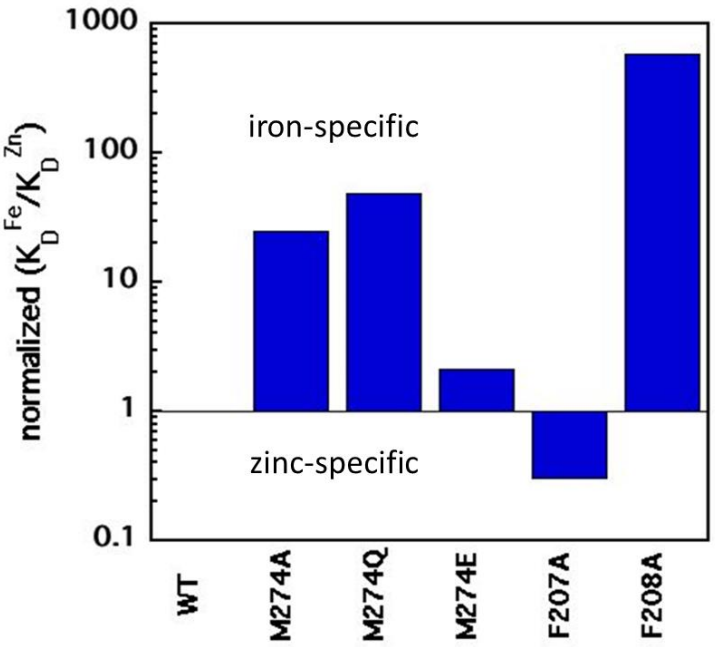

However, F207A showed metal selectivity of <1, implying that these variants had more preference for $Fe^{2+}$ than $Zn^{2+}$. This may be utilized for to the development of protein-based iron sensors using FRET. This mutagenesis study showed that the contribution of each ligand residue in second shell to metal binding, and generated a series of mutants with varying binding affinity and kinetics for $Zn^{2+}$ and $Fe^{2+}$.

*Development of iron sensor*

Iron is the most abundant transition metal in cells; the total cellular concentration is estimated to be approximately 200 μM.[46] Iron is involved in numerous cellular processes from metabolism, electron transport, and DNA synthesis, where disruption of iron regulation has been linked to disorders such as anemia, hemochromatosis, and Alzheimer's.[47,48] Effective fluorescent probes for imaging iron ions in living cellular environments is needed to measure the free iron concentration, leading to a better understanding of biological function and regulation. In the last several years, a series of probes have been developed for $Fe^{2+}$ and $Fe^{3+}$ that may allow new discoveries regarding cellular iron homeostasis.[49–52]

The majority of reported fluorogenic probes for iron imaging in living cells work through a turn-off response, such as Phen Green SK and calcein.[52–54] However, no endogenous biological stimulations were reported in this work. Additionally, these sensors show significant interference from other divalent metal ions, including $Cu^{2+}$, $Ni^{2+}$ and $Co^{2+}$. Furthermore, their utility for cellular imaging experiments has not been established.

One goal of this research was the development of a series of HDAC8 variants with significantly improved properties for sensing iron in cells. Indeed the second shell mutants alter the specificity of HDAC8 for $Fe^{2+}$ and $Zn^{2+}$. In particular, the F208A variant of HDAC8 is a

$Fe^{2+}$-specific protein, binding $Zn^{2+}$ with a $K_D$ >1 nM and $Fe^{2+}$ with a $K_D$ of 0.2 μM. These mutants can be used to develop a sensor to measure readily exchange ion concentrations from a FRET signal between a red fluorescent protein, TagRFP, fused to the C-terminus of HDAC8 as the FRET acceptor and a fluorescein-labeled SAHA (flSAHA) bound to metallated HDAC8 as the donor. Using this construct, the observed FRET/TagRFP fluorescence ratio should reflect metal-bound HDAC8 and vary with the free metal ion concentration. This should allow determination of the readily exchange metal ion concentrations in cells from a comparison of the FRET/TagRFP fluorescence ratio to a metal calibration curve. A similar approach has already proven feasible for sensing free zinc in cells using CAII variants. T199A, Q92A and WT CAII with TagRFP exhibited picomolar apparent affinities for zinc as measured in *E. coli* at pH 7.6, and were sensitive enough to detect subtle differences in intracellular free zinc concentrations.[55] Herein, we demonstrated the availability of HDAC8 variants with altered selectivity for both metals suggesting that iron-specific sensors could be made.

**REFERENCES**


(1) Choudhary, C., Kumar, C., Gnad, F., Nielsen, M. L., Rehman, M., Walther, T. C., Olsen, J. V, and Mann, M. (2009) Lysine acetylation targets protein complexes and co-regulates major cellular functions. *Science (80-. ). 325*, 834–40.

(2) Waltregny, D., Glénisson, W., Tran, S. L., North, B. J., Verdin, E., Colige, A., and Castronovo, V. (2005) Histone deacetylase HDAC8 associates with smooth muscle alpha-actin and is essential for smooth muscle cell contractility. *FASEB J. 19*, 966–8.

(3) Buggy, J. J., Sideris, M. L., Mak, P., Lorimer, D. D., McIntosh, B., and Clark, J. M. (2000) Cloning and characterization of a novel human histone deacetylase, HDAC8. *Biochem. J. 350 Pt 1*, 199–205.

(4) Hu, E., Chen, Z., Fredrickson, T., Zhu, Y., Kirkpatrick, R., Zhang, G. F., Johanson, K., Sung, C. M., Liu, R., and Winkler, J. (2000) Cloning and characterization of a novel human class I histone deacetylase that functions as a transcription repressor. *J. Biol. Chem. 275*, 15254–64.

(5) Deardorff, M. a, Bando, M., Nakato, R., Watrin, E., Itoh, T., Minamino, M., Saitoh, K., Komata, M., Katou, Y., Clark, D., Cole, K. E., De Baere, E., Decroos, C., Di Donato, N., Ernst, S., Francey, L. J., Gyftodimou, Y., Hirashima, K., Hullings, M., Ishikawa, Y., Jaulin, C., Kaur, M., Kiyono, T., Lombardi, P. M., Magnaghi-Jaulin, L., Mortier, G. R., Nozaki, N., Petersen, M. B., Seimiya, H., Siu, V. M., Suzuki, Y., Takagaki, K., Wilde, J. J., Willems, P. J., Prigent, C., Gillessen-Kaesbach, G., Christianson, D. W., Kaiser, F. J., Jackson, L. G., Hirota, T., Krantz, I. D., and Shirahige, K. (2012) HDAC8 mutations in Cornelia de Lange syndrome affect the cohesin acetylation cycle. *Nature 489*, 313–7.

(6) Vannini, A., Volpari, C., Gallinari, P., Jones, P., Mattu, M., Carfí, A., De Francesco, R., Steinkühler, C., and Di Marco, S. (2007) Substrate binding to histone deacetylases as shown by the crystal structure of the HDAC8-substrate complex. *EMBO Rep. 8*, 879–84.

(7) Dowling, D. P., Gattis, S. G., Fierke, C. A., and Christianson, D. W. (2010) Structures of metal-substituted human histone deacetylase 8 provide mechanistic inferences on biological function . *Biochemistry 49*, 5048–56.

(8) Bozym, R. a, Thompson, R. B., Stoddard, A. K., and Fierke, C. a. (2006) Measuring picomolar intracellular exchangeable zinc in PC-12 cells using a ratiometric fluorescence biosensor. *ACS Chem. Biol. 1*, 103–11.

(9) MacKenzie, E. L., Iwasaki, K., and Tsuji, Y. (2008) Intracellular iron transport and storage: from molecular mechanisms to health implications. *Antioxid. Redox Signal. 10*, 997–1030.

(10) Gantt, S. L., Gattis, S. G., and Fierke, C. A. (2006) Catalytic activity and inhibition of human histone deacetylase 8 is dependent on the identity of the active site metal ion. *Biochemistry 45*, 6170–8.

(11) Imlay, J. a. (2008) Cellular defenses against superoxide and hydrogen peroxide. *Annu. Rev. Biochem. 77*, 755–76.

(12) Li, J.-Y., Chen, L.-L., Cui, Y.-M., Luo, Q.-L., Li, J., Nan, F.-J., and Ye, Q.-Z. (2003) Specificity for inhibitors of metal-substituted methionine aminopeptidase. *Biochem. Biophys. Res. Commun. 307*, 172–179.

(13) Christianson, D. W., and Cox, J. D. (1999) Catalysis by metal-activated hydroxide in zinc and manganese metalloenzymes. *Annu. Rev. Biochem. 68*, 33–57.

(14) Krebs, J. F., Ippolito, J. a, Christianson, D. W., and Fierke, C. a. (1993) Structural and functional importance of a conserved hydrogen bond network in human carbonic anhydrase II. *J. Biol. Chem. 268*, 27458–66.

(15) Kiefer, L. L., Krebs, J. F., Paterno, S. a, and Fierke, C. a. (1993) Engineering a cysteine ligand into the zinc binding site of human carbonic anhydrase II. *Biochemistry 32*, 9896–900.

(16) Kiefer, L. L., and Fierke, C. a. (1994) Functional characterization of human carbonic anhydrase II variants with altered zinc binding sites. *Biochemistry 33*, 15233–40.

(17) Lesburg, C. A., and Christianson, D. W. (1995) X-ray Crystallographic Studies of Engineered Hydrogen Bond Networks in a Protein-Zinc Binding Site. *J. Am. Chem. Soc.* 6838–6844.

(18) Kiefer, L. L., Paterno, S. A., Fierke, C. A., and Carolina, N. (1995) Hydrogen Bond Network in the Metal Binding Site of Carbonic Anhydrase Enhances Zinc Affinity and Catalytic Efficiency ? *J. Am. Chem. Soc. 117*, 6831–6837.

(19) Ippolito, J. a, Baird, T. T., McGee, S. a, Christianson, D. W., and Fierke, C. a. (1995) Structure-assisted redesign of a protein-zinc-binding site with femtomolar affinity. *Proc. Natl. Acad. Sci. U. S. A. 92*, 5017–21.

(20) Jackman, J. E., Merz, K. M., and Fierke, C. a. (1996) Disruption of the active site solvent network in carbonic anhydrase II decreases the efficiency of proton transfer. *Biochemistry 35*, 16421–8.

(21) Huang, C. C., Lesburg, C. a, Kiefer, L. L., Fierke, C. a, and Christianson, D. W. (1996) Reversal of the hydrogen bond to zinc ligand histidine-119 dramatically diminishes catalysis and enhances metal equilibration kinetics in carbonic anhydrase II. *Biochemistry 35*, 3439–3446.

(22) Liljas A, Kannan KK, Bergstén PC, Waara I, Fridborg K, Strandberg B, Carlbom U, Järup L, Lövgren S, P. M. (1972) Crystal structure of human carbonic anhydrase C. *Nat New Biol 235*, 131–137.

(23) Yamashita, M. M., Wesson, L., Eisenman, G., and Eisenberg, D. (1990) Where metal ions bind in proteins. *Proc. Natl. Acad. Sci. U. S. A. 87*, 5648–52.

(24) Somoza, J. R., Skene, R. J., Katz, B. a, Mol, C., Ho, J. D., Jennings, A. J., Luong, C., Arvai, A., Buggy, J. J., Chi, E., Tang, J., Sang, B.-C., Verner, E., Wynands, R., Leahy, E. M., Dougan, D. R., Snell, G., Navre, M., Knuth, M. W., Swanson, R. V, McRee, D. E., and Tari, L. W. (2004) Structural snapshots of human HDAC8 provide insights into the class I histone deacetylases. *Structure 12*, 1325–34.

(25) Vannini, A., Volpari, C., Filocamo, G., Casavola, E. C., Brunetti, M., Renzoni, D., Chakravarty, P., Paolini, C., De Francesco, R., Gallinari, P., Steinkühler, C., and Di Marco, S. (2004) Crystal structure of a eukaryotic zinc-dependent histone deacetylase, human HDAC8, complexed with a hydroxamic acid inhibitor. *Proc. Natl. Acad. Sci. U. S. A. 101*, 15064–15069.

(26) Marek, M., Kannan, S., Hauser, A.-T., Moraes Mourão, M., Caby, S., Cura, V., Stolfa, D. a, Schmidtkunz, K., Lancelot, J., Andrade, L., Renaud, J.-P., Oliveira, G., Sippl, W., Jung, M., Cavarelli, J., Pierce, R. J., and Romier, C. (2013) Structural basis for the inhibition of histone deacetylase 8 (HDAC8), a key epigenetic player in the blood fluke Schistosoma mansoni. *PLoS Pathog. 9*, 1–15.

(27) Sankaranarayanapillai, M., Tong, W. P., Maxwell, D. S., Pal, A., Pang, J., Bornmann, W. G., Gelovani, J. G., and Ronen, S. M. (2006) Detection of histone deacetylase inhibition by noninvasive magnetic resonance spectroscopy. *Mol. Cancer Ther. 5*, 1325–34.

(28) Vijayakumar, B., Umamaheswari, A., Puratchikody, A., and Velmurugan, D. (2011) Selection of an improved HDAC8 inhibitor through structure-based drug design. *Bioinformation 7*, 134–41.

(29) Residues, H. C., Hunt, J. A., Ahmed, M., and Fierke, C. A. (1999) Metal Binding Specificity in Carbonic Anhydrase Is Influenced by Conserved. *Biochemistry 38*, 9054–9062.

(30) Mccall, K. A., Huang, C., and Fierke, C. A. (2000) Function and Mechanism of Zinc Metalloenzymes. *J. Nutr. 130*, 1437–1446.

(31) McCall, K. a, and Fierke, C. a. (2004) Probing determinants of the metal ion selectivity in carbonic anhydrase using mutagenesis. *Biochemistry 43*, 3979–3986.

(32) Bozym, R., Hurst, T. K., Westerberg, N., Stoddard, A., Fierke, C. a, Frederickson, C. J., and Thompson, R. B. (2008) Determination of zinc using carbonic anhydrase-based fluorescence biosensors. *Methods Enzymol.* 1st ed., pp 287–309. Elsevier Inc.

(33) Gattis, S. G., Hernick, M., and Fierke, C. a. (2010) Active site metal ion in UDP-3-O-((R)-3-hydroxymyristoyl)-N-acetylglucosamine deacetylase (LpxC) switches between Fe(II) and Zn(II) depending on cellular conditions. *J. Biol. Chem. 285*, 33788–33796.

(34) Finnin, M. S., Donigian, J. R., Cohen, A., Richon, V. M., Rifkind, R. A., Marks, P. A., Breslow, R., and Pavletich, N. P. (1999) Structures of a histone deacetylase homologue bound to the TSA and SAHA inhibitors. *Nature 401*, 188–193.

(35) Hernick, M., and Fierke, C. a. (2005) Zinc hydrolases: the mechanisms of zinc-dependent deacetylases. *Arch. Biochem. Biophys. 433*, 71–84.

(36) Smith, B. C., and Denu, J. M. (2007) Acetyl-lysine analog peptides as mechanistic probes of protein deacetylases. *J. Biol. Chem. 282*, 37256–65.

(37) Rajagopalan, P. T. R., and Yu, X. C. (2008) Peptide Deformylase : A New Type of Mononuclear Iron Protein. *J. Am. Chem. Soc. 7863*, 12418–12419.

(38) Tripp, B. C., Bell, C. B., Cruz, F., Krebs, C., and Ferry, J. G. (2004) A role for iron in an ancient carbonic anhydrase. *J. Biol. Chem. 279*, 6683–7.

(39) Irving, H. Williams, R. J. P. (1948) Order of stability of metal complexes. *Nature 162*, 746–747.

(40) Vinkenborg, J. L., Nicolson, T. J., Bellomo, E. a, Koay, M. S., Rutter, G. a, and Merkx, M. (2009) Genetically encoded FRET sensors to monitor intracellular Zn2+ homeostasis. *Nat. Methods 6*, 737–40.

(41) MacKenzie, E. L., Iwasaki, K., and Tsuji, Y. (2008) Intracellular iron transport and storage: from molecular mechanisms to health implications. *Antioxid. Redox Signal. 10*, 997–1030.

(42) Cells, M., Epsztejn, S., Kakhlon, O., Glickstein, H., Breuer, W., and Cabantchik, Z. I. (1997) Fluorescence Analysis of the Labile Iron Pool of. *Anal. Biochem. 40*, 31–40.

(43) Dudev, T., and Lim, C. (2008) Metal binding affinity and selectivity in metalloproteins: insights from computational studies. *Annu. Rev. Biophys. 37*, 97–116.

(44) Sprang, S., Standing, T., Fletterick, R. J., Stroud, R. M., Finer-Moore, J., Xuong, N. H., Hamlin, R., Rutter, W. J., and Craik, C. S. (1987) The three-dimensional structure of Asn102 mutant of trypsin: role of Asp102 in serine protease catalysis. *Science 237*, 905–9.

(45) Craik, C. S., Roczniak, S., Largman, C., and Rutter, W. J. (1987) The Catalytic Role of the Active Site Aspartic Acid in. *Science (80-. ). 237*, 909–913.

(46) Outten, C. E., and O'Halloran, T. V. (2001) Femtomolar sensitivity of metalloregulatory proteins controlling zinc homeostasis. *Science (80-. ). 292*, 2488–92.

(47) Barnham, K. J., Masters, C. L., and Bush, A. I. (2004) Neurodegenerative diseases and oxidative stress. *Nat. Rev. Drug Discov. 3*, 205–14.

(48) Hider, R. C., and Kong, X. (2013) Iron speciation in the cytosol: an overview. *Dalton Trans. 42*, 3220–9.

(49) Chen, J.-L., Zhuo, S.-J., Wu, Y.-Q., Fang, F., Li, L., and Zhu, C.-Q. (2006) High selective determination iron(II) by its enhancement effect on the fluorescence of pyrene-tetramethylpiperidinyl (TEMPO) as a spin fluorescence probe. *Spectrochim. Acta. A. Mol. Biomol. Spectrosc. 63*, 438–43.

(50) García-Beltrán, O., Mena, N., Yañez, O., Caballero, J., Vargas, V., Nuñez, M. T., and Cassels, B. K. (2013) Design, synthesis and cellular dynamics studies in membranes of a new coumarin-based "turn-off" fluorescent probe selective for Fe2+. *Eur. J. Med. Chem. 67*, 60–3.

(51) Hirayama, T., Okuda, K., and Nagasawa, H. (2013) A highly selective turn-on fluorescent probe for iron(ii) to visualize labile iron in living cells. *Chem. Sci. 4*, 1250–1256.

(52) Petrat, F., Rauen, U., and de Groot, H. (1999) Determination of the chelatable iron pool of isolated rat hepatocytes by digital fluorescence microscopy using the fluorescent probe, phen green SK. *Hepatology 29*, 1171–9.

(53) Breuer, W., Epsztejn, S., Millgram, P., and Cabantchik, I. Z. (1995) Transport of iron and other transition metals into cells as revealed by a fluorescent probe. *Am. J. Physiol. 268*, C1354–61.

(54) Petrat, F., Groot, H. D. E., and Rauen, U. (2001) Subcellular distribution of chelatable iron: a laser scanning microscopic study in isolated hepatocytes and liver endothelial cells. *Biochem. J 69*, 61–69.

(55) Wang, D., Hurst, T. K., Thompson, R. B., and Fierke, C. A. (2011) Genetically encoded ratiometric biosensors to measure intracellular exchangeable zinc in Escherichia coli. *J. Biomed. Opt. 16*, 087011.

# CHAPTER 4

# INVESTIGATING THE HDAC8-PCBP1 INTERACTION BY KINETIC AND MASS-SPECTROMETRIC ANALYSIS[1]

## INTRODUCTION

Histone deacetylase 8 (HDAC8) catalyzes the hydrolysis of ε-*N*-acetyl lysine residues on proteins acetylated by histone acetyltransferases.[1] It serves as an essential epigenetic regulatory enzyme in gene transcription.[2] Upon its discovery, this enzyme was identified as a Zn(II)-dependent metalloenzyme.[3] However, *in vitro* activity and binding affinity studies suggest that Fe(II) could be the native metal cofactor *in vivo*.[4] Additionally, HDAC activity in cell lysates is sensitive to oxygen exposure.[4] These data suggest that HDAC8 might be activated by either Zn(II) or Fe(II), depending on the cellular environment. The readily exchangeable concentration of cellular Zn(II) fluctuates under a variety of conditions, such as upon generation of reactive oxygen species.[4] The determinants of Fe(II) / Zn(II) metal selectivity of proteins in a cell are currently unclear and could be facilitated by interactions with other proteins, such as metallochaperones.

In cells, a variety of evidence suggests that the majority of class I HDAC enzymes form complexes with other proteins. HDAC isozymes - 1 and 2 associate with the large protein complexes Mi2/NURD (nucleosome remodelling and histone deacetylase), SIN3A and Co-REST (co-repressor for element-1-silencing transcription factor) *in vivo* (Figure 1).[5,6,7] Given that HDAC8 is a class I enzyme, it is possible that other proteins may form complexes with HDAC8,



[1]All Co-IP experiments were carried out by the Philpott lab at NIH.

which could affect the biological function of the enzyme, including altering the metal selectivity to alter the activity of HDAC8 in the cell.

**Figure 4.1** Three main HDAC1/2-containing complexes. Mammalian Class-I HDAC1 and HDAC2 are abundant, ubiquitously expressed and share a high degree of sequence similarity. They are located almost exclusively in the nucleus as part of multi-protein complexes which regulate gene expression by modulating chromatin structure. Stable HDAC8 complexes have not been well-characterized, although mass spectrometry of HDAC8 pull-downs have suggested some proteins that complex with HDAC8[8].

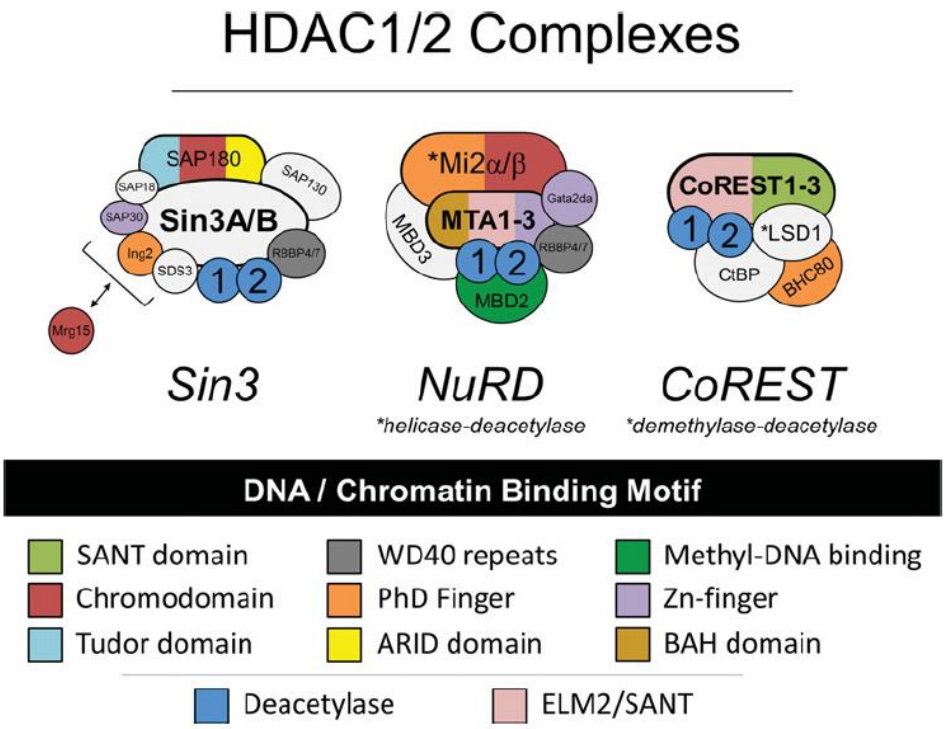


In fact, mass spectrometric analysis of HDAC8 pull-downs suggests a number of binding parterners.[8] This possibility raises multiple questions, including whether these interacting proteins alter the metal status of HDAC8.

The mechanism by which HDAC8 recognizes and incorporates the cognate metal ions (Zn(II) or Fe(II)) in the cell is unknown. Metal incorporation for a number of metalloproteins is facilitated by metallochaperones. For example, cytosolic copper and nickel chaperones have

been described for cytochrome c oxidase and urease activation, respectively.[9,10] No zinc-specific metallochaperones have been identified so far. However, several potential iron-specific metallochaperones are being investigated for roles in iron homeostasis, particularly in the assembly of Fe-S clusters.[11–14,15–17] These chaperone candidates include the IscA family of proteins and frataxin for delivery of iron for iron-sulfur cluster assembly.[18,19] Furthermore, in 2008, the Philpott lab reported that poly r(C)-binding protein 1 (PCBP1) can function as a cytosolic iron chaperone in the delivery of iron to ferritin, a cellular iron storage protein.[20]

A recent mass spectrometric analysis led to the first proposed global protein interaction network for all 11 human HDACs, including HDAC8.[8] This interactome network was assembled from protein–protein interactions in human CEM T cells. The study identified HDAC8 associations with multiple members of the cohesin complex (SMC1A, SMC3, and STAG2) which are involved in sister chromatid segregation during mitosis. Additionally, this analysis suggested that HDAC8 might interact with the PCBP family of iron-metallochaperones.[20] However, based on statistical modelling using I-DIRT and SAINT, the HDAC8-PCBP1/2 interactions were characterized as non-specific.

Within the PCBP family, PCBP1 is one of the four homologous proteins that include PCBP2, PCBP3, and PCBP4. This family of proteins bind RNA and are ubiquitously expressed in mammalian cells in both the cytosol and the nucleus.[21] In a genetic screen using budding yeast, human PCBP1 was identified by the Philpott lab as an iron chaperone that delivers iron to human ferritin.[20] Additional functional assays in yeast indicate that PCBP1 facilitates the incorporation of iron into ferritin through a direct protein-protein interaction.[22] Subsequent studies have identified additional targets for iron delivery through the formation of a hetero-oligomeric complex of PCBP1 and 2: the prolyl hydroxylases (PHDs) and deoxyhypusine hydroxylase

(DOHH).[23].[22] This study demonstrates that the two chaperones function cooperatively to deliver iron to several hydroxylases.[24] The full range of proteins that the PCBP family may function as metallochaperones is currently unexplored.

Herein we investigate the interaction between HDAC8 and the recently identified Fe(II) chaperone, poly (rC) binding protein 1 (PCBP1), to evaluate whether this family of metallochaperones plays a role in the formation of cellular Fe(II)-HDAC8. We demonstrate that addition of PCBP1 to HDAC8 decreases the metal dissociation rate constant for Fe(II) but not Zn(II) and alters the catalytic activity of Fe(II)-HDAC8. To evaluate complex formation we coupled Nano-electrospray ionization (nano-ESI) mass spectrometry (MS)[25] with ion mobility mass spectrometry (IM-MS) to gain information about both stoichiometry and geometry of the protein complexes (Figure 2).[26] Using IM-MS under native conditions, we demonstrate the formation of a HDAC8-PCBP1 complex. Furthermore, co-immunoprecipitation experiments from T-Rex 293 cells demonstrate the formation of cellular complexes. Taken together, these data suggest that PCBP1 functions as a metallochaperone for the formation of Fe(II)-HDAC8.

**Figure 4.2** Scheme of ion mobility-mass spectrometry data acquisition. Ions are generated at the ion source (lower left), and are allowed to drift in an ion guide filled with neutral gas molecules under the influence of an electric field. The ions migrate through this region according to their size-to-charge ratio. They are then injected into a time-of-flight (ToF) mass analyzer under vacuum for mass-to-charge (*m/z*) analysis. The resulting data are 3-dimensional, containing ion intensity, size, and mass information. The various dimensions of the data can be shown as a contour plot (middle, bottom), or 2D selections in drift time or m/z (lower right).

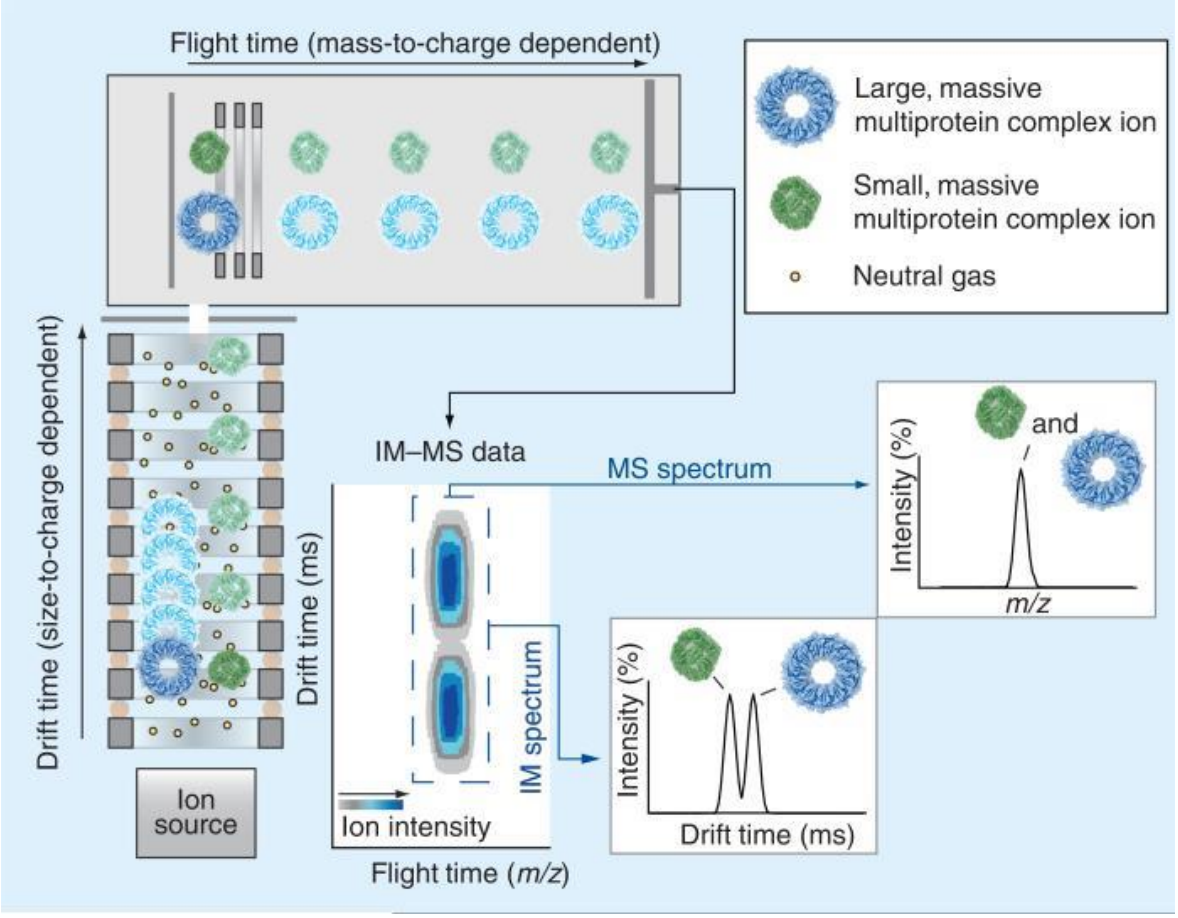

## MATERIALS AND METHODS

*General*

All solutions were prepared in "metal-free" plasticware, with reagents that do not contain extraneous metal ions and/or were treated with Chelex (Biorad). The metal content of solutions, reagents and proteins was measured using inductively coupled plasma mass spectrometry (ICP-MS; Dr. Ted Huston, Univ. of Michigan). HDAC8 was over-expressed in BL21(DE3) *E. coli* transformed with pET-derived expression plasmids and purified according to published procedures.[4] All work with Fe(II) was performed anaerobically in a $N_2/H_2$ atmosphere glove bag from Coy Labs. Dissolved oxygen was removed from $ddH_2O$ by sparging with argon and incubating for 24 h in the glove box. $FeCl_2$ was dissolved in anaerobic $ddH_2O$ and used within 1 h. Enzyme and substrate (<10 μl) were each equilibrated in the glove box for at least 2 h at 4 ℃ before Fe(II) was added; Fe(II) was incubated with apo-HDAC8 for 1hr prior to beginning each assay.

*Co-IP using anti-flag resin and Western blots*

(All Co-IP were carried out by the Philpott lab, NIH)

Tetracycline-inducible flag-tagged PCBP1 or PCBP2 constructs (single copy) were stably transfected into T-REx-293 cells via the FlpIn recombinase system from Invitrogen. Based on the western blots, the level of flag-PCBP1 is about the same as the amount of native PCBP1, but this effectively doubles the concentration of PCBP1 in the cell.

For western blots, proteins were transferred to a nitrocellulose membrane via iBlot (Invitrogen) after separation using 4~12% Bis-Tris NuPAGE. The membrane was blocked with 5%

milk in phosphate buffered saline (PBS) and blotted with either anti-HDAC8 (sc-11405 from Santa Cruz, diluted 1:200) or anti-PCBP1[20] and the respective secondary antibodies (anti-rabbit IgG and anti-chicken IgY from Li-Cor) in PBS-T plus 0.02% sodium azide. Images of the blots were produced using a Li-Cor imaging system.

*Expression and purification of apoPCBP1*

Chemically competent BL21(DE3) cells were transformed with pCDF encoding $His_6$SUMO-tagged PCBP1.[22] Starter cultures (10 mL) were inoculated by addition of a single colony and grown in LB media with 100 μg/ μl streptomycin for 5 hr at 37 ℃ and 250 rpm. The starter culture was diluted (1:1000) into 2 L of LB with appropriate antibiotics in a 6 L culture flask. The temperature was decreased to 15 ℃ at induction. Expression was induced by addition of 0.1 mM IPTG,and the cells were incubated overnight at 15 ℃. Cells from the 2 L growth were harvested, resuspended in 30 ml buffer A (20 mM Tris [pH 7.9], 250 mM NaCl, 30 mM imidazole, 10% glycerol, and 2.5 mM TCEP) with one EDTA-free protease inhibitor cocktail tablet (Roche). Resuspended cells were lysed using a microfluidizer. The extract was centrifuged at 6000 g for 30 min and the supernatant was loaded onto a nickel column. Protein fractionation was carried out using a linear gradient in buffer A from 30 mM to 500 mM imidazole, to buffer B (20 mM Tris [pH 7.9], 250 mM NaCl, 500 mM imidazole, 10% glycerol, 2.5 mM TCEP), with PCBP1 eluting at 110–230 mM imidazole. The $His_6$-SUMO tag was cleaved by incubating with 1 unit/μl *Saccharomyces cerevisiae* SUMO protease (Life Techonologies) overnight at 4 ℃. The protein was buffer exchanged using dialysis with buffer A before passing over the nickel column a second time to separate the tag from the untagged protein. The protein was dialyzed overnight at 4 ℃ first against buffer A containing 1 mM EDTA to remove metals and then against buffer A

to remove EDTA. Finally, the protein was fractionated on a PD-10 column to remove any remaining EDTA. Apo-PCBP1 was concentrated to 100 – 200 μM, flash-frozen and stored at –80℃.

*Measurement of HDAC8 activity as a function of [apoPCBP1]*

Metallated HDAC8 was prepared by incubating apo-HDAC8 (10 μM) with stoichiometric Zn(II) or 1 – 2 equivalents of Fe(II) for 1 hr at 4 ℃. To analyze the effects of PCBP1 on HDAC8 catalytic activity, 2 μM Zn(II)- or Fe(II)-HDAC8 was incubated with varying concentrations of apo-PCBP1 (1 – 35 μM) in assay buffer (20 mM HEPES, pH 8, 3 mM KCl, 137 mM NaCl) for 1 min at 25 ℃ and then either immediately diluting the enzyme and assaying the catalytic activity, and then assaying the catalytic activity of HDAC8. In these assays, the final enzyme concentration was 0.5 μM with 50 μM Fluor de Lys p53 substrate. At various times the reaction was quenched by the addition of Trichostatin A (TSA) and trypsin which catalyzed cleavage of the coumarin group from the product. The initial rate for deacetylation was measured from the linear change in the fluorescent ratio (product : ex = 340 nm, em = 450 nm over substrate : ex = 340 nm, em = 380 nm)) over time. The initial rates were plotted as a function of the incubation time at pH 8 and fit to the following first order exponential equation. $Y=A * \exp(-k_{off} * X) + c$

*Measurement of metal (Zn(II) / Fe(II)) dissociation rate constant ($k_{off}$)*

The first order rate constant for dissociation of Zn(II) or Fe(II) bound to HDAC8 in the absence or presence of apoPCBP1 was measured by the time-dependent loss of catalytic activity upon incubation with EDTA. HDAC8 reconstituted with stoichiometric Zn(II) or Fe(II) was

incubated with varying concentrations of apoPCBP1 (0 – 10 μM) to form a complex followed by dilution into assay buffer containing 1 mM EDTA. At various times (0 – 60 min) an aliquot was diluted 10-fold into assay buffer containing the Fluor de Lys p53 substrate. At various times, the reactions were quenched by the addition of TSA and Enzo Developer II and the linear initial rate measured. The dissociation rate constant was calculated from a fit of a first order exponential equation to the time-dependent decrease in the initial rate after dilution into EDTA. The observed rate constants are not dependent on the concentration of EDTA (0 – 5 mM).

*Sample preparation for IM-MS analysis*

ApoHDAC8 and apoPCBP1 at each 30 μM were prepared in 20 mM HEPES, pH 8. The samples were then buffer-exchanged using a Micro Bio-Spin 6 column (Bio-Rad, Hercules, CA) equilibrated with 500 mM aqueous ammonium acetate, pH 7 just prior to IM-MS analysis.[27] Both of buffer-exchanged proteins were incubated at 25 ℃ for 10 min to form apoHDAC8-apoPCBP1 complex.

*Synapt G2 Instrumentation*

All experiments were performed on a Synapt G2 ESI quadrupole-ion mobilioty separation- time-of-flight (Q-IMS-TOF) mass spectrometer (Waters,Milford, MA), equipped with a nanoflow ESI source in collaboration with the laboratory of Professor Brandon Ruotolo.[28] The ‘tri-wave’ region of the instrument consists of three main traveling-wave ion guide sections, enclosed from the main vacuum system, coupled to smaller traveling-wave ion guides that operate within the main vacuum system for increased conductance of the gas load within the enclosed regions of the instrument. All mass spectra were collected under positive ion mode

using cesium iodide for calibration. A capillary voltage of 1.68kV was applied. Sampling cone voltage and source temperature were maintained at 50V and 20 ℃ during signal acquisition. Backing pressure was at 7-8 mbar. To optimize the mass resolution, a trap collision voltage ranging from 30-50V were applied, with argon being used in the trap region as the collision gas, with a pressure of $2.56e^{-2}$ mbar. The ion mobility measurements were carried out using $N_2$ as the mobility buffer gas, at a pressure of 3.5 mbar. Data acquisition and processing were carried out using MassLynx V4.1 software.[29]

**RESULTS**

*In-vivo Co-Immunoprecipitation* (All Co-IP were carried out by Philpott lab at NIH)

Since PCBP1 functions as a metallochaperone for a number of iron(II)-dependent enzymes[22,23,30], we proposed that this protein might also mediate delivery of iron to HDAC8. As a first step, we collaborated with the Philpott lab to investigate the formation of an HDAC8-PCBP1 complex in cells using co-immunoprecipitation. The Philpott laboratory constructed T-REx 293 cell lines containing either an empty vector (EV; pcDNA5) or a vector expressing flag-epitope-tagged PCBP1 under the regulation of tetracycline. They were stably transfected, i.e., the FP1 construct was integrated into the chromosome, using the Flp-In system. The T-Rex 293 cells were subject to iron supplementation by addition of ferric ammonium citrate (FAC) or iron chelation by incubation with deferoxamine (DFO) for 5 hr, 16 hr, or no treatment. The flag-tagged PCBP1 was immunoprecipitated using an anti-Flag antibody and then probed for the co-precipitation of HDAC8 using an anti-HDAC8 antibody (Figure 3). HDAC8 was detected in immunoprecipitates of flag-PCBP1 from cells expressing endogenous levels of both proteins. No

PCBP1 or HDAC8 was detected in immunoprecipitates cells containing the empty vector as a negative control. These data suggested that PCBP1 and HDAC8 physically interact in cells. Co-immunoprecipitation of PCBP1 and HDAC8 was also detected in iron-deficient (deferoxamine-treated) and iron-sufficient (ferric ammonium citrate) growth conditions. Longer incubations of cells with FAC or DFO or decreased DFO concentration did not affect the levels of immunoprecipitated HDAC8 and PCBP1. Overall, alteration of growth conditions to manipulate cellular iron levels had little effect on the total levels of PCBP1 and HDAC8 in the whole-cell lysates.

**Figure 4.3** *In vivo* pull-down data to investigate the interaction between PCBP1 and HDAC8. T-REx 293 cells containing integrated copies of empty vector (EV), FLAG-PCBP1 (FP1) under the control of a tetracycline-regulatable promoter were treated with 1 µg/ml doxycycline for 24 h. Cells were lysed using glass beads in 50 mM Tris (pH 7.4), 40 mM KCl, 1 mM PMSF, 5 mM DTT, and protease inhibitor cocktail and the lysates were subjected to Western blotting with anti-PCBP1 (Santa Cruz Biotechnology) T-REx 293 cells were treated with A) 20 µM $FeCl_3$ for 5hr, or 100 DFO for 5hr or B) 20 µM $FeCl_3$ for 16hr or 25 µM DFO for 16hr. PCBP1 was immunoprecipitated using anti-PCBP1 as a negative control. Immune complexes analyzed by western blotting for PCBP1. WCE: Whole cell extract, SN: Supernatant.

| | FAC Treatment | DFO Treatment |
|---|---|---|
| A | 20 µM , 5hr | 100 µM , 5hr |
| B | 20 µM , 16hr | 25 µM , 16hr |

- Cells : T-Rex 293 Cells with Inducible FP1 or EV + Doxycycline (1 ug/mL); 24 h
- FAC : Ferric Ammonium Citrate
- DFO : Deferoxamine

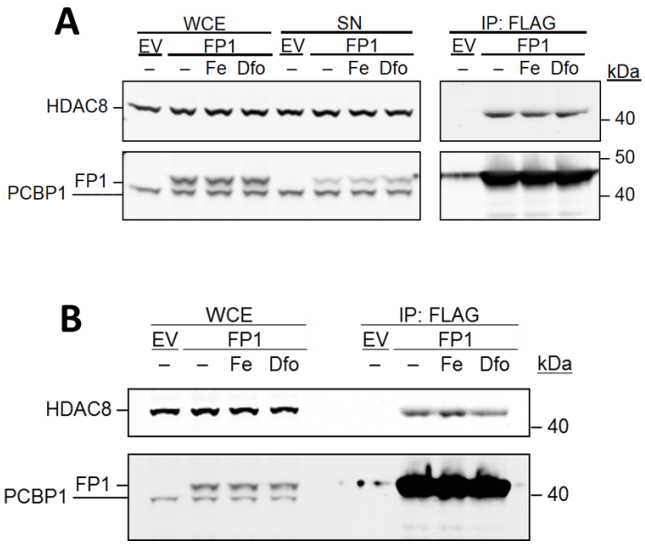

*Purification of apoPCBP1 from E.coli*

We next questioned whether PCBP1 altered the metal-dependent activation of HDAC8 *in vitro*. A $His_6$-SUMO-tagged version of PCBP1 was subcloned into a pET vector for recombinant expression in BL21(DE3) *E. coli*. Using this vector, overexpression of PCBP1 was induced by the addition of IPTG and the protein was purified to homogeneity using a procedure modified from Nandal et. al.[22]

**Figure 4.4** SDS-PAGE analysis of the purification of recombinant PCBP1. Panel A : Lane 1 – 6 are PCBP1-His fractions purified using 1st Ni-IMAC. Panel B : Lane 1 is combined fraction from 1st Ni-IMAC column (panel A, lane 1-6) and lane 2 is after incubations with SUMO protease. The red arrow shows SUMO cleaved PCBP1. Panel C : Lane 1 shows the flow-through after the 2nd Ni-IMAC column. Lane 2 is eluent from 20 mM imidazole fraction (red arrow indicates PCBP1 with correct MW) while lane 3 shows proteins eluted upon addition of 250 mM imidazole. Panel D: Lane 1 is MW markers. Lane 2 is PCBP1 after dialysis against 1 mM EDTA first and then against no EDTA. (red arrow indicates PCBP1 with correct MW)

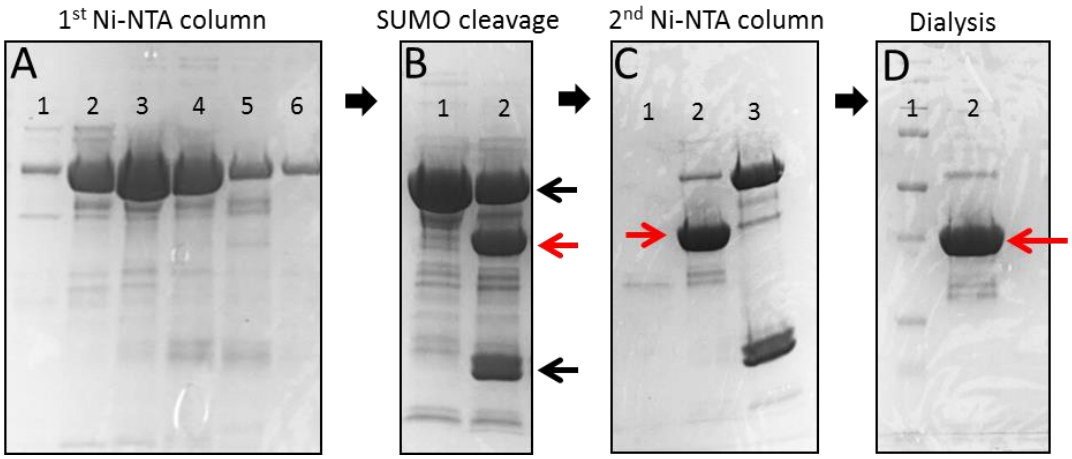


$His_6$-PCBP1 bound to an immobilized Ni(II) ion affinity chromatography (IMAC) column and was eluted from the column using a 25-500 mM imidazole gradient, as determined by SDS-PAGE and staining with Coomassie Blue (Figure 4, panel A). Next, SUMO protease was added to the combined fractions containing $His_6$-SUMO-PCBP1 to cleave the SUMO-tag (Figure 4, panel B, lanes 1 and 2) and this mixture was dialyzed overnight against 20 mM Tris buffer, pH

7. Following cleavage and dialysis, the enzyme was bound to a second immobilized Ni(II) ion affinity chromatography column, and eluted by the addition of 25 mM imidazole (Figure 4, panel C, lane 2). The protein was then dialyzed against buffer containing 1 mM EDTA to remove all metal ions followed by dialysis against buffer alone to remove EDTA (Figure 4, panel D). This procedure routinely yields apo-PCBP1 containing <0.1 mol total bound metal ion / mol enzyme (Table 1). The molecular mass of the purified protein was in accord with the size of the PCBP1 product (37.5 kDa) deduced from the amino acid sequence.

**Table 4.1** Metal ion content of apo-PCBP1. Metal-free PCBP1 was generated by dialyzing the recombinant protein with 1 mM EDTA followed by dialysis and gel filtration to removed EDTA. Metal ion content of the apo-protein sample was determined by ICP mass spectrometry. The ratio of metal ion to protein was determined by dividing the metal ion concentration, as determined by ICP mass spectrometry, by the protein concentration as determined by nanodrop.

| | molar ratio of metal : protein | | | | | |
|---|---|---|---|---|---|---|
| | Zn(II) | Fe(II) | Co(II) | Ni(II) | Cu(II) | Mn(II) |
| PCBP1 | 0.04 | 0.02 | <0.01 | 0.02 | 0.01 | <0.02 |
| Buffer | <0.01 | <0.01 | <0.01 | <0.01 | <0.01 | <0.02 |

*Measurement of metal-bound HDAC8 activity in the presence of apo-PCBP1*

We examined the effect of apo-PCBP1 on the reactivity of metal-bound HDAC8 using a steady-state kinetic assay. The initial rate for deacetylation catalyzed by HDAC8 was measured *in vitro* using the commercially available Fluor de Lys® (FdL) assay. The initial rate for deacetylation catalyzed by Fe(II)-bound HDAC8 increased ~ 2-fold upon addition of 8 μM apo-PCBP1 while higher concentrations (16 – 33 μM) of PCBP1 decrease activity (Figure 5, panel A). In contrast, incubation of apoPCBP1 with Zn(II)-bound HDAC8 has little effect on the initial rate for deacetylation.

**Figure 4.5** Measurement of the activity of Zn(II) and- Fe(II)-bound HDAC8 as a function of apo-PCBP1concentration. (a) Apo-HDAC8 (2 μM) was incubated with divalent metal ions (Fe(II) or Zn(II)) at 4 ℃ for 1 hr and then diluted to 0.5 μM by the addition of Fluor de Lys HDAC8 substrate (50 μM) at 25 ℃ in 20 mM HEPES, pH 8.0, 137 mM NaCl and 3 mM KCl in the presence of varying concentrations of apo-PCBP1. The initial rates for deacetylation were determined from the time-dependent change in fluorescence (product $\lambda_{ex}$ = 340 nm, $\lambda_{em}$ = 450 nm) and substrate ($\lambda_{ex}$ = 340 nm, $\lambda_{em}$ = 380 nm)). The observed initial rates for each metal ion were normalized to the highest initial rate for a given metal ion. (b) Apo-HDAC8 (2 μM) was incubated with excess amount of Fe(II) (5:1) at 4 ℃ for 1 hr and then diluted to 0.5 μM by the addition of Fluor de Lys HDAC8 substrate (50 μM) at 25 ℃ in 20 mM HEPES, pH 8.0, 137 mM NaCl and 3 mM KCl in the presence of varying concentrations of apo-PCBP1. The initial rates for deacetylation were determined from time-dependent changes in fluorescence, as described in (a).

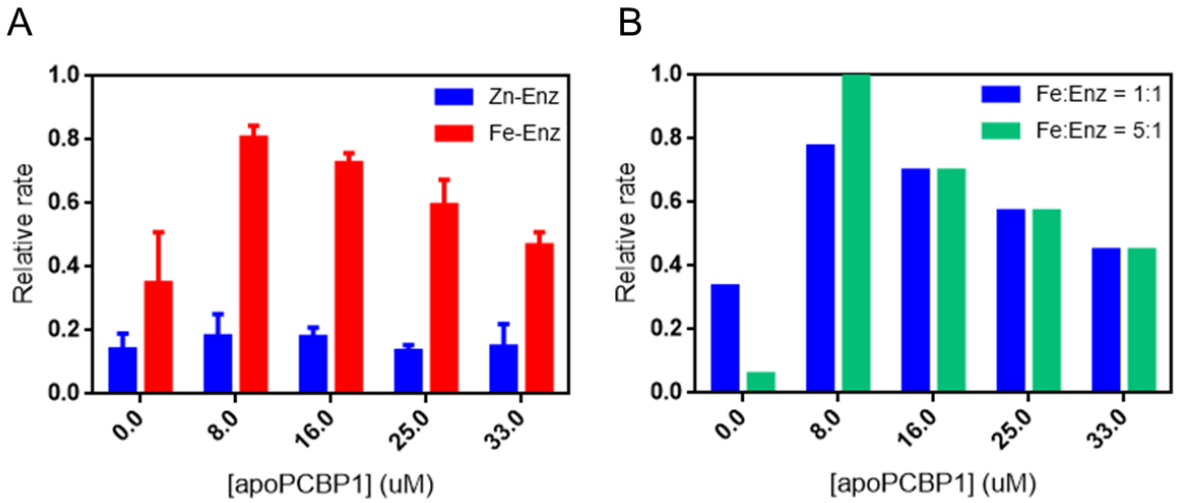


The reduced activity of Fe(II)-bound HDAC8 at higher concentrations of apoPCBP1 could be explained by decreased levels of Fe(II)-bound HDAC8 caused by PCBP1 competing for Fe(II). PCBP1 binds three atoms of ferrous iron with dissociation constants ($K_D$) of 0.9 μM for the first Fe(II) and 5.8 μM for the remaining two atoms, while HDAC8 has an Fe(II) $K_D$ of 0.2 μM.[20] To test this possibility, we measure the effect of PCBP1 on the Fe(II)-HDAC8 activity in the presence of excess concentrations of Fe(II). At high concentrations of PCBP1 (>10 μM) the activity of Fe(II)-bound HDAC8 in the presence of PCBP1 was independent of the metal stoichiometry, suggesting that the inhibition of HDAC8 at high PCBP1 is not due to a decrease in Fe(II)-HDAC8 (Figure 5, panel B). Therefore, interactions between PCBP1 and HDAC8 lead

to both that the gain and loss of Fe(II)-HDAC8 activity, demonstrating the formation of multiple complexes. Additionally, the increase in activity at lower concentrations of PCBP1 indicates that the initial PCBP1 binding site is not the active site of HDAC8. However, reduced activity at low concentration of PCBP1 with excess concentration of Fe(II) was observed probably due to rapid oxidation of Fe(II) or experimental error. More work is needed to more carefully assess the effect of PCBP1 on the activity of Fe(II)-bound HDAC8.

*Effect of apo-PCBP1 on metal dissociation rate constant of HDAC8*

To determine whether apoPCBP1 effects the kinetics of metal binding to HDAC8, we measured the metal dissociation rate constant ($k_{off}$) for Fe(II) and Zn(II) bound to HDAC8 in the presence and absence of apoPCBP1 (Figure 6).

**Figure 4.6** Measurement of Zn(II) and- Fe(II) dissociation rate constants ($k_{off}$) for HDAC8 as a function of apo-PCBP1 concentration. The $k_{off}$ values for HDAC8-bound metal ions were determined from the time-dependent decrease in activity upon dilution of the enzyme into 1 mM EDTA. The activity is measured using the FdL assay, as described in the legend of Figure 5. A first-order exponential was fit to the data to calculate the $k_{off}$ values. A) Measurement of Zn $k_{off}$ as a function of PCBP1 concentrations. B) Measurement of Fe $k_{off}$ as a function of PCBP1 concentrations

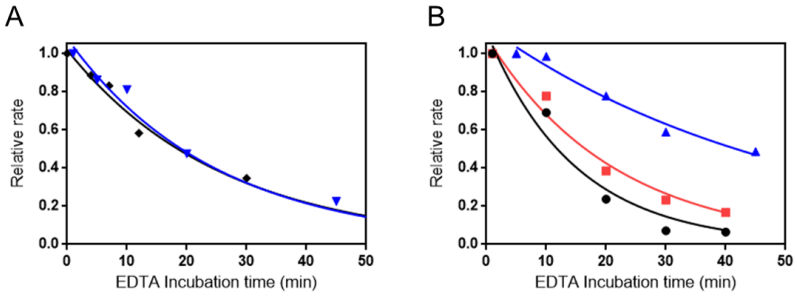


| [apoPCBP1] | Zn(II) $k_{off}$ | Fe(II) $k_{off}$ |
|---|---|---|
| 0uM | 0.04 ± 0.004 | 0.05 ± 0.004 |
| 2.5uM | - | 0.04 ± 0.006 |
| 7.5uM | 0.04 ± 0.007 | 0.02 ± 0.007 |

Addition of apoPCBP1 does not alter the Zn dissociation rate constant, however, $k_{off}$ for Fe(II) decreases with increasing concentration of apoPCBP1. A hyperbolic fit to the dependence of $k_{off}$ on apoPCBP1 indicates a $K_{1/2}$ of 6 ± 2 μM. These data suggest that apoPCBP1 interacts with HDAC8 and specifically decreases the dissociation of Fe(II) bound to HDAC8. Furthermore, these data would be consistent with apoPCBP1 enhancing the affinity of HDAC8 for Fe(II). However, additional work is needed to more precisely define the role of PCBP1 on HDAC8 activity and metal binding affinity and specificity.

*Identification of a complex between HDAC8 and PCBP1 by IM-MS*

Under *in vitro* conditions PCBP1 likely affects the Fe(II) dissociation rate constant and catalytic activity by directly interacting with HDAC8. To further characterize the interactions of PCBP1 with HDAC8, we used ion mobility mass spectrometry (IM-MS) to directly measure the binding behavior of apo- or metal-bound HDAC8 with apo- or Fe(II)-bound PCBP1. Ion mobility separation coupled to mass spectrometry offers unique structural and conformational details and has recently been introduced as a novel tool for the analysis of intact protein complexes.[31] We tested the formation of HDAC8-PCBP1 complexes using recombinant, purified proteins. Each protein was buffer-exchanged with 500 mM aqueous ammonium acetate solution, pH 7, and then the two proteins were mixed in varying concentrations and incubated for 10 min before mass spectrometric analysis. The mixture was ionized by nanoESI, and then separated by ion mobility drift time as well as *m/z* values. Close analysis within *m/z* window 4000 - 5200 showed several well-resolved peaks that correspond to A) HDAC8 monomer, B) PCBP1 monomer, and C) HDAC8-PCBP1 complex, as indicated by comparison to the spectra of each protein alone (Figure 7).

**Figure 4.7** IM-MS analysis of each protein and complex. Protein complexes are ionized by nESI in a range of charge states, and then a single charge state is selected for activation in a quadrupole mass filter. Spectrum of intact protein complex between apo-HDAC8 and apo-PCBP1. Proteins states colored as follows: HDAC8 (blue), PCBP1 (orange). Same colors used throughout. Values of *m/z* for each protein monomer are recorded in table below.

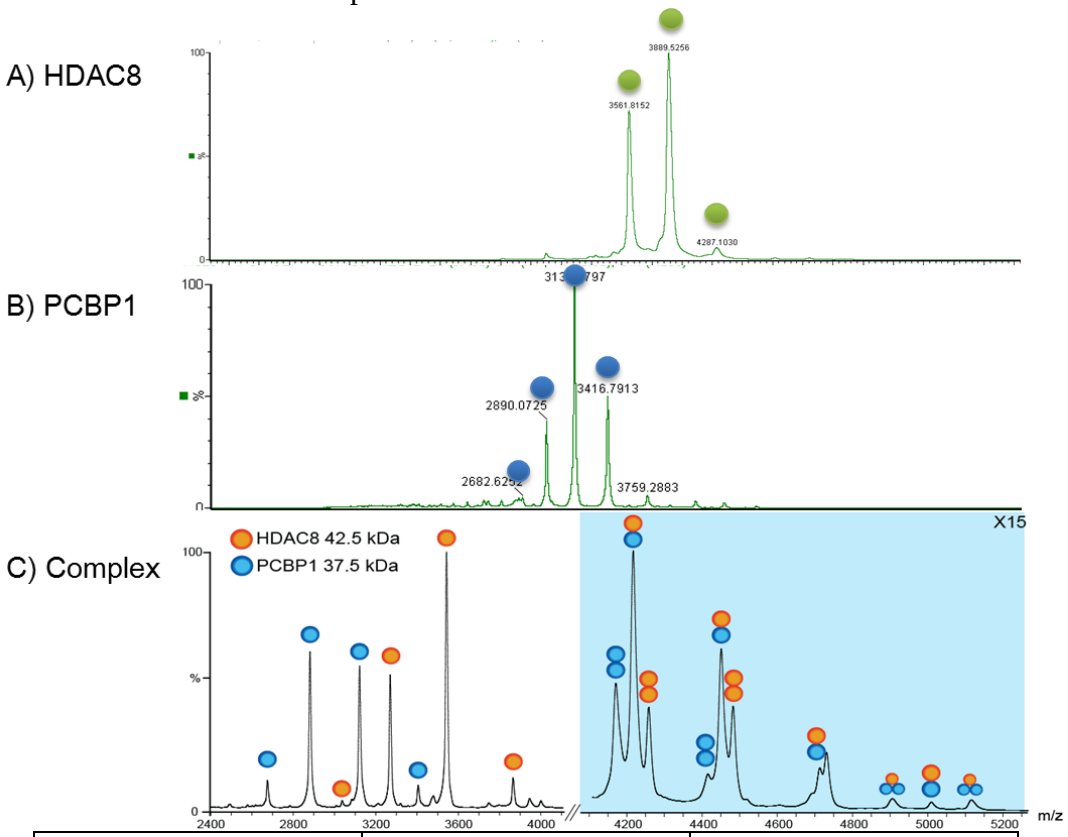


| HDAC8 (42.5kDa) | | PCBP1 (37.5kDa) | | Complex (80kDa) | |
|---|---|---|---|---|---|
| *m/z* | z | *m/z* | z | *m/z* | z |
| 3277 | 13 | 2890 | 13 | 4217 | 19 |
| 3551 | 12 | 3131 | 12 | 4452 | 18 |
| 3874 | 11 | 3414 | 11 | 4714 | 17 |
| 4261 | 10 | 3755 | 10 | 5008 | 16 |

Furthermore, each intact homo-monomer was detected at four distinct charge states; $13^+$, $12^+$, $11^+$, and $10^+$. Four charge states ($19^+$, $18^+$, $17^+$, and $16^+$) were also observed for the hetero-complex under the same experimental conditions. Therefore, the IM-MS spectra revealed the

presence of a complex between HDAC8 and PCBP1 with a mass of 80 kDa, in agreement with the calculated mass of the HDAC8-PCBP1 complex.

To further verify the identity of the hetero-complex, tandem MS was applied to the *m/z* peaks responsible for complex formation and the precursor ions were collisional activated in the trap region, prior to ion mobility separation. Dissociated PCBP1 monomers from the complex are observed when trap collision voltage exceeds 140V (Figure 8). This result consolidates the identity of peaks reflecting the HDAC8-PCBP1 complex.

**Figure 4.8** MS/MS analysis of complex peak by increasing trap energy. Protein complexes is selected for activation in a quadrupole mass filter. Proteins are colored as follows: HDAC8 (blue), PCBP1 (orange). A 1.68kV capillary voltage, 50V sampling cone voltage and 20 ℃ source temperature were maintained during signal acquisition. Backing pressure was at 7-8 mbar.

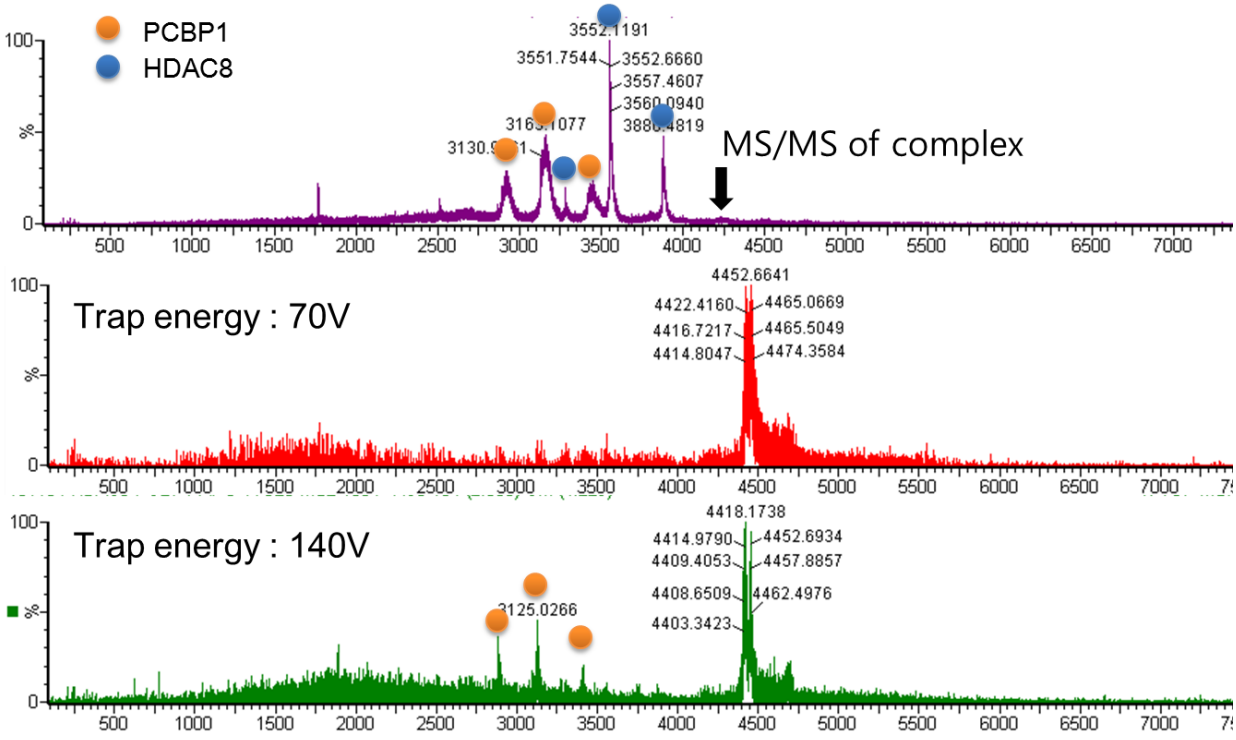


As protein samples are transferred from solution phase to gas phase by electro-spray, it is possible that two or more protein molecules are trapped in the same water droplet, and

subsequently being detected by the mass analyzer and interpreted as complex formation. To examine whether the hetero-complex we observed was due to this ESI artifact, we carried out the following negative control experiment.

We tested the formation of hetero-complexes in the IM-MS experiment between human carbonic anhydrase II (CAII) and either HDAC8 or PCBP1. We chose to use CAII since there is no evidence that this protein forms a protein-protein complex with either HDAC8 or PCBP1. We incubated stoichiometric concentrations (5-10 μM) of CAII with HDAC8 or PCBP1 and repeated the IM-MS analysis. No peaks consistent with the formation of CAII-HDAC8 or CAII-PCBP1 hetero-complexes were observed (Figure 9). These IM-MS results strengthen our hypothesis that HDAC8 binds to PCBP1 in a specific manner.

*Measurement of binding affinity ($K_D$) between apoHDAC8 and apoPCBP1 using IM-MS*

Previously protein-protein binding affinities ($K_D$ = 2.2 ± 0.7 μM) for β-lactoglobulin and hemoglobin were determined by direct ESI-MS.[32] Subsequent studies with using direct ESI-MS-based titration of concanavalin A, whose dimeric form is in equilibrium with its tetramer in solution, were able to determine the $K_a$ values for the dimer-tetramer equilibria. These researchers showed that the titration method was essential for measuring reasonable $K_a$ values of protein-protein interactions in equilibrium by mass spectrometry.[33] Taking into account the response factors (probability of being ionized, transmitted, and detected), we adapted the protocol published by the Klassen group[32,34] Based on the well-established protocol from the Klassen method[35], we plan to expand its utility from protein-ligand interactions to protein-protein scenarios.[32,33]

**Figure 4.9.** IM-MS analysis of HDAC8 or PCBP1 after incubating with carbonic anhydrase II (CAII). apo-HDAC8 or apo-PCBP1 was incubated with apo-CAII under same assay conditions (HDAC8: 10 μM, PCBP1: 15 μM, and CAII: 3 μM) to monitor possible complexation by IM-MS.

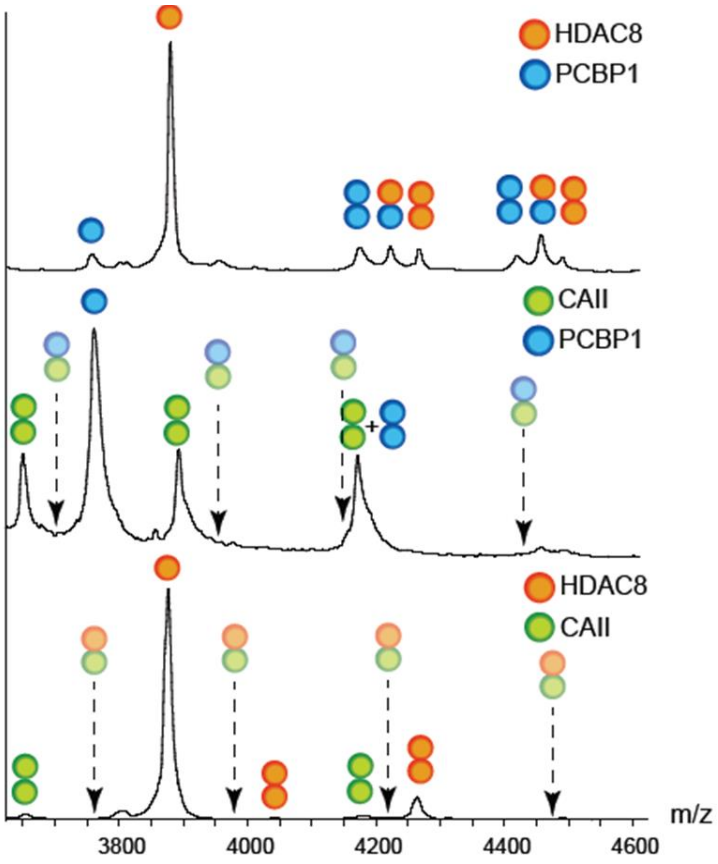


To obtain an estimate for values, several factors need to be considered. First, loss of sample can occur after buffer exchange. This can be accounted for the actual concentrations of each protein after buffer exchange with a nanodrop, before forming the complex. Second, to account for potential non-uniform surface properties of each individual protein, as well as the complex, we performed a series of titrations of each individual protein, and plotted the log (signal intensity) vs. the actual protein concentration.

The results showed the two proteins were equally detected equally well (Figure 10A). Third, the quadrupole setting, potential disruption of complex by collision-induced dissociation

(CID), as well as formation of non-specific complex binding were investigated and have developed corresponding control experiments to account for these factors. Finally, we performed our $K_D$ measurements over a wide range of different concentrations and reported the average value. The total ion intensity of the HDAC8 and PCBP1 monomer peaks in the IM-MS spectrum were integrated, and the ratio of these two species were defined as R, which serves as a gas phase analog of the solution phase concentration ratio of the two species at equilibrium. The following series of control experiments were performed to detect all of the possible sources of error sources. We first confirmed that the intensities of each of the peaks assigned to HDAC8 and PCBP1 were related to their actual concentrations in buffer solution over appropriate concentration ranges. For various concentrations, we integrated the areas under the peaks representing the monomer populations of each protein to calculate the response factor (Figure 10A). The measured peak intensity is linearly dependent on the concentration of each protein after buffer exchange that was injected into the mass spectrometer. This result demonstrates that both proteins behave similarly in IM-MS, although the slope of the line is slightly varied for the two proteins. The peak intensity of the HDAC8-PCBP1 complex was measured at varying concentrations of HDAC8 and PCBP1. Taking into account the variation in ionization, preliminary dissociation constants were determined for these data using the equation as summarized in Figure 10B. There was significant variability in the calculated value of $K_D$ depending on the protein concentration (21 – 82 μM). The average of these values was $K_D$ = 51 μM with a standard deviation of 21 μM which reflects the affinity of the interaction between apo-HDAC8 and PCBP1. Dissociation constants determined in this way at different protein concentrations range within a factor of four. The spread in the ESI-MS-derived $K_D$ values for HDAC8 and PCBP1 is somewhat larger, between 20 and 80 μM. However, this level of variability is quite common when measuring

dissociation constants using the IM-MS method.[36]

**Figure 4.10** Measurement of the value $K_D$ for apo-HDAC8 and apo-PCBP1 using IM-MS. Relative abundance of HDAC8 and PCBP1 versus solution concentration of each protein. (A) Correlation between log-transformed monomer intensity of each protein measured by IM-MS and actual concentration of each protein after buffer exchange (B) Determination of $K_D$ by MS-Based Titration from multiple spectra from nine different experimental datasets. $K_D$ and associated error is represented with bold text.

A)

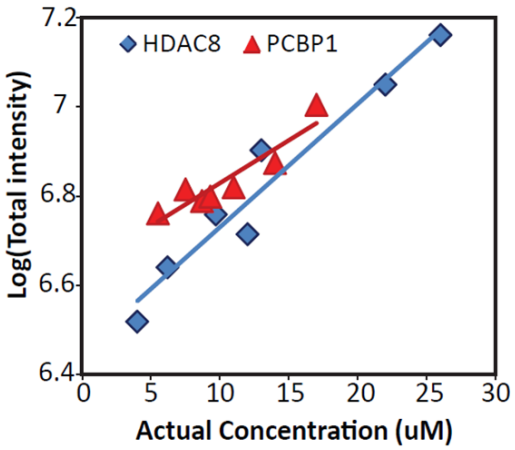


B)

| HDAC8 (μM) | PCBP1 (μM) | $K_D$ (μM) |
|---|---|---|
| 6 | 13 | **21** |
| 6 | 13 | **28** |
| 6 | 13 | **29** |
| 10 | 10 | **60** |
| 10 | 10 | **82** |
| 10 | 10 | **72** |
| 18 | 15 | **56** |
| 18 | 15 | **59** |
| 18 | 15 | **63** |

$K_D = 51 \pm 21$ μM

## DISCUSSION

The identity of the native metal cofactor in a given enzyme *in vivo* is vital for determining how the enzyme is regulated and for developing potent inhibitors; however, the *in vivo* metal can be difficult to distinguish. A previous study showed that HDAC8 can switch from the Fe(II)-bound form to the Zn(II)-bound form *in vitro*.[4] It may be possible that HDAC8 switches metals *in vivo*, and this could be facilitated by a complex mechanism that requires additional regulatory proteins or chaperones to properly control metal homeostasis. Here we

investigated the possible interaction between HDAC8 and PCBP1, the iron chaperone to ferritin, using kinetic and mass-spectrometric analysis. Preliminary *in vivo* co-IP experiments indicate that PCBP1 and HDAC8 form a complex in T-REx HEK293 cells regardless of iron conditions, and subsequent IM-MS analyse have demonstrated complex formation under *in vitro* conditions.

*HDAC8-PCBP1 interaction in T-REx 293 cells*

Previously, PCBP1 was shown to act as an iron chaperone for ferritin, prolyl, asparagyl, and deoxyhypusine hydroxylase in mammalian cells. Here we have presented evidences that PCBP1 has an interaction with HDAC8 in T-REx 293 cells under Fe(II)-sufficient or deficient conditions. PCBP1 co-immunoprecipitated with HDAC8 in FAC-supplemented and DFO-chelated T-REx 293 cells. These studies suggest that PCBP1 and HDAC8 can form a hetero-oligomeric complex in the cell. A recent study revealed that PCBP1 and PCBP2 played a synergistic role in iron delivery to PHDs, but that they could not functionally replace each other.[24] Additionally when purified, recombinant PCBP1 was shown to restore activity to PHDs in lysates from cells lacking PCBP1 but not from cells lacking PCBP2, this suggested that the two chaperones functioned cooperatively to deliver iron to PHD.[22] This suggests that both PCBP1 and PCBP2 might be required to form a stable complex with and facilitate iron uptake in HDAC8.

*Kinetic analysis of HDAC8 with PCBP1*

To explore the effect of PCBP1 on HDAC8, we measured the kinetics for dissociation of Zn(II) or Fe(II) from HDAC8 in the presence or absence of PCBP1 *in vitro*. The rate constants for dissociation of Fe(II) from the HDAC8-metal complex were slower in the presence of PCBP1.

However, little change in metal dissociation was observed for Zn(II)-bound HDAC8. Additionally PCBP1 only affected the activity of Fe(II)-HDAC8, not Zn(II)-PCBP1. One possible mechanism for this could be the formation of an Fe(II)-HDAC8 complex with PCBP1 which modestly decreases dissociation of Fe(II) through structural rearrangement (~2.5-fold, Figure 6), suggesting that in the context of a cell, binding partners including PCBP1 may contribute to form or stabilize the Fe(II)-bound HDAC8 and regulate its biological function. Zn(II)-HDAC8 might be able to form a complex with PCBP1, however, the catalytic activity and zinc dissociation rate constant are unaffected by binding PCBP1.

One possible mechanism for inhibition of the catalytic mechanism of HDAC8 by PCBP1 is competition for binding Fe(II). If the Fe(II) affinities do not change significantly upon formation of a HDAC8-PCBP1 complex, PCBP1 ($K_D^{Fe}$ = 0.9 ~ 5.8 μM[20]) should significantly compete with HDAC8 for binding Fe(II) at concentrations above 10 μM. However, increasing the Fe(II) concentration in these assays does not decrease inhibition by PCBP1 (Figure 5), indicating that PCBP1 does not compete for Fe(II) binding to HDAC8. This result suggests that the Fe(II) affinity of HDAC8 is enhanced by complex formation with PCBP1. This enhanced affinity is consistent with the decrease in the Fe(II) dissociation rate constant under these conditions. These results are consistent for a role of PCBP1 in regulating the cellular metal content of HDAC8.

*Probing the HDAC8-PCBP1 affinity by IM-MS*

To examine the HDAC8•PCBP1 complex, we developed an ion-mobility mass spectrometry experiment that could be further developed in the future to measure the complex under metal-bound conditions. These experiments demonstrate that HDAC8 binds to PCBP1

with a $K_D$ of ~50 μM in the absence of metal. Control experiments with CAII demonstrated that the observed binding between HDAC8 and PCBP1 is not non-specific based on the fact that no complex formation with CAII as observed under the same experimental conditions. These findings are consistent with the co-IP results, and taken together the data show that, HDAC8 and PCBP1 interact with micromolar affinity in the absence of metal ions. To gain more insight into biologically relevant metal-bound species, IM-MS experiments should be completed using samples with varying metal concentrations to form metal-bound HDAC8 and/or PCBP1 under the same assay conditions. Since both proteins bind metals *in vitro* and *in vivo*, we predict both that the metallated HDAC8-PCB1 complex should form with higher affinity and that HDAC8 in this complex should have a higher affinity for Fe(II), as proposed above. For these experiments, it is essential to use conditions where Fe(II)-HDAC8 is stabilized under aerobic conditions. To this end, we demonstrated that addition of 5 mM ascorbic acid maintained the catalytic activity of Fe(II)-HDAC8 in air for 2 hours (Figure 11). A future direction will be to evaluate the HDAC8•PCBP1 binding affinity and stoichiometry as a function of Fe(II) concentration. This will provide additional insight into the functional role of complex formation.

**Figure 4.11** Conditions to stabilize the activity of Fe(II)-HDAC8 outside of the glovebox. Activity of Fe(II)-bound HDAC8 was assayed using the FdL assay under exposure to air in the presence or in the absence of 5 mM ascorbic acid.

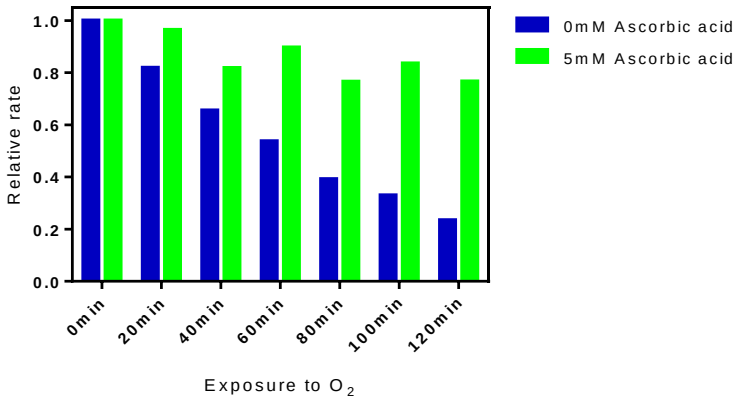

**REFERENCE**


(1) Barnes, P. J., Adcock, I. M., and Ito, K. (2005) Histone acetylation and deacetylation: importance in inflammatory lung diseases. *Eur. Respir. J. 25*, 552–63.

(2) Minucci, S., and Pelicci, P. G. (2006) Histone deacetylase inhibitors and the promise of epigenetic (and more) treatments for cancer. *Nat. Rev. Cancer 6*, 38–51.

(3) Finnin, M. S., Donigian, J. R., Cohen, A., Richon, V. M., Rifkind, R. A., Marks, P. A., Breslow, R., and Pavletich, N. P. (1999) Structures of a histone deacetylase homologue bound to the TSA and SAHA inhibitors. *Nature 401*, 188–193.

(4) Gantt, S. L., Gattis, S. G., and Fierke, C. A. (2006) Catalytic activity and inhibition of human histone deacetylase 8 is dependent on the identity of the active site metal ion. *Biochemistry 45*, 6170–8.

(5) Denslow, S. a, and Wade, P. a. (2007) The human Mi-2/NuRD complex and gene regulation. *Oncogene 26*, 5433–8.

(6) Force, J., Saxena, R., Schneider, B. P., Storniolo, A. M., Sledge, G. W., Chalasani, N., and Vuppalanchi, R. (2014) Nodular Regenerative Hyperplasia After Treatment With Trastuzumab Emtansine. *J. Clin. Oncol. 2010*, 1–4.

(7) Hdac, D., Complex, H., Peinado, H., Ballestar, E., Esteller, M., and Cano, A. (2004) Snail Mediates E-Cadherin Repression by the Recruitment of the Sin3A / Histone Snail Mediates E-Cadherin Repression by the Recruitment of the Sin3A / Histone Deacetylase 1 ( HDAC1 )/ HDAC2 Complex. *Mol. Cell. Biol. 24*, 306–319.

(8) Joshi, P., Greco, T. M., Guise, A. J., Luo, Y., Yu, F., Nesvizhskii, A. I., and Cristea, I. M. (2013) The functional interactome landscape of the human histone deacetylase family. *Mol. Syst. Biol. 9*, 1–21.

(9) Colpas, G. J. (2000) In Vivo and in Vitro Kinetics of Metal Transfer by the Klebsiella aerogenes Urease Nickel Metallochaperone, UreE. *J. Biol. Chem. 275*, 10731–10737.

(10) Complex, P., Heaton, D. N., George, G. N., Garrison, G., and Winge, D. R. (2001) The Mitochondrial Copper Metallochaperone Cox17 Exists as an Oligomeric ,. *Biochemistry 40*, 743–751.

(11) Rae, T. D., P.J. Schmidt, R.A. Pufahl, V.C. Culotta, T. V. O. (1999) Undetectable Intracellular Free Copper: The Requirement of a Copper Chaperone for Superoxide Dismutase. *Science (80-. ). 284*, 805–808.

(12) Pufahl, R. A. (1997) Metal Ion Chaperone Function of the Soluble Cu(I) Receptor Atx1. *Science (80-. ). 278*, 853–856.

(13) O'Halloran, T. V, and Culotta, V. C. (2000) Metallochaperones, an intracellular shuttle service for metal ions. *J. Biol. Chem. 275*, 25057–60.

(14) Kuchar, J., and Hausinger, R. P. (2004) Biosynthesis of metal sites. *Chem. Rev. 104*, 509–25.

(15) Tottey, S., Harvie, D. R., and Robinson, N. J. (2005) Understanding how cells allocate metals using metal sensors and metallochaperones. *Acc Chem Res 38*, 775–83.

(16) Mansy, S.S., Cowan, J. A. (2004) Iron - Sulfur Cluster Biosynthesis : Toward an Understanding of Cellular Machinery and Molecular Iron - Sulfur Cluster Proteins : Biological. *Acc Chem Res 37*, 719–725.

(17) Waldron, K. J., Rutherford, J. C., Ford, D., and Robinson, N. J. (2009) Metalloproteins and metal sensing. *Nature 460*, 823–30.

(18) Jensen, L. T., and Culotta, V. C. (2000) Role of Saccharomyces cerevisiae ISA1 and ISA2 in Iron Homeostasis Role of Saccharomyces cerevisiae ISA1 and ISA2 in Iron Homeostasis. *Mol. Cell. Biol. 20*, 3918–3927.

(19) Bulteau, A.-L., O'Neill, H. a, Kennedy, M. C., Ikeda-Saito, M., Isaya, G., and Szweda, L. I. (2004) Frataxin acts as an iron chaperone protein to modulate mitochondrial aconitase activity. *Science (80-. ). 305*, 242–5.

(20) Shi, H., Bencze, K. Z., Stemmler, T. L., and Philpott, C. C. (2008) A cytosolic iron chaperone that delivers iron to ferritin. *Science (80-. ). 320*, 1207–10.

(21) Makeyev, A. V, and Liebhaber, S. A. (2002) The poly ( C ) -binding proteins : a multiplicity of functions and a search for mechanisms . The poly ( C ) -binding proteins : A multiplicity of. *RNA 8*, 265–278.

(22) Nandal, A., Ruiz, J. C., Subramanian, P., Ghimire-Rijal, S., Sinnamon, R. A., Stemmler, T. L., Bruick, R. K., and Philpott, C. C. (2011) Activation of the HIF prolyl hydroxylase by the iron chaperones PCBP1 and PCBP2. *Cell Metab. 14*, 647–57.

(23) Frey, A. G., Nandal, A., Park, J. H., Smith, P. M., Yabe, T., Ryu, M.-S., Ghosh, M. C., Lee, J., Rouault, T. a, Park, M. H., and Philpott, C. C. (2014) Iron chaperones PCBP1 and PCBP2 mediate the metallation of the dinuclear iron enzyme deoxyhypusine hydroxylase. *Proc. Natl. Acad. Sci. U. S. A. 111*, 8031–8036.

(24) Leidgens, S., Bullough, K. Z., Shi, H., Li, F., Shakoury-Elizeh, M., Yabe, T., Subramanian, P., Hsu, E., Natarajan, N., Nandal, A., Stemmler, T. L., and Philpott, C. C. (2013) Each member

of the poly-r(C)-binding protein 1 (PCBP) family exhibits iron chaperone activity toward ferritin. *J. Biol. Chem. 288*, 17791–802.

(25) Rusconi, F., Guillonneau, F., and Praseuth, D. (2003) Contributions of mass spectrometry in the study of nucleic acid-binding proteins and of nucleic acid-protein interactions. *Mass Spectrom. Rev. 21*, 305–48.

(26) Heck, A. J. R. (2008) Native mass spectrometry : a bridge between interactomics and structural biology. *Nat. Methods 5*, 927–933.

(27) Bush, M. F., Hall, Z., Giles, K., Hoyes, J., Robinson, C. V, and Ruotolo, B. T. (2010) Collision cross sections of proteins and their complexes: a calibration framework and database for gas-phase structural biology. *Anal. Chem. 82*, 9557–65.

(28) Giles, K., Williams, J. P., and Campuzano, I. (2011) Enhancements in travelling wave ion mobility resolution. *Rapid Commun. Mass Spectrom. 25*, 1559–66.

(29) Hernández, H., and Robinson, C. V. (2007) Determining the stoichiometry and interactions of macromolecular assemblies from mass spectrometry. *Nat. Protoc. 2*, 715–26.

(30) Shi, H. (2013) A cytosolic iron chaperone that delivers iron to ferritin. *Science (80-. ). 1207*, 1207–1210.

(31) Ruotolo, B. T., Giles, K., Campuzano, I., Sandercock, A. M., Bateman, R. H., and Robinson, C. V. (2005) Evidence for macromolecular protein rings in the absence of bulk water. *Science (80-. ). 310*, 1658–61.

(32) Liu, J., and Konermann, L. (2011) Protein-protein binding affinities in solution determined by electrospray mass spectrometry. *J. Am. Soc. Mass Spectrom. 22*, 408–17.

(33) Boeri Erba, E., Barylyuk, K., Yang, Y., and Zenobi, R. (2011) Quantifying protein-protein interactions within noncovalent complexes using electrospray ionization mass spectrometry. *Anal. Chem. 83*, 9251–9.

(34) Rabuck, J. N., Hyung, S.-J., Ko, K. S., Fox, C. C., Soellner, M. B., and Ruotolo, B. T. (2013) Activation state-selective kinase inhibitor assay based on ion mobility-mass spectrometry. *Anal. Chem. 85*, 6995–7002.

(35) Wang, W., Kitova, E. N., and Klassen, J. S. (2003) Influence of Solution and Gas Phase Processes on Protein - Carbohydrate Binding Affinities Determined by Nanoelectrospray Fourier Spectrometry. *Anal. Chem. 75*, 4945–4955.

(36) Powell, K. D., Ghaemmaghami, S., Wang, M. Z., Ma, L., Oas, T. G., and Fitzgerald, M. C. (2002) A general mass spectrometry-based assay for the quantitation of protein-ligand binding interactions in solution. *J. Am. Chem. Soc. 124*, 10256–7.

# CHAPTER 5

# INHIBITION OF LpxC[1]

## INTRODUCTION

In Gram-negative bacteria, the outer layer of the cell envelope is predominantly comprised of lipopolysaccharides (LPS), which are anchored to the membrane through a core Lipid A component.[64,164] Lipid A biosynthesis is essential for growth in nearly all Gram-negative bacteria. LpxC is an essential metal-dependent enzyme in Gram-negative bacteria that catalyzes the deacetylation of UDP-3-*O*-(acyl)-*N*-acetylglucosamine in the biosynthesis of lipid A (Figure 1).[2] For the majority of Gram-negative bacteria, the first step in the lipid A biosynthetic pathway,

**Figure 5.1** LpxC-catalyzed reaction to lipid A biosynthetic pathway

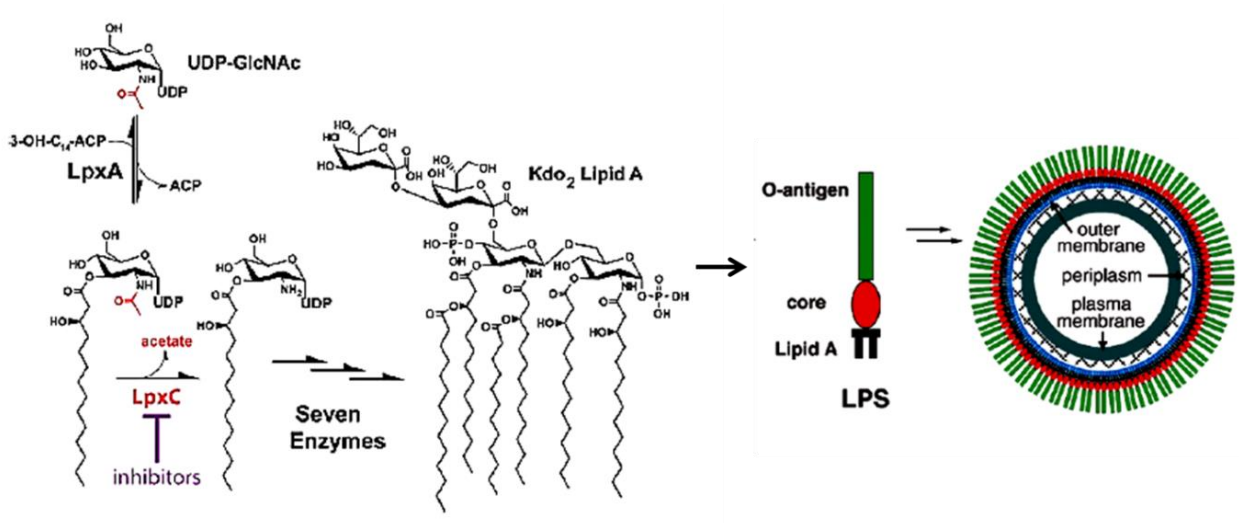


catalyzed by LpxA, is thermodynamically unfavorable and reversible.[165] Therefore, the second reaction catalyzed by LpxC is the first committed step of lipid A biosynthesis. For this reason,



[1]This was a collaboration with Seth Lab at UCSD and all metal binding fragments provided by them is explicitly labeled within the chapter.

LpxC is considered to be an antibacterial pharmaceutical target. Since inhibition of LpxC is bactericidal for most Gram-negative bacteria, it is considered an attractive target for treatment of multidrug-resistant Gram-negative infections.[65]

Small molecule inhibitors targeting LpxC were first discovered in the late 1980s using compound screens that measured inhibition of $^{3}$H-galactose uptake in *Escherichia coli* cells.[166] Subsequent lead optimization studies led to the development of L-161,240, a hydroxamate-containing phenyloxazoline compound (Figure 2).[166] L-161,240 had antibacterial activity comparable to ampicillin against *E. coli*, but was ineffective against *Pseudomonas aeruginosa*.[166] Additional experimentation demonstrated that the antibacterial specificity of L-161,240 toward *E.*

**Figure 5.2** Summary of known LpxC inhibitors

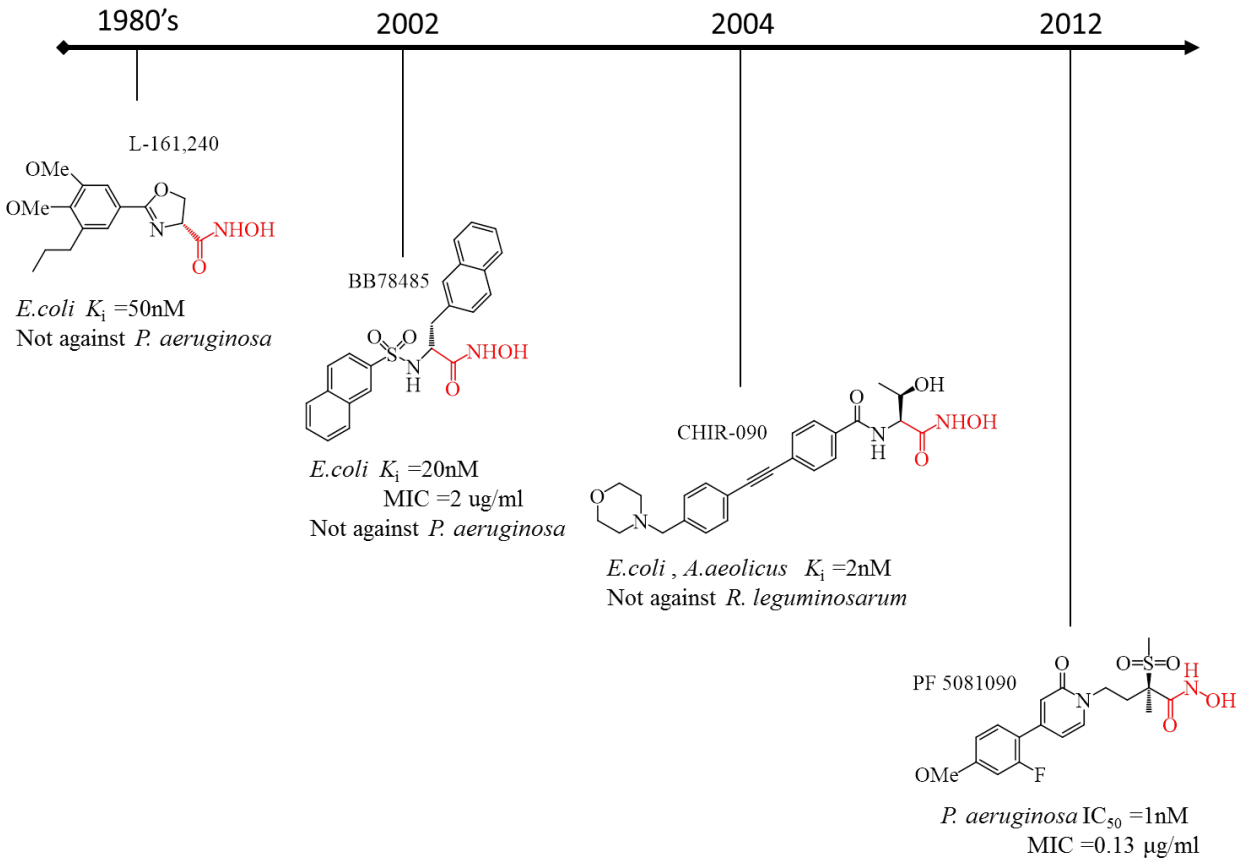

*coli* is due to the greater binding affinity of this compound with *E. coli* LpxC (EcLpxC) compared to *P. aeruginosa* LpxC (PaLpxC) rather than differences in the intrinsic resistance mechanisms of these two bacterial strains, such as membrane permeability or drug efflux.[167] Subsequent drug development efforts yielded a series of sulfonamide-based compounds from British Biotech, such as BB-78485, which prevented *E. coli* growth with an activity better than that of L-161,240, but remain ineffective against *P. aeruginosa*.[168,169] In 2004, scientists at Chiron synthesized the compound CHIR-090 that showed promise as a lead compound.[170] CHIR-090 is the best LpxC inhibitor reported to date, killing both *E. coli* and *P. aeruginosa* in bacterial disk diffusion assays with an efficacy comparable to that of ciprofloxacin. CHIR-090 has a $K_i$ of 2 nM for *Aquifex aeolicus* LpxC, and exhibits behavior typical of a slow, non-covalent tight-binding inhibitor.[170] Recently, a new series of LpxC inhibitors, such as pyridone methylsulfone hydroxamate (PF5081090), have been reported.[171] These compounds have improved solubility and free fraction when compared to the previously developed biphenyl methylsulfone hydroxamate series, such as BB-78485, and showed higher Gram-negative antibacterial activity.[171]

All inhibitors described above are structurally similar in that they contain both a hydroxamate group for coordinating with the active site metal ion (Zn/Fe) and a hydrophobic tail which mimics the hydroxy-myristate fatty acid group found in the natural substrate. However, most hydroxamate-based inhibitors are associated with severe toxicity and suffer from poor oral bioavailability since the hydroxamate groups readily hydrolyzes, leaving the corresponding carboxylic acid with a loss of inhibitory and antibacterial activity.[172] Thus, there is an urgent need for the development of non-hydroxamate based inhibitors for LpxC.

In this chapter, a library of non-hydroxamate inhibitors targeting LpxC is screened and assayed to identify more potent, broad spectrum inhibitors of Lipid A biosynthesis.

## MATERIAL AND METHODS

### *General methods*

All solutions were prepared in "metal-free" plasticware with reagents without extraneous metal ions, as verified by inductively coupled plasma mass spectrometry (ICP-MS, Dr. Ted Huston, University of Michigan). Reagents were of the highest quality available from Sigma-Aldrich, unless noted.

### *Preparation of E. coli* LpxC

Wild-type *E. coli* LpxC (EcLpxC) was overexpressed using a T7 expression vector and purified according to published procedures.[66] All purification steps were carried out at 4 ℃ for EcLpxC. Following lysis using a microfluidizer, the cell debris was pelleted by centrifugation, and the supernatant was loaded onto a DEAE-Sepharose column in 25 mM HEPES, pH 7, 2 mM dithiothreitol. EcLpxC were eluted with a linear salt gradient (0–250 mM KCl). The LpxC was further fractionated using a Reactive Red 120 column with a linear gradient (0–250 mM KCl). LpxC purified by this method was >95% pure as assessed by SDS-PAGE and stored at -80 ℃. All metals were removed from the purified enzymes by incubation with metal chelators

(DPA/EDTA), as described previously.[66] The apoLpxC was reconstituted with stoichiometric amounts of $ZnSO_4$ or $FeCl_2$ prior to use in assays.

*LC-MS Assay condition*

The LpxC substrate, UDP-3-*O*-(R-3-hydroxy-myristoyl)-*N*-acetyl-glucosamine, was gift from Cubist Pharmaceuticals (Lexington, MA). The assay measures the enzymatic deacetylation of the synthetic LpxC substrate by mass spectrometry using a computer-controlled fluidic system combined with a triple quadrupole mass spectrometer (BioTrove RapidFire). The enzyme assay was conducted in 96-well polypropylene plates (Corning no. 3363) in a total volume of 50 μL. Substrate, UDP-3-*O*-(R-3-hydroxy-myristoyl)-*N*-acetyl-glucosamine, was first added to wells (final assay concentration 100 nM). Compounds (5 μL in 100% DMSO: compound final concentration range 50 μM to 200 μM) were added at room temperature. The reaction was initiated by the addition of LpxC (final assay concentration 1 nM) in buffer 20 mM Bis-Tris Propane (BTP)) pH 7.5, 1 mM TCEP, 10% DMSO and, 1 mg/ml bovine serum albumin (BSA). After incubation at room temperature for 30 min, reactions were stopped by the addition of 0.25 N HCl (20 μL) and the plates sealed with Thermowell sealing tape (Corning Incorporation) and cooled to –80 ℃. The frozen plates were then sent on dry ice to Biotrove, Inc. for analysis using the RapidFire ultra-highthroughput mass spectrometry system, consisting of a proprietary computer-controlled fluidic robot interfaced with a Sciex API-4000 triple-quadrupole mass spectrometer.[173] The product and substrate peak areas were determined and a percent substrate conversion was calculated in Microsoft Excel. The percent inhibition was calculated by comparison to the activity in the absence of inhibitor.

Known hydroxamate inhibitor (L-161240, BB-78485, and CHIR-090) and nonhydroxamate inhibitor (196904) was provided by Cubist Pharmaceuticals. Metal-binding fragment library (CFL and DTP series) were provided by Prof. Cohen lab at UCSD.

## RESULTS

### *High-throughput screen for LpxC inhibitors*

We used a label-free method to characterize the activities of inhibitors against *E. coli* LpxC using a high-throughput mass spectrometry method developed by BioTrove, Inc. (Woburn, MA).[173] This method has been used for a screening assay with results comparable to an assay using radiolabeled substrate.[173] LpxC catalyzes deacetylation of UDP-3-*O*-(acyl)-*N*-acetylglucosamine, generating an expected mass species for substrate at 833 amu and for the product at 791 amu (Figure 3). Integration of the peak areas to quantify the substrate and product indicates a linear conversion of substrate to product as a function of incubation time; the substrate ion signal decreases while the product ion signal increases. The initial rate of product formation (<20% reaction) as a function of either substrate or inhibitor concentration can be calculated to measure kinetic values ($k_{cat}/K_M$ or $IC_{50}$) using this method. The purified *E. coli* LpxC (1 nM) was incubated with 100 nM chemically synthesized substrate (UDP-3-*O*-[(*R*)-3-hydroxymyristoyl]-*N*-acetylglucosamine) in buffer in the presence or in the absence of inhibitor. At specified time, duplicate reactions were quenched by the addition of 0.25 N HCl and then the fraction of product was analyzed by mass spectrometry.

**Figure 5.3** Measuring conversion of substrate and product using RapidFire mass spectrometry

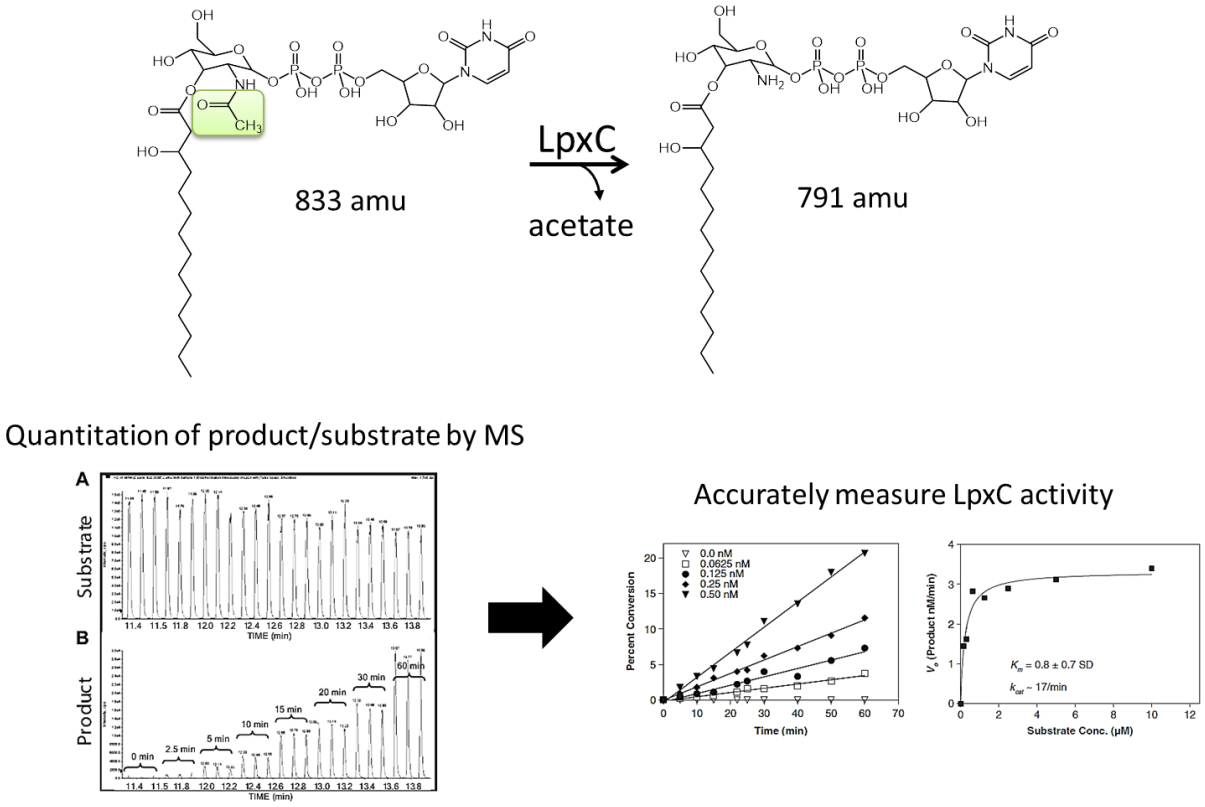


To examine whether the RapidFire mass spectrometric high-throughput assay accurately reflects LpxC inhibition, stopped assays in the presence of previously reported LpxC inhibitors were carried out in parallel (Figure 4). Under these conditions, all of the inhibitors decrease the activity to <0.1% of the LpxC activity in the absence of inhibitor while CHIR-090 ($K_i$ = 2 nM) showed the most potent inhibitory activity.. Under these assay conditions, the relative initial rate in the presence of the inhibitor is in good agreement with the relative inhibitory potency of the compounds previously measured.[65] These data demonstrate that the assay accurately measures the relative inhibitory potency of these compounds.

**Figure 5.4** Control experiments of known LpxC inhibitors using the RapidFire MS assay. Inhibition by known LpxC inhibitors (10 μM) was measured in buffer (20 mM Bis-Tris-Propane pH = 7.5, 1 mM TCEP, 1 mg/ml BSA) with 100 nM substrate and 1 nM EcLpxC at room temperature in the presence of varying concentrations of hydroxamate inhibitors. After 60 min at room temperature, the reaction was quenched and then product formation was analyzed using the RapidFire MS assay. H2O is a negative control and ZnEnz is a positive control without inhibitor. HOPO-2 is an internal control. CHIR-090, L161,240, BB-78485, and PF5081090 are potent well-known inhibitors against LpxC.

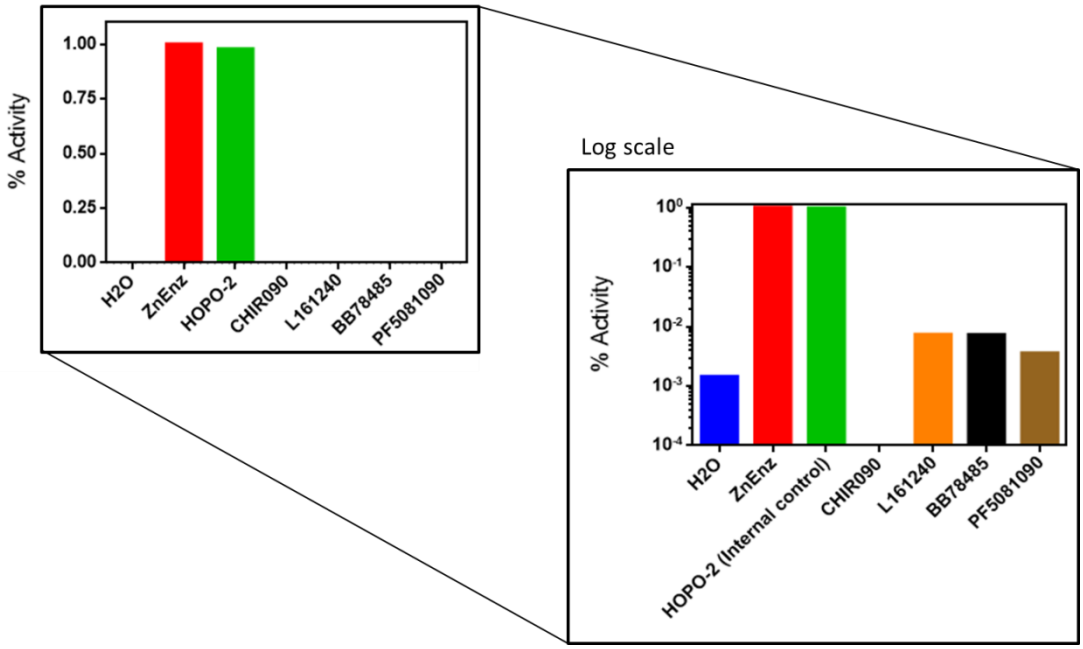


*Metal-dependence of $IC_{50}$ values of LpxC inhibitors*

Recent experiments have demonstrated that under most conditions, LpxC in *E. coli* is activated by a Fe(II) cofactor[67] while the majority of screens have investigated inhibition of Zn(II)-LpxC. Therefore, we investigated whether the identity of the active site metal affects the affinity of inhibitors containing either a hydroxamate or a carboxylate group that directly interacts with the metal ion. The carboxylate inhibitor (196904) was designed and synthesized by Cubist Pharmaceuticals. Two of the known hydroxamic acid inhibitors of LpxC, L-161240 and CHIR-090, inhibit Fe(II)-LpxC ~2-fold better than the zinc-bound enzyme, consistent with the

enhanced $k_{cat}/K_M$ value for the iron-enzyme (Figure 5).

This same trend was also observed for the metal-dependence of inhibition of human deacetylase HDAC8 by the hydroxamic acid inhibitor, SAHA.[43] However, the inhibitor BB-78485 has ~2-fold higher affinity for Fe(II)-LpxC than Zn(II)-LpxC and the $IC_{50}$ value for the carboxylate inhibitor, 196904, did not vary based on the metal cofactor bound to LpxC (Figure 4).

**Figure 5.5** Determination of $IC_{50}$ for hydroxamate and carboxylate inhibitors. LpxC activity was assayed using the conditions described in the legend of Figure 4 including 100 nM substrate and 1 nM EcLpxC in the presence of varying concentrations of hydroxamate and carboxylate inhibitors. After 60 min at room temperature, the reaction was quenched and then product formation was analyzed using the RapidFire MS assay.

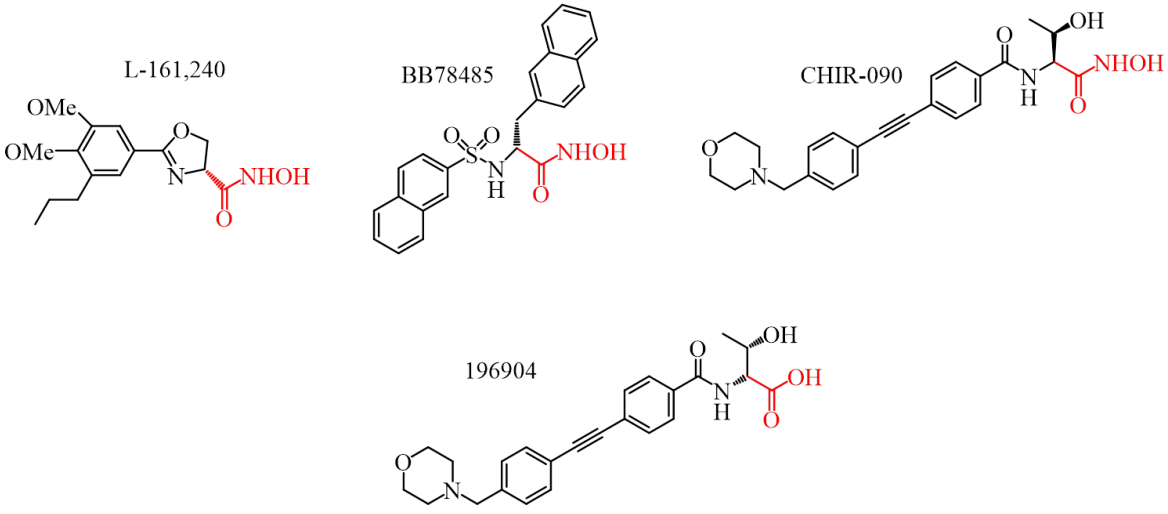


| $IC_{50}$ (μM) | L-161240 | BB-78485 | CHIR-090 | 196904 |
|---|---|---|---|---|
| Zn(II) | 11 ± 1 | 90 ± 17 | 0.2 ± 0.01 | 0.9 ± 0.1 |
| Fe(II) | 6 ± 0.6 | 190 ± 40 | 0.1 ± 0.002 | 0.9 ± 0.1 |

*Screening non-hydroxamate compound library as LpxC inhibitors*

Inhibitors having hydroxamate functional group as metal-binding site encounter many obstacles that have limited their effectiveness in the clinic, although the hydroxamate-containing

compounds have been approved as drugs, such as ibuproxam and suberoylanilide hydroxamic acid (SAHA).[174] For example, hydroxamic acids can readily hydrolyze *in vivo* to the corresponding carboxylic acid, resulting in poor pharmacokinetics.[175] Herein, a library of >200 non-hydroxamate metal-binding fragments, synthesized by the laboratory of Prof. Seth Cohen at UCSD, has been screened to evaluate inhibitor potency for *E. coli* LpxC using the mass spectrometric.assay (Figure 6). This library, containing 96 structural cores, was prepared from chelators with two to four donor atoms for binding metal ions and to provide sufficient solubility for screening.[176,177] The chelating groups include picolinic acids, hydroxyquinolones, pyrimidines, hydroxypyrones, hydroxypyridinones and salicylic acids. This CFL library was previously screened against various enzymes (anthrax lethal factor, LF), a non-heme iron enzyme (5-lipoxygenase, 5-LO), a dinuclear copper enzyme (tyrosinase, TY), and a heme iron enzyme (inducible nitric oxide synthase, iNOS) in order to generate novel metal-binding fragments for a wide range of metalloenzymes.[177,178]

All of the compounds compounds were soluble in the assay buffer and did not appear to aggregate under the assay conditions. This 96-member library (CFL) was screened against EcLpxC, at a fragment concentration of 200 μM, using a label-free mass spectrometry assay to identify LpxC inhibitors. The results of the screens are presented in a heatmap (Figure 6) representing the percent remaining activity of EcLpxC in the presence of the library compounds. Out of the 96 compounds, 34 compounds decreased activity ≥ 2-fold and 3 compounds decreased the activity >10-fold at 200 μM. Most of the hydroxypyrones series (CFL-D: 1d-11d) inhibited

LpxC >2 fold with some compound inhibiting >10-fold. Additionally, several of the sulfur- containing hydroxypyridinethiones (CDL-E) inhibit LpxC >5-fold. Salicylic acid

**Figure 5.6.** Screening chelator fragment library (CFL) for compounds that inhibit LpxC. Heatmap representing the results from the screens of CFL-1.1 against Zn(II)-EcLpxC carried out as described in the legend of Figure 4. Cells are color-coded by the percent of the remaining activity: brown (80-100%), red (60-80%), green (40-60%), orange (20-40%), pale grey (10-20%) and white (no detection).

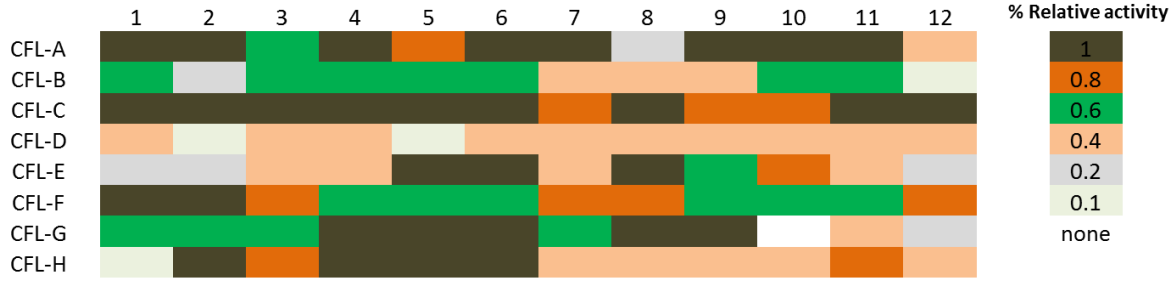


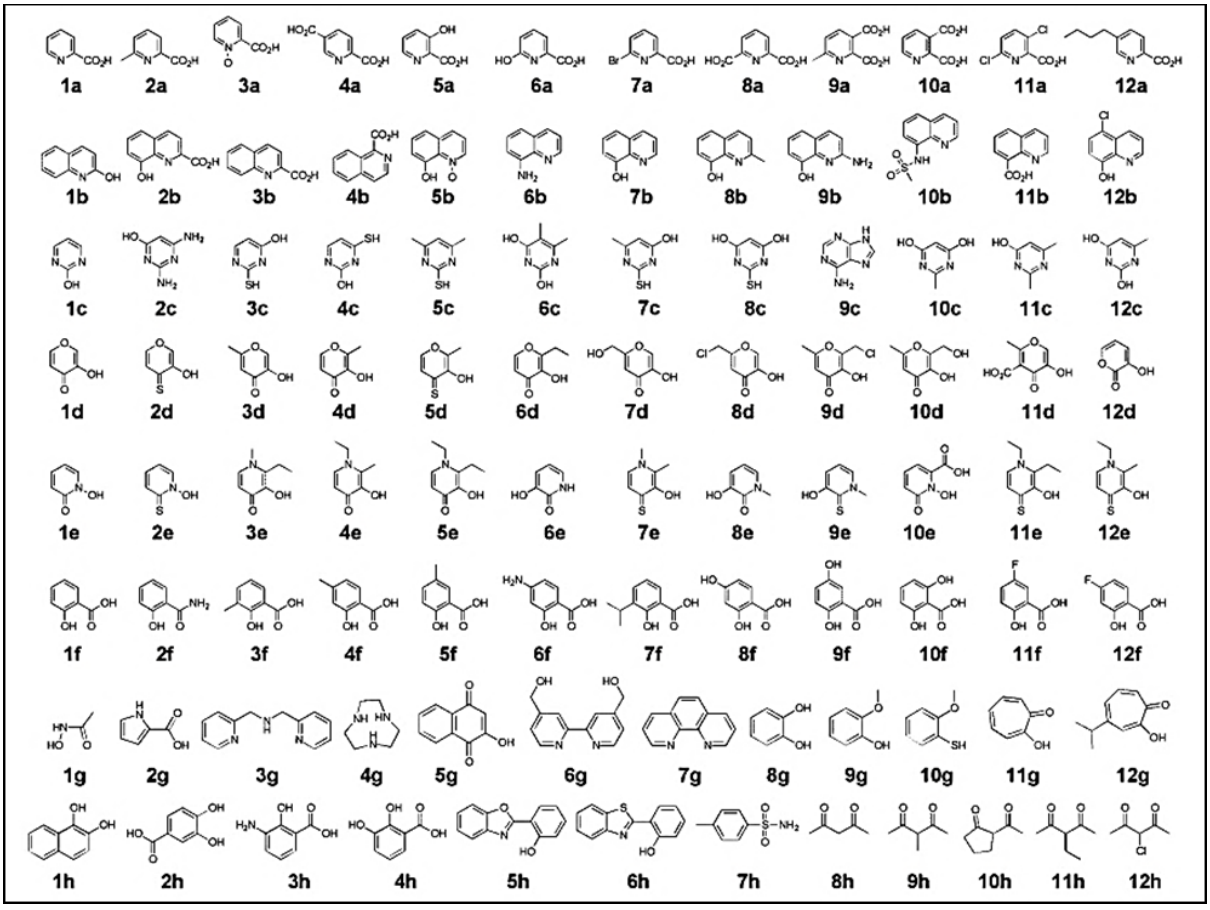


derivatives (CFL-F) and the CFL-C series generally inhibited LpxC <2-fold. Additionally, several other compounds (12b, 12g, 1h) inhibit LpxC.

Based on these initial results, the Cohen lab synthesized another candidate library (DTP series) and this library of inhibitors was screened using the mass spectrometric assay (Figure 7). This library is composed of derivatives of 5-hydroxy-2-(hydroxymethyl)-4H-pyran-4-one. 8 out of the 9 DTP series compound inhibit LpxC >2-fold at 50 μM. Dose-response scores for inhibition of *E.coli* LpxC were determined for the top scoring compounds and $IC_{50}$ values were calculated (Figure 7). The compound DTP-088 was the most potent inhibitor against Zn(II)-bound LpxC with $IC_{50} \approx 2$ nM, which is comparable to the potent inhibitor, CHIR-090.

**Figure 5.7** Measurement of $IC_{50}$ values of selected compounds from the DTP series. Dose-response curves of inhibition of EcLpxC by DTP derivatives (0 – 100 μM) were measured in buffer (20 mM Bis-Tris-Propane pH = 7.5, 1 mM TCEP, 1 mg/ml BSA) with 100 nM substrate and 1 nM EcLpxC at room temperature. The $IC_{50}$ values were calculated by fitting the following equation to the data: $activity_I = activity_0 / (1 + [I] / IC_{50})$. The $IC_{50}$ values for metal-binding fragments that inhibit activity by ≥50% are listed in the table.

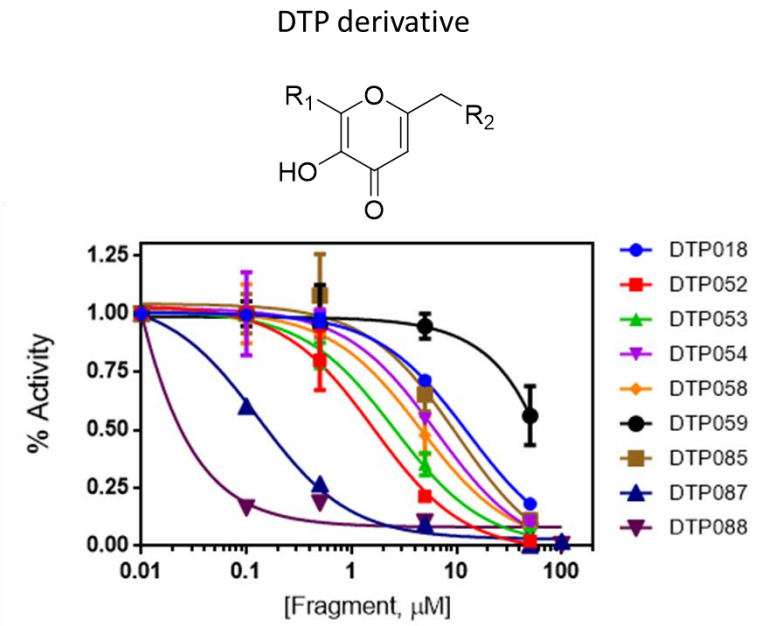


| | DTP-018 | DTP-052 | DTP-053 | DTP-054 | DTP-058 |
|---|---|---|---|---|---|
| $IC_{50}$ (μM) | 11.7 ± 0.5 | 1.3 ± 0.1 | 2.5 ± 0.3 | 5.5 ± 0.7 | 4.4 ± 0.06 |
| | DTP-059 | DTP-085 | DTP-087 | DTP-088 | |
| $IC_{50}$ (μM) | 67.0 ± 9.2 | 9.0 ± 5.1 | 0.13 ± 0.02 | 0.002 ± 0.009 | |

## DISCUSSION

In this chapter, we addressed two important issues: 1) the effect of the active site metal ion (Zn/Fe) on the inhibitor affinity to better correlate the *in vitro* inhibitor potency with the *in vivo* activity, and 2) a searching for potent non-hydroxamate inhibitors of LpxC to overcome the *in vivo* limitations of hydroxamate inhibitors.

LpxC containing a single catalytic Fe(II) has 6~8-fold higher activity than Zn(II)-LpxC.[45] The increases in $k_{cat}/K_M$ and $k_{cat}$ upon substitution of Zn(II) with Fe(II) are proposed to be attributable mainly to an enhancement in the chemical step. The inhibitor potency could be altered by these changes in the active site metal ion or by changes in interactions with the substrate binding pocket. We demonstrated that the affinity of Fe(II)-EcLpxC for a hydroxamate inhibitor is altered less than 2-fold compared to the Zn(II)-enzyme.

This result is consistent with high resolution structures showing that the Fe(II)-geometry in LpxC-hydroxamate complexes is five-coordinate.[169,179] In contrast to Fe-LpxC, extended X-ray absorption fine structure (EXAFS) spectroscopic studies and x-ray crystal structures of Zn(II)-LpxC from *A. aeolicus* and *P. aeruginosa* with hydroxamate inhibitors suggest a 4-coordinate zinc ion (tetrahedral geometry).[179,180] These data imply that the geometry of the metal site is flexible so that the Fe(II) site appears to adopt a five-coordinate structure even in the absence of added inhibitors. In general, the alteration between 4- and 5-coordinate geometries could explain a modest decrease in the inhibitor affinity of Zn(II)-LpxC from Fe(II)-LpxC.

Although hydroxamate functional groups rank among the most potent inhibitors of LpxC,

many hydroxamates exhibit limited inhibitory activity *in vivo* following oral administration. This low activity has been attributed to the rapid metabolism of the hydroxamate group to the corresponding inactive carboxylic acid. To date, few high affinity LpxC inhibitors with other metal-binding groups have been reported. To overcome the limitations of the hydroxamate moiety we screened a library of potential inhibitors that contained other metal-binding moieties to identify LpxC inhibitors *in vitro*, and possibly *in vivo*. This library was originally assembled and screened against five matrix metalloproteinase (MMP) family members to identify new MMP inhibitors.[176] The best compounds for inhibition of MMPs are library of hydroxypyridinone and hydroxypyridinethione fragments. For LpxC the best inhibitors generally contained a hydroxypyrones (CFL-D) or hydroxypyridinethiones (CDL-E). However, the best inhibitor was identified in a second library based on a DTP scaffold. Notably, the compound DTP-088 showed the most potent inhibition (nM range) from a non-hydroxamate inhibitor identified to date. This compound has suitable properties as a lead compound. The mode of inhibition as well as the structure of the compound bound to LpxC will provide further insight into the development of novel antibacterial compounds targeting LpxC.

Investigators have focused on inhibiting the first committed step in lipid A biosynthesis catalyzed by the metal-dependent deacetylase, LpxC for many years. The most potent hydroxamate inhibitor identified so far, CHIR-090, has been characterized in terms of both the inhibitory mechanism and the structure of the LpxC-inhibitor complex. However, the narrow spectrum of antibacterial activity and pathogen resistance due to mutations and the high lipophilicity have been problematic for development of CHIR-090 as a novel antibiotic. Therefore, there is an urgent need to generate more potent, broad spectrum inhibitors that target LpxC. The work in this chapter improves our understanding of the role of metal cofactors and

metal chelators in developing inhibitors of LpxC. The identification of a potent non-hydroxamate inhibitor of LpxC will be fundamental for developing the next-generation, potent inhibitors targeting LpxC and may lead to novel antibiotics.

**REFERENCE**

(1) Raetz, C. R. H. (1993) Bacterial Endotoxins : Extraordinary Lipids That Activate Eucaryotic Signal Transduction O-Antigen. *J Biol Chem 175*, 5745–5753.

(2) Raetz, C. R. H., and Whitfield, C. (2002) Lipopolysaccharide endotoxins. *Annu. Rev. Biochem. 71*, 635–700.

(3) S, M., Bull, G., Galloway, S. M., Kelly, M., Mohan, S., and Radikag, K. (1993) UDP-N-acetylglucosamine Acyltransferase of Escherichia coli. *J Biol Chem 268*, 19858–19865.

(4) Barb, A. W., Zhou, P., Hsieh, J., Koutmou, K. S., Rueda, D., Koutmos, M., Walter, N. G., and Fierke, C. A. (2008) Mechanism and inhibition of LpxC: an essential zinc-dependent deacetylase of bacterial lipid A synthesis. *Curr Pharm Biotechnol 9*, 9–15.

(5) Onishi, H. R., Pelak, B. a, Gerckens, L. S., Silver, L. L., Kahan, F. M., Chen, M. H., Patchett, a a, Galloway, S. M., Hyland, S. a, Anderson, M. S., and Raetz, C. R. (1996) Antibacterial agents that inhibit lipid A biosynthesis. *Science (80-. ). 274*, 980–2.

(6) Mdluli, K. E., Witte, P. R., Kline, T., Barb, A. W., Erwin, A. L., Mansfield, B. E., McClerren, A. L., Pirrung, M. C., Tumey, L. N., Warrener, P., Raetz, C. R. H., and Stover, C. K. (2006) Molecular validation of LpxC as an antibacterial drug target in Pseudomonas aeruginosa. *Antimicrob. Agents Chemother. 50*, 2178–84.

(7) Clements, J. M., Coignard, F., Johnson, I., Chandler, S., Palan, S., Waller, A., Wijkmans, J., Hunter, M. G., and Hemother, A. N. A. G. C. (2002) Antibacterial Activities and Characterization of Novel Inhibitors of LpxC. *Antimicrob. Agents Chemother. 46*, 1793–1799.

(8) Mochalkin, I., Knafels, J. D., and Lightle, S. (2008) Crystal structure of LpxC from Pseudomonas aeruginosa complexed with the potent BB-78485 inhibitor. *Protein Sci. 17*, 450–457.

(9) McClerren, A. L., Endsley, S., Bowman, J. L., Andersen, N. H., Guan, Z., Rudolph, J., and Raetz, C. R. H. (2005) A slow, tight-binding inhibitor of the zinc-dependent deacetylase LpxC of lipid A biosynthesis with antibiotic activity comparable to ciprofloxacin. *Biochemistry 44*, 16574–83.

(10) Montgomery, J. I., Brown, M. F., Reilly, U., Price, L. M., Abramite, J. a, Arcari, J., Barham, R., Che, Y., Chen, J. M., Chung, S. W., Collantes, E. M., Desbonnet, C., Doroski, M., Doty, J., Engtrakul, J. J., Harris, T. M., Huband, M., Knafels, J. D., Leach, K. L., Liu, S., Marfat, A., McAllister, L., McElroy, E., Menard, C. a, Mitton-Fry, M., Mullins, L., Noe, M. C., O'Donnell, J., Oliver, R., Penzien, J., Plummer, M., Shanmugasundaram, V., Thoma, C., Tomaras, A. P., Uccello, D. P., Vaz, A., and Wishka, D. G. (2012) Pyridone methylsulfone hydroxamate LpxC inhibitors for the treatment of serious gram-negative infections. *J. Med. Chem. 55*, 1662–70.

(11) Jacobsen, F. E., Lewis, J. a, and Cohen, S. M. (2007) The design of inhibitors for medicinally relevant metalloproteins. *ChemMedChem 2*, 152–71.

(12) Jackman, J. E., Raetz, C. R., and Fierke, C. a. (1999) UDP-3-O-(R-3-hydroxymyristoyl)-N-acetylglucosamine deacetylase of Escherichia coli is a zinc metalloenzyme. *Biochemistry 38*, 1902–11.

(13) Langsdorf, E. F., Malikzay, A., Lamarr, W. a, Daubaras, D., Kravec, C., Zhang, R., Hart, R., Monsma, F., Black, T., Ozbal, C. C., Miesel, L., and Lunn, C. a. (2010) Screening for antibacterial inhibitors of the UDP-3-O-(R-3-hydroxymyristoyl)-N-acetylglucosamine deacetylase (LpxC) using a high-throughput mass spectrometry assay. *J. Biomol. Screen. 15*, 52–61.

(14) Hernick, M., Gattis, S. G., Penner-Hahn, J. E., and Fierke, C. a. (2010) Activation of Escherichia coli UDP-3-O-[(R)-3-hydroxymyristoyl]-N-acetylglucosamine deacetylase by Fe2+ yields a more efficient enzyme with altered ligand affinity. *Biochemistry 49*, 2246–55.

(15) Gantt, S. L., Gattis, S. G., and Fierke, C. A. (2006) Catalytic activity and inhibition of human histone deacetylase 8 is dependent on the identity of the active site metal ion. *Biochemistry 45*, 6170–8.

(16) Fisher, J. F., and Mobashery, S. (2006) Recent advances in MMP inhibitor design. *Cancer Metastasis Rev. 25*, 115–36.

(17) Summers, J. B., Gunn, B. P., Mazdiyasni, H., Goetze, a M., Young, P. R., Bouska, J. B., Dyer, R. D., Brooks, D. W., and Carter, G. W. (1987) In vivo characterization of hydroxamic acid inhibitors of 5-lipoxygenase. *J. Med. Chem. 30*, 2121–6.

(18) Pellecchia, M., and Cohen, S. M. (2011) Chelator Fragment Libraries for Targeting Metalloproteinases. *ChemMedChem 5*, 195–199.

(19) Jacobsen, J. a, Fullagar, J. L., Miller, M. T., and Cohen, S. M. (2011) Identifying chelators for metalloprotein inhibitors using a fragment-based approach. *J. Med. Chem. 54*, 591–602.

(20) Agrawal, A., Johnson, S. L., Jacobsen, J. a, Miller, M. T., Chen, L.-H., Pellecchia, M., and Cohen, S. M. (2010) Chelator fragment libraries for targeting metalloproteinases. *ChemMedChem 5*, 195–9.

(21) Gattis, S. G., Hernick, M., and Fierke, C. a. (2010) Active site metal ion in UDP-3-O-((R)-3-hydroxymyristoyl)-N-acetylglucosamine deacetylase (LpxC) switches between Fe(II) and Zn(II) depending on cellular conditions. *J. Biol. Chem. 285*, 33788–33796.

(22) Whittington, D. a, Rusche, K. M., Shin, H., Fierke, C. a, and Christianson, D. W. (2003) Crystal structure of LpxC, a zinc-dependent deacetylase essential for endotoxin biosynthesis. *Proc. Natl. Acad. Sci. U. S. A. 100*, 8146–50.

(23) McClure, C. P., Rusche, K. M., Peariso, K., Jackman, J. E., Fierke, C. a., and Penner-Hahn, J. E. (2003) EXAFS studies of the zinc sites of UDP-(3-O-acyl)-N-acetylglucosamine deacetylase (LpxC). *J. Inorg. Biochem. 94*, 78–85.

# CHAPTER 6

# SUMMARY AND FUTURE WORKS

## SUMMARY

A bound metal ion is essential for histone deacetylase 8 activity. The metal ion enhances the enzyme activity by activating the water nucleophile and polarizing the substrate, and stabilizing charge in the tetrahedral intermediate and the transition state. Thus, it was intriguing that HDAC8 shows different catalytic efficiency and peptide selectivity with bound Fe(II) or Zn(II), which are the most abundant metals in cells.[1]

Also this enzyme has is inhibited by incubation with metal chelators.[2] To date, the most potent compounds that effectively inhibit HDAC activity contain a metal-binding moiety such as a hydroxamate.[3] After aerobic purification, HDAC was isolated with a bound Zn(II) and was therefore categorized as a Zn(II)-dependent metalloenzyme. However, additional data supported activation of HDAC8 by Fe(II). Based on the crystal structure, the HDAC metal ligands are unusual for a mononuclear zinc metalloenzyme in that two of the three ligands are negatively charged carboxylates.[4] Also Fe(II)-HDAC8 is more active than Zn(II)-HDAC8 *in vitro*.[1] Lastly, the HDAC8 activity is ~4-fold larger when the cells are lysed and assayed under anaerobic compared to aerobic conditions.[1] In light of these observations, the work in this thesis addressed two important unanswered questions: 1) What are the metal binding kinetics and thermodynamics of HDAC8, and 2) What are the structural determinants of metal specificity and, potentially, metal switching? The overall goals of this thesis were to characterize the metal

binding kinetics and thermodynamics of a class I histone deacetylase, HDAC8, and furthermore to investigate the possible determinants that lead the enzyme to switch between Zn(II) and Fe(II) as an active site cofactor.

*1. Measurement of metal-binding properties of WT HDAC8 using newly-developed FP assay*

I have investigated the metal binding kinetics using HDAC8 using a newly-developed fluorescence polarization (FP) assay with a fluorescein-labeled SAHA (flSAHA). First, the kinetic/thermodynamic values ($k_{on}$, $k_{off}$, $K_D$) of flSAHA binding to apo- and metal (Zn(II)/Fe(II))-bound HDAC8 were determined using the FP assay and stopped-flow spectrometry. We noted that the binding affinity of flSAHA to metal-bound HDAC8 was fairly high and were comparable to selected HDAC8 inhibitors, SAHA. Association rate constants of flSAHA to Zn/Fe-bound HDAC8 were also fast enough to allow me to measure metal-binding kinetics of HDAC8.

Then, using the FP binding assay and the conventional FdL activity assay, the metal (Zn(II)/Fe(II)) binding kinetics and thermodynamics ($k_{off}$ and $K_D$) of HDAC8 were investigated. Interestingly, $k_{off}$ of both metals were comparable, while $K_D$ values varied from the picomolar to micromolar range for Zn(II) and Fe(II), respectively. These affinities are comparable to the readily exchangeable Zn(II) and Fe(II) concentrations in cells, consistent with either metal cofactor activating HDAC8.

*2. Second shell residues determine the metal (Zn/Fe) selectivity and reactivity of HDAC8*

To characterize the structural determinants of metal switching in HDAC8, mutations of conserved second shell ligands (M274, F207, F208) which are unique to HDAC8 were generated using site-specific mutagenesis. The catalytic activity ($k_{cat}/K_M$) and metal affinity and kinetics ($k_{off}$, and $K_D$) were assayed using the FP binding assay and the FdL assay for both Zn(II) and Fe(II). These results indicated the importance of these residues for both the Zn(II) / Fe(II) affinities and catalytic activities of HDAC8. Notably, the M274E mutant has enormously enhanced selectivity for Fe(II) compared to Zn(II) compared to that of WT. This Fe(II)-specific HDAC8 mutant has properties which may be ideal for combining with flSAHA for development of a cellular iron-sensor (chapter 3, figure 7). In future, more mutations of these amino acids (M274L, F207Y, F208Y) will be made and assayed to further delineate the role of second shell ligand on metal selectivity. Although Met is located in HDAC8, other class I HDACs contain Leu as their conserved residue. It would be interesting to see if S atom has an effect on reactivity or metal binding affinity through interaction with His180. F207A mutant shows preference for Zn(II), while F208A has an strong affinity for Fe(II). By placing an hydroxyl group from Tyr residue instead of Phe, we could determine the role of hydrophobic interaction in pre-orienting the metal environment of HDAC8.

A collaboration with Dr. David Christianson at the University of Pennsylvania to crystallize both Zn(II)- and Fe(II)-HDAC8 of mutants showing a higher preference for one metal will visualize changes in the metal geometry and the surrounding protein residues that are important for metal selectivity. These experiments will advance our understanding of the underlying principles of metal selectivity function in the context of second shell ligand

environment.

*3. Investigation of HDAC8-PCBP1 interaction by kinetic and mass-spec analysis*

Many of the HDAC isozymes form complexes with a variety of other proteins[5,6]. Indeed, mass spectrometry and pull-down data suggest that poly (rC) binding protein 1 (PCBP1), an iron chaperone of ferritin, interacts with HDAC.[7] Therefore, the effect of PCBP1 on the activity and metal dissociation kinetics of HDAC8 were measured to explore the PCBP1 as a potential metallochaperone candidate. Co-IP data indicated that PCBP1 physically interacted with HDAC8 *in vivo* regardless of the cellular iron conditions. Using IM-MS in collaboration with Prof. Ruotolo lab, an HDAC8-PCBP1 complex was identified with a $K_D$ for the two apo proteins of ~50 μM. The $k_{off}$ of Fe(II) from HDAC8 was decreased in the presence of apo-PCBP1, whereas $k_{off}$ for Zn(II) was not altered. Additionally, only the catalytic activity of Fe(II)-bound HDAC8 was affected by apo-PCBP1, implying that the protein interaction site for PCBP1 on HDAC8 must not occur at the active site.

*4. LpxC inhibition*

There is a need for the development of non-hydroxamate metal-binding inhibitors for LpxC, since most hydroxamate-based inhibitors lead to severe toxicity and poor oral bioavailability. To search for novel non-hydroxamate inhibitors of the LpxC enzyme, we collaborated with Cubist pharmaceutical and Prof. Cohen at University of California, San Diego to assay current potent inhibitors and their novel lead compounds. The affinity of Fe(II)-EcLpxC

for a known hydroxamate inhibitor (L161240, CHIR-090) increases by a small degree (~2-fold), consistent with crystal structures indicating that the metal geometry in LpxC-hydroxamate complexes is 5-coordinate. This change in affinity is likely due to alteration of the geometry of the metal-ligand coordination leading to alterations in interactions with other active site groups. Subsequently, a library of novel potent metal-binding fragments were screened using the Cubist HTS MS assay and found to have submicromolar inhibitory affinity.

## FUTURE WORKS

### *Metal switching in HDAC8*

In HDAC8, many questions about the *in vivo* metal still remain unclear. The current evidence strongly suggests that Fe(II)-bound HDAC8 can form *in vivo*. Therefore, identification of the cellular conditions that lead to formation of the Fe(II)-HDAC8 or Zn(II)-HDAC8 is the most important question to ask to understand the biological implications of metal switching. If HDAC8 does switch the native metal *in vivo* in response to cellular factors, this would suggest that many members of HDAC superfamily should be examined to identify cellular conditions that lead to metal switching.

If the metal bound to HDAC8 does not to correlate with the metal content in the media, as observed for the bacterial deacetylase LpxC[8], it will be interesting to identify other stimuli, such as binding partners[7] or metallochaperones, that are responsible for determining the identity of the native active site metal. In eukaryotic cells, extracellular metal ion concentrations might not be variable enough to induce switching, but other changes, such as oxidative stress or

potential alterations in the substrate pool, might lead to metal switching.[9] In this model, the enzyme-bound Fe(II) dissociates from the enzyme and is replaced by Zn(II) which is increased due to oxidative stress. Metal switching could also be enhanced by oxidation of HDAC8-bound Fe(II) to Fe(III) which has lower affinity.

Based on evidence that Fe(II)-HDAC8 is more active than Zn(II)-HDAC8, an important future direction is to probe native metal ion bound to HDAC8 *in vivo* in mammalian cells under a variety of cellular conditions. The pull-down method used to evaluate the native metal ion bound to LpxC[8] could be optimized to probe metals bound to HDAC8 in tissue culture cells. Determining the physiological metal bound to HDAC8 under various condition (such as ± $H_2O_2$ and during cell division) will shed light on whether the novel metal switching mechanism of HDAC8 has cellular importance, such as acting as a protective redox mode.

Probing substrate selectivity of HDAC8 second shell mutants using short acetylated peptides will shed light on the molecular recognition of metal ion in HDAC8. This can be done in collaboration with the Schueler-Furman lab at the Hebrew University of Jerusalem who has been working on models to predict HDAC8 substrates through multiple iterations of reactivity prediction using the Rosetta FlexPepBind platform. These results suggest that metal switching may alter the substrate/peptide selectivity, providing a potential mechanism to regulate HDAC activity *in vivo*. This experiment needs to be extended to be performed with tissue culture cells, since HDAC8 binds a mixture of Fe(II) and Zn(II) when expressed in mammalian tissue culture cells. If the metal selectivity is mainly determined by structural factors, such as second shell ligand, then the metals bound to HDAC8 expressed in tissue culture cells should vary with mutants in second shell environment.

*Development of iron sensor*

Effective fluorescent probes for imaging iron ions in living cellular environments is needed to measure free iron concentration more accurately, leading to an enhanced understanding of the biological function of iron. In the last several years, a series of probes have been developed for Fe(II) and Fe(III) that may allow new discoveries regarding cellular iron homeostasis.[10,11] However, current fluorogenic agents for cellular iron detection are limited to fluorescence quenching readouts. For example, calcein is a commercially available fluorophore that has been used for turn-off Fe(II) detection. This reagent is about ten-fold more selective for Fe(II) over Fe(III) but also shows significant interference from other metal ions, including Cu(II), Ni(II) and Co(II). There is urgent need to develop more specific sensor which can used in *in vivo* accurately.

An application goal of the second shell mutant study was the development of a series of HDAC8 variants, such as M274Q or F208A, with significantly improved properties for sensing iron in cells. Various mutations in the second shell ligand of HDAC8 generate distinct metal specificity for $K_D^{Zn}/K_D^{Fe}$. The proposed sensing scheme is to use HDAC8 as the metal recognition element and couple this to binding of fl-SAHA to visualize bound metal ions. Wild-type HDAC8 is not sufficiently selective for Fe(II) such that it would likely reflect both cellular Fe(II) and Zn(II) levels. However, a variant of HDAC8 second shell ligand (e.g. F208A) binds Zn(II) with a $K_D$ > nM while retaining an Fe(II) $K_D$ of 0.2 μM. The enhanced selectivity for iron is ideal for the development of an Fe(II) sensor, although the molecular determinants of selectivity are not yet understood. For metal sensing, a red fluorescent protein, TagRFP, will be fused to the C-terminus of the HDAC8 mutant as a FRET acceptor and fluorescein-labeled

SAHA (flSAHA) bound to the active site will function as the FRET donor. The FRET signal will reflect metal-bound HDAC8 since flSAHA requires an active site metal ion to bind with high affinity. This sensor will be calibrated for measuring free iron in *E. coli* cells and then adapted for use in tissue culture cells. This approach has already proven feasible for sensing readily exchangeable zinc in cells using CAII variants. T199A, Q92A, H94N and WT CAII fused with TagRFP bound a fluorescent ligand (dapoxylsulfonamide) to reflect zinc binding.[12] These sensors successfully measured picomolar zinc concentrations in *E. coli* at pH 7.6, and were very sensitive for detecting subtle differences in intracellular free zinc concentrations.[39] Herein, we prepared HDAC8 variants with altered selectivity for both metals suggesting that iron-specific sensors could be made.

*Development of LpxC inhibitor*

A majority of current compounds efficiently inhibit the growth of *E. coli* and are selective inhibitors for EcLpxC. Because square pyramidal geometry has been observed for all hydroxamate containing inhibitors, this zinc coordination has generally been regarded as a primary restraint for design of LpxC inhibitors. However, there is growing evidences that LpxC is activated by Fe(II) or Zn(II) based on cellular conditions.[8,13] The affinity of Fe(II)-EcLpxC for a hydroxamate inhibitor increases by a small degree (~2-fold), consistent with the five-coordinate (square pyramidal) metal geometry in LpxC-hydroxamate complexes. Next efforts to identify potent inhibitors which coordinate the metal ion at the active site of LpxC are required to determine the behavior of this enzyme *in vivo* and prevent overestimation of current inhibitors.

## CLOSING REMARKS

The work presented here has provided insight into the metal binding mechanism of HDAC8 and determinants of metal switching of HDAC8. Since metal switching is proposed to be a common phenomenon among certain metallohydrolases, affecting the activity and regulation of numerous proteins, it is critical that we better understand this mechanism. This research provides insight into the specific role of structural elements (e.g., second shell residues or monovalent cation binding) in eukaryotic cells and furthermore will be useful in developing an iron-specific metal sensor or more potent HDAC inhibitors.

**REFERENCE**

(1) Gantt, S. L., Gattis, S. G., and Fierke, C. A. (2006) Catalytic activity and inhibition of human histone deacetylase 8 is dependent on the identity of the active site metal ion. *Biochemistry 45*, 6170–8.

(2) Hassig, C. A., Tong, J. K., Fleischer, T. C., Owa, T., Grable, P. G., Ayer, D. E., and Schreiber, S. L. (1998) A role for histone deacetylase activity in HDAC1-mediated transcriptional repression. *Proc. Natl. Acad. Sci. U. S. A. 95*, 3519–24.

(3) De Ruijter, A. J. M., van Gennip, A. H., Caron, H. N., Kemp, S., and van Kuilenburg, A. B. P. (2003) Histone deacetylases (HDACs): characterization of the classical HDAC family. *Biochem. J. 370*, 737–49.

(4) Vannini, A., Volpari, C., Filocamo, G., Casavola, E. C., Brunetti, M., Renzoni, D., Chakravarty, P., Paolini, C., De Francesco, R., Gallinari, P., Steinkühler, C., and Di Marco, S. (2004) Crystal structure of a eukaryotic zinc-dependent histone deacetylase, human HDAC8, complexed with a hydroxamic acid inhibitor. *Proc. Natl. Acad. Sci. U. S. A. 101*, 15064–15069.

(5) Denslow, S. A., and Wade, P. A. (2007) The human Mi-2/NuRD complex and gene regulation. *Oncogene 26*, 5433–8.

(6) Hdac, D., Complex, H., Peinado, H., Ballestar, E., Esteller, M., and Cano, A. (2004) Snail Mediates E-Cadherin Repression by the Recruitment of the Sin3A / Histone Snail Mediates E-Cadherin Repression by the Recruitment of the Sin3A / Histone Deacetylase 1 ( HDAC1 )/ HDAC2 Complex. *Mol. Cell. Biol. 24*, 306–319.

(7) Joshi, P., Greco, T. M., Guise, A. J., Luo, Y., Yu, F., Nesvizhskii, A. I., and Cristea, I. M. (2013) The functional interactome landscape of the human histone deacetylase family. *Mol. Syst. Biol. 9*, 1–21.

(8) Gattis, S. G., Hernick, M., and Fierke, C. A. (2010) Active site metal ion in UDP-3-O-((R)-3-hydroxymyristoyl)-N-acetylglucosamine deacetylase (LpxC) switches between Fe(II) and Zn(II) depending on cellular conditions. *J. Biol. Chem. 285*, 33788–33796.

(9) Imlay, J. A. (2008) Cellular defenses against superoxide and hydrogen peroxide. *Annu. Rev. Biochem. 77*, 755–76.

(10) García-Beltrán, O., Mena, N., Yañez, O., Caballero, J., Vargas, V., Nuñez, M. T., and Cassels, B. K. (2013) Design, synthesis and cellular dynamics studies in membranes of a new coumarin-based “turn-off” fluorescent probe selective for Fe2+. *Eur. J. Med. Chem. 67*, 60–3.

(11) Hirayama, T., Okuda, K., and Nagasawa, H. (2013) A highly selective turn-on fluorescent probe for iron(ii) to visualize labile iron in living cells. *Chem. Sci. 4*, 1250–1256.

(12) Kiefer, L. L., Paterno, S. A., Fierke, C. A., and Carolina, N. (1995) Hydrogen Bond Network in the Metal Binding Site of Carbonic Anhydrase Enhances Zinc Affinity and Catalytic Efficiency ? *J. Am. Chem. Soc. 117*, 6831–6837.

(13) Hernick, M., Gattis, S. G., Penner-Hahn, J. E., and Fierke, C. A. (2010) Activation of Escherichia coli UDP-3-O-[(R)-3-hydroxymyristoyl]-N-acetylglucosamine deacetylase by Fe2+ yields a more efficient enzyme with altered ligand affinity. *Biochemistry 49*, 2246–55.